Femtosecond few-cycle mid-infrared laser pulses

Liu, Xing; Bache, Morten; Zhou, Binbin; Bang, Ole

Publication date:
2016

Document Version
Publisher's PDF, also known as Version of record

Femtosecond few-cycle mid-infrared laser pulses

Xing Liu

March 15, 2016

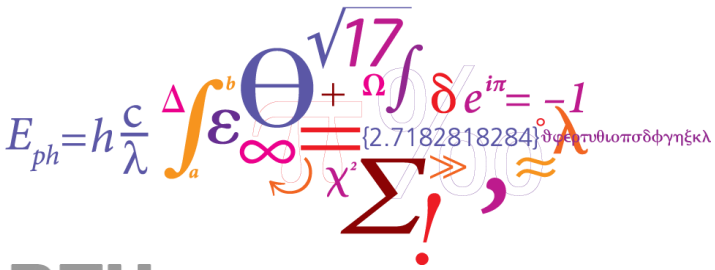

DTU
Technical University
of Denmark

Preface

The work presented in this thesis has been carried out as my Ph.D. project in the period October 16th 2012 – March 15th 2016. The work took place at the Department of Photonics Engineering (DTU Fotonik), Technical University of Denmark. The Ph.D. project is funded by the Danish Council for Independent Research (274-08-0479, 11-106702, held by main supervisor Dr. Morten Bache) and supported by the basic funding of the Department of Photonics Engineering (DTU Fotonik).The main supervisor Dr. Morten Bache, Associate Professor at DTU Fotonik,Technical University of Denmark. The co-supervisors is Dr. Binbin Zhou also from DTU Fotonik.

Acknowledgement

With this part, I would like to express my gratitude to those who have helped me during my whole PhD study at DTU Fotonik.

Firstly, I would appreciate my main supervisor Professor Morten Bache who has given me the opportunity to work and study at DTU Fotonik as a PhD student. As my tutor, Professor Morten shows great patience to my work and shares his knowledge and experience with me. It's his consistent supporting and encouragement that push me to move forward. Besides a great supervisor, he is also a good friend for me. I would be very happy if I had the opportunity to work with him in the future.

I also want to give my warm thanks to my co-supervisor Dr. Binbin Zhou. I appreciate him for helping me on experiments, sharing your experiences with me in the lab, and his careful instructions to me in each experiment. The experimental skills taught by him greatly help me for my PhD study.

Many thanks to Dr. Hairun Guo for fruitful discussions a lot with me on simulations. Thanks to Dr. Minhao Pu and Dr. Radu Alureanu for helping me with the experiments on the microscope stage. I would also like to thank all my friends, colleagues.

Finally, I want to show my affection to my parents. During the three year study life, I lose the opportunity to enjoy time with them. Their continuous support and encouragement help me cover the difficulties in my PhD study. I hope this work will make all of guys feel proud of me.

Abstract

The few-cycle pulses of mid-infrared (mid-IR, wavelength 2-10 microns) have attracted increasing attention owing to their great potentials for high order harmonic generation, time-resolved spectroscopy, precision of cutting and biomedical science.

In this thesis, mid-IR frequency conversion by the ultra-fast soliton was proposed, which exploit optical solitons in near-IR for generating the mid-IR pulses.

Firstly, we show numerically that ultrashort self-defocusing temporal solitons colliding with a weak pulsed probe in the near-IR can convert the probe to the mid-IR. A near perfect conversion efficiency is possible for a high effective soliton order. The near-IR self-defocusing soliton can form in a quadratic nonlinear crystal (beta-barium borate) in the normal dispersion regime due to cascaded (phase-mismatched) second-harmonic generation, and the mid-IR converted wave is formed in the anomalous dispersion regime between $\lambda = 2.2 - 2.4$ μm as a resonant dispersive wave. This process relies on non-degenerate four-wave mixing mediated by an effective negative cross-phase modulation term caused by cascaded soliton-probe sum-frequency generation.

Secondly, a self-pumped soliton-driven tunable mid-IR optical parametric amplifier is demonstrated for the first time in a standard periodically poled lithium niobate (PPLN) bulk crystal. The new type of resonant radiation is generated through a three wave mixing (TWM) process. The poling pitch gives a parametrically tunable resonant radiation from λ =4.2 - 5.5 μm with only one fixed pump wavelength, a feature absent in Kerr media.

Finally, we experimentally observe supercontinuum generation spanning 1.5 octaves, generated in a 10 mm long silicon-rich nitride waveguide pumped by 100 pJ femtosecond pulses from an erbium fiber laser. The waveguide has a large nonlinear Kerr coefficient and two zero dispersion wavelengths giving broadband anomalous dispersion centered around the pump wavelength. This is achieved by slightly increasing the silicon content over stoichiometric silicon nitride and waveguide geometry engineering. The spectral broadening relies on exciting a soliton and two dispersive waves. In the same waveguide using orthogonal pump polarization, optical wave-breaking occurs as the pump dispersion becomes normal. The numerical simulations indicate that the supercontinua are highly coherent.

Through numerical simulations and experiments, we find out soliton based on generating the mid-IR is a compact and simple approach, and could have great potentials.

Resumé

Impulser med varighed af få optiske cyklusser med bølgelængder i det melleminfrarøde (MIR, bølgelængde 2-20 mikrometer) har fået stigende opmærksomhed på grund af deres store potentiale til høj-harmonisk generering, tidsopløst spektroskopi, og biomedicinsk videnskab.

I denne afhandling blev en ny teknik til MIR frekvenskonvertering af en ultra-kort soliton foreslået, der udnytter optiske solitoner i nær-IR til generering af MIR impulser.

For det første viser vi numerisk at når ultrakorte selv-defokuserende tidslige solitoner kolliderer med en svag pulseret probeimpuls i nær-IR, kan dette konvertere proben til MIR. En næsten perfekt virkningsgrad er muligt for en højere ordens effektiv solitontal. Den nær-IR selv-defokuserende soliton kan dannes i en kvadratisk ikke-lineær krystal (beta-bariumborat) i det normale dispersionsområde via kaskade (fase-mismatched) anden-harmonisk generering, og den MIR konverterede bølge dannes i det anormale dispersionsområde mellem 2,2-2,4 mikrometer som en resonant dispersiv bølge. Denne proces bygger på ikke-degenereret fire-bølge blanding medieret af en effektiv negativ kryds-fasemodulation som er forårsaget af kaskade soliton-probe sum-frekvens generering.

For det andet, bliver en selv-pumpet soliton-drevet tunbar MIR optisk parametrisk forstærker demonstreret for første gang i en standard periodisk polet lithium niobat (PPLN) krystal. Denne nye type resonant stråling frembringes gennem en tre bølge blanding proces. Afstanden mellem polingdomænerne giver en parametrisk tunbar resonant stråling fra 4,2 - 5.5 mikrometer med kun én enkelt pumpe bølgelængde, en funktion som ikke kan genskabes i Kerr ikke-lineære medier.

Endelig har vi eksperimentelt observeret superkontinuum generering der spænder over 1,5 oktaver, genereret i en 10 mm lang silicium-rig nitrid bølgeleder pumpet af 100 pJ femtosekund impulser fra en erbium fiberlaser. Bølgelederen har en stor ulineær Kerr koefficient og to nul-dispersions bølgelængder, hvilket giver bredbåndet anormal dispersion centreret omkring pumpens bølgelængde. Dette opnås ved at bruge en smule større silicium indhold i forhold til støkiometrisk siliciumnitrid og ved hjælp af en passende konstrueret bølgeledergeometri. Den spektrale udvidelse er afhængig af eksitere en soliton og to dispersive bølger. I samme bølgeleder ved anvendelse ortogonal polarisering af pumpen, observerede vi optisk bølge-brydning som forekommer fordi pumpens dispersion bliver normal. De numeriske simulationer viser, at de dannede superkontinua er meget kohærente.

Gennem numeriske simuleringer og eksperimenter har vi vist, at soliton-baseret generering af MIR bredbåndet stråling er en kompakt og enkel metode som har et stort potentiale.

Contents

Chapter 1

Introduction

1.1 Project Background

Over the past decade, ultrashort pulse have become an indispensable tool in the physics, medical, telecommunication sectors, time-resolved spectroscopy in chemistry, biology, materials science and defense security. In particular, ultrashort pulses in the mid-infrared (mid-IR, wavelength 2-10 microns) have great potential for probing and manipulating atomic and molecular dynamics, which provide a powerful tool for imaging molecular structure by detecting the chemical bonds, such as the important C-H,O-H and N-H bonds. For the industrial applications, mid-infrared laser dominate in materials processing, precision of cutting and medical treatment applications [1].

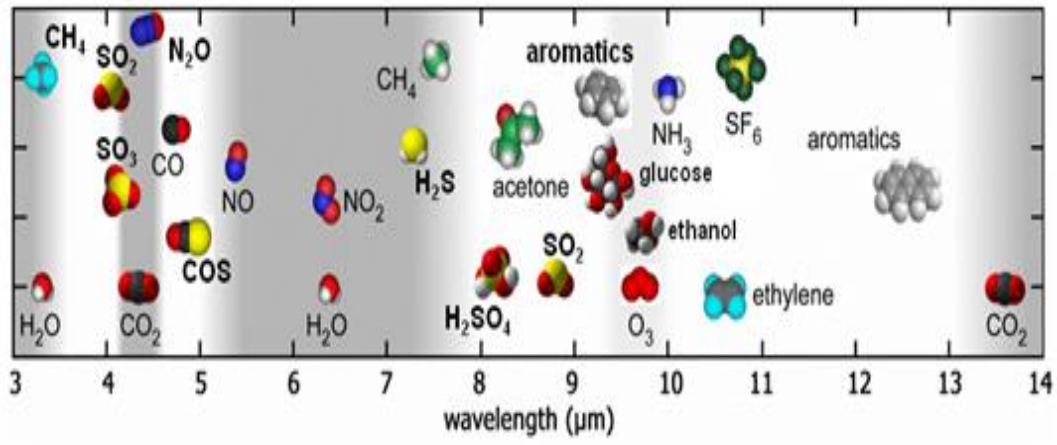

Fig 1 Molecular resonances in the mid-IR spectral region [8]

Much effort has been invested in developing mid-IR sources in the past few years. With the development of novel mid-IR materials and technology, the availability of mid-IR light sources have been the dramatic increasing and improvement recently. The commonly used methods for generating ultrashort mid-IR radiation are based on nonlinear optical parametric processes—including difference frequency generation (DFG) [9], optical parametric amplification (OPA) [11], and optical parametric oscillators (OPO) [13] and quantum cascade lasers (QCL) [14]. These technologies can span much of the mid-IR spectral region using tunable or broadband pump sources. Such devices pumped by solid-state laser systems operating in the near-infrared require critical

phase-matching condition, synchronized pump wavelengths or low conversion efficiencies [7], which results in a need to find a new alternative solution for generating mid-IR.

The motivation behind the new project is to bridge the near-IR ultrafast laser technology and the demand of ultrashort pulses in the mid-IR. One possible method relies on ultra-fast frequency conversion by the soliton, which potentially can generate mid-infrared pulses.

1.2 Project Description

The temporal soliton is a fascinating and ubiquitous property of nonlinear waves which can maintain their temporal shape by balance between the effects of dispersion and nonlinearity. Solitons have been found to play the major role for supercontinuum generation (SCG) in photonic crystal fiber (PCF) since 2000[15]. When pumping a PCF in the region of anomalous dispersion leads to the broadest spectrum broadening, which determined by soliton-related dynamics, especially dispersion wave (DW) generation [16].The spectral of DW location is a result of a phase-matching condition to the soliton [19]. The SCG is achieved through complex processes in the PCF including self-phase modulation (SPM) effect, dispersive radiation emitted by soliton, four wave mixing (FWM), and Raman nonlinearity etc. Although SC sources operating in the visible and near-infrared (NIR) spectral regions have been great developed and commercialized [20], it is still a challenging to achieve the SC generation in the mid-IR regions. The common used fiber is the silica PCF, because its dispersion and zero-dispersion wavelength (ZDW) can be tailored. However, the transmission window is determined by the multi phonon absorption, the maximum phonon energy of silica glass limits the emission wavelength up to 2.5μm [22]. The soft-glass including fluoride, tellurite, and chalcogenide fibers is a platform highly suitable for mid-IR generation, exhibit high Kerr nonlinearities and excellent transmission properties in the mid-IR [24]. However, the material ZDW of e.g. As_2Se_3 is 7.4 μm. It is challenging to shift down the ZDW that operating wavelengths of common ultrafast pulsed lasers.

One possible method is to exploit ultrashort self-defocusing nonlinearity solitons generated in the quadratic crystals [32]. When the SHG is phase mismatched, the energy conversion between the fundamental wave (FW) and the second harmonic (SH) will become weak and periodically repeated. In this process, FW can be given rise to an intensity-related nonlinear phase shift, like the cubic Kerr nonlinearity. Therefore, such energy and phase shifts can also be used to dynamically counteract the spreading caused by nonlinearity and dispersion, forming a temporal quadratic solitons. The compressed temporal solitons have been experimentally demonstrated in the barium borate (BBO) [35] and lithium niobate (LN) [37].Spectrally soliton dominate in the infrared, where the group velocity dispersion (GVD) is typically normal. The longer part of SC in the mid-infrared range most often spans through the range of anomalous GVD and is associated with an ultrashort DW, which has been experimentally observed in the crystal lithium thioindate (LIS) [38], LN crystal [40], BBO crystal [41] and waveguides [42].

Another possible method is to employ silicon nitride which transparency window covers from the UV to > 6 μm. The nonlinear coefficient in bulk is ten times larger than silica glass. This material does not display two-photon absorption in the telecommunications wavelength band and waveguides can be engineered with very low propagation losses. More importantly the waveguide have also the ability to tailor the dispersion in a wide range. Such features indicate that silicon nitride is a good candidate material for mid-IR [43].

Therefore, based on above descriptions, we proposed the project “Femtosecond few-cycle mid-infrared laser pulses”. What was out looked in this project is the fact that interaction of solitons with DW, in this process associated frequency conversion processes can be efficient and practically important for mid-IR. The idea is to explore the soliton interaction with dispersive wave from a PCF to a quadratic crystal and CMOS-compatible waveguide. Our primary aims here are to explain

the frequency conversion effects resulting from the soliton-radiation interaction and leading to SCG, which will bring the new insights into nonlinear optics.

1.3 Achievements and Milestones

The achievements and milestones of this project are listed as follows:

• We numerically for the first time demonstrated in a quadratic nonlinear crystal a self-defocusing near-IR soliton colliding with a weak near-IR probe induces a cascaded SFG nonlinearity generating a self- defocusing Kerr-like cross phase modulation term. This allows a resonant mid-IR wave to become phase matched. A complete probe-resonant wave conversion is possible when colliding with a higher-order soliton.

• We developed couple analytic wave equations (CAWEs), which firstly confirmed the new mid-IR radiation a standard periodically poled lithium niobate (PPLN) bulk crystal. The soliton drives resonant radiation in the mid-IR, through a three-wave mixing process with a large degree of tunability in the wavelength.

• We investigate the SCG in a dispersion engineered silicon-rich nitride waveguide by pumping with low-energy pulses (80-140 pJ) from an erbium fiber oscillator. In the transverse-electric (TE) polarization case a soliton and two dispersive waves were excited to give a 1.5 octave SC (from 800-2250 nm at -30 dB).

Bibliography

[1] M. Ebrahim Zadeh and I. T. Sorokina, Mid-Infrared Coherent Sources and Applications (Springer, 2005).

[2] M. Groot and R. Van Grondelle, “Femtosecond time-resolved infrared spectroscopy,” in “Biophysical Techniques in Photosynthesis,” vol. 26 of Advances in Photosynthesis and Respiration, T. J. Aartsma and J. Matysik, eds. (Springer Netherlands, 2008), pp. 191–200.

[3] L. Dhar, J. A. Rogers, and K. A. Nelson, “Time-resolved vibrational spectroscopy in the impulsive limit,” Chem. Rev. 94, 157–193 (1994).

[4] E. Tokunaga, T. Kobayashi, and A. Terasaki, “Frequency-domain interferometer for

femtosecond time-resolved phase spectroscopy," Opt. Lett.17, 1131–1133 (1992).

[5] K. Iwata, T. Takaya, H. Hamaguchi, A. Yamakata, T. Ishibashi, H. Onishi, and H. uroda, "Carrier dynamics in TiO2 and Pt=TiO2 powders observed by femtosecond time-resolved near-infrared spectroscopy at a spectral region of 0.9-1.5 _m with the direct absorption method," J Phys.Chem. B 108, 20233–20239 (2004).

[6] A. L. Smeigh, M. Creelman, R. A. Mathies, and J. K. McCusker, "Femtosecond time-resolved optical and raman spectroscopy of photoinduced spin crossover: Temporal resolution of low-to-high spin optical switching," J Am. Chem. Soc. 130, 14105–14107 (2008).

[7] H. Pires, M.Baudisch, D.Sanchez, M.Hemmer and J.Biegert, "Ultrashort pulse generation in the mid-IR," Progress inQuantumElectronics431–30(2015)

[8] http://www.daylightsolutions.com/technology/qcl_technology.htm

[9] F. Seifert, V. Petrov, and M. Woerner, "Solid-state laser system for the generation of midinfrared femtosecond pulses tunable from 3.3 to 10 μm," Opt. Lett. 19, 2009–2011 (1994).

[10] R. A. Kaindl, M. Wurm, K. Reimann, P. Hamm, A. M. Weiner, and M. Woerner, "Generation, shaping, and characterization of intense femtosecond pulses tunable from 3 to 20 μm," J. Opt. Soc. Am. B 17, 2086–2094 (2000).

[11] Giedrius Andriukaitis, Tadas Balčiūnas, Skirmantas Ališauskas, Audrius Pugžlys, Andrius Baltuška, Tenio Popmintchev, Ming-Chang Chen, Margaret M. Murnane, and Henry C. Kapteyn, "90 GW peak power few-cycle mid-infrared pulses from an optical parametric amplifier," Opt. Lett. 36, 2755-2757 (2011)

[12] Xiaoping Liu, Richard M. Osgood, Jr, Yurii A. Vlasov and William M. J. Green, "Mid-infrared optical parametric amplifier using silicon nanophotonic waveguides," Nature Photonics 4, 557 - 560 (2010)

[13] Martin Gebhardt, Christian Gaida, Pankaj Kadwani,Alex Sincore, Nils Gehlich, Cheonha Jeon, Lawrence Shah, and Martin Richardson, "High peak-power mid-infrared ZnGeP2 optical parametric oscillator pumped by a Tm:fiber master oscillator power amplifier system," Opt. Lett. 39, 1212-1215 (2014)

[14] Y.Yao,A.J.Hoffman and C.F.Gmachl,"Mid-infrared quantum cascade lasers," Nat. Photon.6(7) 432–439, (2012)

[15] J. K. Ranka, R. S. Windeler, and A. J. Stentz, "Visible continuum generation in air silica microstructure optical fibers with anomalous dispersion at 800 nm," Opt. Lett. 25, 25-27 (2000).

[16] J. M. Dudley, G. Genty, and S. Coen, "Supercontinuum generation in photonic crystal fibers,"

Rev. Mod. Phys. 78, 1135-1184 (2006).

[17] A. V. Husakou and J. Herrmann, "Supercontinuum generation of higher-order solitons by fission in photonic crystal fibers," Phys. Rev. Lett. 87, 203901 (2001).

[18] I. Cristiani, R. Tediosi, L. Tartara, and V. Degiorgio, "Dispersive wave generation by solitons in microstructured optical fibers,'' Opt. Express 12, 124-135 (2004).

[19] D. V. Skryabin and A. V. Yulin, "Theory of generation of new frequencies by mixing of solitons and dispersive waves in optical fibers,'' Phys. Rev E 72, 016619 (2005)

[20] http://www.leukos-systems.com/spip.php?rubrique23

[21] http://www.nktphotonics.com/

[22] Bach, H. & Neuroth, N. The Properties of Optical Glasses (Springer-Verlag, 1995)

[23] J.S. Sanghera, L. B. Shaw, I.D. Aggarwal, "Chalcogenide glass-fiber-based Mid-IR sources and applications," IEEE Journal of Selected Topics in Quantum Electronics, 15, 114-119 (2009)

[24] G. Qin, X. Yan, C. Kito, M. Liao, C. Chaudhari, T. Suzuki, Y. Ohishi, "Ultrabroadband supercontinuum generation from ultraviolet to 6.28 μm in a fluoride fiber," Appl. Phys. Lett. 95, 161103 (2009)

[25] N. Granzow, S.P. Stark, M.A. Schmidt, A.S. Tverjanovich, L. Wondraczek, P. St. J. Russell, "Supercontinuum generation in chalcogenide-silica step-index fibers," Opt. Express 19, 21003-21010 (2011)

[26] C. Xia, Z. Xu, M.N. Islam, F.L. Terry, M.J. Freeman, A. Zakel, J. Mauricio, "10.5 W time-averaged power mid-IR supercontinuum generation extending beyond 4 μm with direct pulse pattern modulation," IEEE Journal of Selected Topics in Quantum Electronics, 15, 422- 434 (2009)

[27] D. Buccoliero, H. Steffensen, O. Bang, H. Ebendorff-Heidepriem, T. M. Monro, "Thulium pumped high power supercontinuum in lossdetermined optimum lengths of tellurite photonic crystal fiber,"Appl. Phys. Lett. 97, 061106 (2010)

[28] J. Swiderski, M. Michalska, G. Maze, "Mid-IR supercontinuum generation in a ZBLAN fiber pumped by a gain-switched mode-locked Tm-doped fiber laser and amplifier system," Opt. Express 21, 7851-7857 (2013)

[29] O.P. Kulkarni, V.V. Alexander, M. Kumar, M. J. Freeman, M.N. Islam, F.L. Terry, Jr., M. Neelakandan, A. Chan, "Supercontinuum generation from ~1.9 to 4.5μm in ZBLAN fiber with high average power generation beyond 3.8 μm using a thulium-doped fiber amplifier," J. Opt. Soc. Am. B 28, 2486-2498 (2011)

[30] Christian Rosenberg Petersen, Uffe Møller,Irnis Kubat, Binbin Zhou, Sune Dupont, Jacob Ramsay, Trevor Benson, Slawomir Sujecki, Nabil Abdel-Moneim, Zhuoqi Tang, David Furniss, Angela Seddon and Ole Bang,“ Mid-infrared supercontinuum covering the 1.4–13.3μm molecular fingerprint region using ultra-high NA chalcogenide step-index fibre. Nature Photon. 8, 830–834 (2014).

[31] Xin Jiang, Nicolas Y. Joly, Martin A. Finger, Fehim Babic, Gordon K. L. Wong , John C. Traver and Philip St. J. Russell, , “Deep-ultraviolet to mid-infrared supercontinuum generated in solid-core ZBLAN photonic crystal fibre,” Nature Photonics 9, 133 - 139 (2015)

[32] R. DeSalvo, H. Vanherzeele, D. J. Hagan, M. Sheik-Bahae, G. Stegeman,and E. W. V. Stryland, “Self-focusing and self-defocusing by cascaded second-order effects in KTP,” Opt. Lett. 17, 28–30 (1992).

[33] M. L. Sundheimer, J. D. Bierlein, C. Bosshard, E. W. V. Stryland,and G. I. Stegeman, “Large nonlinear phase modulation in quasi-phasematched KTP waveguides as a result of cascaded second-order processes,”Opt. Lett. 18, 1397–1399 (1993).

[34] G. I. Stegeman, M. Sheik-Bahae, E. V. Stryland, and G. Assanto, “Large nonlinear phase shifts in second-order nonlinear-optical processes,” Opt.Lett. 18, 13–15 (1993).

[35] S. Ashihara, J. Nishina, T. Shimura, and K. Kuroda, “Soliton compression of femtosecond pulses in quadratic media,” J. Opt. Soc. Am. B 19, 2505–2510 (2002).

[36] J. Moses and F. W. Wise, “Soliton compression in quadratic media: high energy few-cycle pulses with a frequency-doubling crystal,” Opt. Lett. 31, 1881–1883 (2006).

[37] B. B. Zhou, A. Chong, F. W. Wise, and M. Bache, “Ultrafast and octave-spanning optical nonlinearities from strongly phase-mismatched quadratic interactions,” Phys. Rev. Lett. 109, 043902 (2012).

[38] B. Zhou, H. Guo, X. Liu, and M. Bache, “Octave-spanning mid-IR supercontinuum generation with ultrafast cascaded nonlinearities,” in “CLEO:2014,” (Optical Society of America, 2014), p. JTu4A.24.

[39] M. Bache, H. Guo, and B. Zhou, “Generating mid-IR octave-spanning supercontinua and few-cycle pulses with solitons in phase-mismatched quadratic nonlinear crystals,” Opt. Mater. Express 3, 1647–1657 (2013).

[40] B Zhou, H Guo, M Bache, “Energetic mid-IR femtosecond pulse generation by self-defocusing soliton-induced dispersive waves in a bulk quadratic nonlinear crystal,” Optics express 23 (5), 6924-6936 (2015)

[41] B Zhou, M Bache, “Dispersive waves induced by self-defocusing temporal solitons in a beta-barium-borate crystal,” Optics letters 40 (18), 4257-4260 (2015)

[42] C. R. Phillips, C. Langrock, J. S. Pelc, M. M. Fejer, I. Hartl, and M. E.Fermann, “Supercontinuum generation in quasi-phasematched waveguides,” Opt. Express 19, 18754–18773 (2011).

[43] . M. Chavez Boggio, D. Bodenmüller, T. Fremberg, R. Haynes, M. M. Roth, R. Eisermann, M. Lisker, L. Zimmermann, and M. Böhm, "Dispersion engineered silicon nitride waveguides by geometrical and refractive-index optimization," J. Opt. Soc. Am. B 31, 2846-2857 (2014) C. J.

[44] Clemens J. Krückel, Víctor Torres-Company, Peter A. Andrekson, Daryl T. Spencer, Jared F. Bauters, Martijn J. R. Heck, and John E. Bowers, "Continuous wave-pumped wavelength conversion in low-loss silicon nitride waveguides," Opt. Lett. 40, 875-878 (2015)

[45] D. J. Moss, R. Morandotti, A. L. Gaeta, and M. Lipson, “New CMOS-compatible platforms based on silicon nitride and Hydex for nonlinear optics,” Nature Phot. 7(8), 597–607 (2013).

[46] K. Luke et al., “Overcoming Si_3N_4 film stress limitations for high quality factor ring resonators,” Opt. Express 21, 22829-22833 (2013).

Chapter 2

Numerical Models for Pulse Propagation in Nonlinear Media

2.1 Introduction

In this chapter we will derive the numerical models describing the propagation of ultrashort laser pulses. We will refer to three main models: nonlinear wave equations in frequency domain (NWEF), nonlinear envelope equation (NEE) and coupled wave equations (CWEs) for field propagation.

2.2 Maxwell equations

Starting from Maxwell equations in a nonmagnetic dielectric medium [1]:

$$\nabla \times \mathrm{E} + \frac{\partial \mathrm{B}}{\partial \mathrm{t}} = 0$$

$$\nabla \times \mathrm{H} + \frac{\partial \mathbf{D}}{\partial \mathrm{t}} = \mathrm{J}$$

$$\nabla \cdot \mathrm{B} = 0$$

$$\nabla \cdot \mathrm{J} = \rho \tag{2.1}$$

where **D** is the displacement filed, J the total current density and H is the magnetizing field at the positions and time (x, y, z, t). For the electric displacement field we have the relation

$$\mathbf{D} = \varepsilon_0 \mathrm{E} + \mathbf{P} \tag{2.2}$$

where ε_0 is the vacuum permittivity **P** is the polarization density .

It is useful to write this decomposition in the frequency domain. With the Fourier transform $\hat{\mathrm{F}}(\omega) = \int_{-\infty}^{\infty} \mathrm{F}(\mathrm{t}) \mathrm{e}^{-\mathrm{i}\omega \mathrm{t}} \mathrm{dt}$, the nonlinear polarization in frequency domain is:

$$\hat{\mathrm{P}}(\mathrm{z}, \omega) = \varepsilon_0 \chi^{(1)}(\omega) \hat{\mathrm{E}}(\mathrm{z}, \omega) + \hat{\mathrm{P}}_{\mathrm{NL}}(\mathrm{z}, \omega) \tag{2.3}$$

where $\chi^{(1)}(\omega)$ is the linear electric susceptibility. The electric displacement is rewritten as:

$$\hat{\mathrm{D}} = \varepsilon_0 \mathrm{n}^2(\omega) \hat{\mathrm{E}} + \hat{\mathrm{P}}_{\mathrm{NL}} \tag{2.4}$$

where $\mathrm{n}(\omega) = (1 + \chi^{(1)}(\omega))^{1/2}$ is the frequency-dependent refractive index of the medium.

Applying the operator $\nabla \times \left(\nabla \times \hat{\mathrm{E}}\right) = \nabla\left(\nabla \cdot \hat{\mathrm{E}}\right) - \nabla^2 \hat{\mathrm{E}}$ to Eq. (2.1) and combining its temporal Fourier counterpart with Eq. (2.2) and Eq. (2.4), we can obtain:

$$\nabla^2 \hat{\mathrm{E}} + \mathrm{k}^2(\omega) \hat{\mathrm{E}} = -\mu_0 \omega^2 \hat{\mathrm{P}}_{\mathrm{NL}} \tag{2.5}$$

where $k(\omega) = \omega n(\omega)/c$ is the wave-vector at the frequency ω.

In the time domain:

$$\nabla^2 E - \frac{1}{c^2}\frac{\partial^2 E}{\partial t^2} = \mu_0 \frac{\partial^2 P}{\partial t^2} \tag{2.6}$$

2.3 Nonlinear wave equations in frequency domain (NWEFs)

Let us consider the quadratic and cubic polarization when the ultrashort pulse propagation in the nonlinear medium. The second nonlinear polarization occur only in a non-centrosymmetric crystal can arise from a $\chi^{(2)}$ nonlinearity [2]. The component of second nonlinear polarization depends quadratically on the electric field of an incident light:

$$\widehat{P}_i^{(2)}(\omega) = \varepsilon_0 \sum_{m,n}\left(\hat{\chi}^{(2)}_{j;m,n} F[E_m E_n]\right) \tag{2.7}$$

where i,m,n =o or e, $\hat{\chi}^{(2)}_{j;m,n}$ is the effective second-order nonlinear susceptibility.

The third-order nonlinear polarization can be written as:

$$\widehat{P}_i^{(3)}(\omega) = \varepsilon_0 \sum_{a_1,a_2,a_3}\left(\hat{\chi}^{(3)}_{j;a_1,a_2,a_3}[1-f_R]F\left[E_{a_1}E_{a_2}E_{a_3}\right] + f_R F\left[E_{a_1}E_{a_2}E_{a_3}\right]\right) \tag{2-8}$$

where $\hat{\chi}^{(3)}_{j;a_1,a_2,a_3}$ is the effective third-order nonlinear susceptibility, f_R indicates the relative fraction of the material Raman effects. Thus, the Eq. (2-5) can be expanded to two equations corresponding to the ordinary and extraordinary waves in frequency domain with the slowly varying spectral amplitude approximation (SVSAA) [4]:

$$\frac{\partial \tilde{E}_o}{\partial z} + ik_o(\omega) = -i\frac{\omega^2}{2k_o(\omega)c^2}\left\{\sum_{\alpha_1,\alpha_2}(\hat{\chi}^{(2)}_{o:\alpha_1\alpha_2} F\left[E_{\alpha_1}E_{\alpha_2,}\right] + \sum_{o:\alpha_1\alpha_2\alpha_3}(\hat{\chi}^{(3)}_{o:\alpha_1\alpha_2\alpha_3}(1-f_R)F\left[E_{\alpha_1}E_{\alpha_2,}E_{\alpha_3,}\right] + f_R \cdot F[F^{-1}\left[\bar{h}_R(\omega)F\left[E_{\alpha_1}E_{\alpha_2,}\right]\right]\tilde{E}_{\alpha_3,}])\right\} \tag{2-9}$$

$$\frac{\partial \tilde{E}_e}{\partial z} + ik_e(\omega) = -i\frac{\omega^2}{2k_e(\omega)c^2}\left\{\sum_{\alpha_1,\alpha_2}(\hat{\chi}^{(2)}_{e:\alpha_1\alpha_2} F\left[E_{\alpha_1}E_{\alpha_2,}\right] + \sum_{e:\alpha_1\alpha_2\alpha_3}(\hat{\chi}^{(3)}_{e:\alpha_1\alpha_2\alpha_3}(1-f_R)F\left[E_{\alpha_1}E_{\alpha_2,}E_{\alpha_3,}\right] + f_R \cdot F[F^{-1}\left[\bar{h}_R(\omega)F\left[E_{\alpha_1}E_{\alpha_2,}\right]\right]\tilde{E}_{\alpha_3,}])\right\} \tag{2-10}$$

where $\bar{h}_R(\omega)$ is the Raman response function in the frequency domain, the NWEF [5] provides a power tool for modelling the ultrashort pulse propagation in the nonlinear medium , automatically

including all types of nonlinear interactions and the anisotropy of the nonlinearities.

2.4 The analytic Signal

We consider now real electric field E(z,t) the nonlinear polarization $P_{NL}(z,t)$ propagating in the nonlinear medium:

$$E(z,t) = \left[A(z,t)e^{-i\beta_0 z + i\omega_0 t} + c.c\right]/2, \tag{2-11}$$

$$P_{NL}(z,t) = \left[A_P(z,t)e^{-i\beta_0 z + i\omega_0 t} + c.c\right]/2, \tag{2-12}$$

where z is the propagation direction, t is the time variable and ω_0 is a reference frequency. The Fourier transform of the analytic signal which is a complex function is denoted by:

$$E_\omega = \frac{1}{2\pi}\int_{-\infty}^{+\infty} E(z,t)\exp(-i\omega t)dt, \tag{2-13}$$

$$P_{NL,\omega} = \frac{1}{2\pi}\int_{-\infty}^{+\infty} P_{NL}(z,t)\exp(-i\omega t)dt \tag{2-14}$$

The analytic signal can also be defined alternatively by using the Hilbert transform:

$$\varepsilon(z,t) = E(z,t) + i\varkappa[E(z,t)] \tag{2-15}$$

where the Hilbert transform of the electric field is $\varkappa[E(z,t)] = \frac{1}{\pi}\mathbb{P}\int_{-\infty}^{+\infty} dt'\, E(z,t')/(t-t')$, the symbol $\mathbb{P}\int_{-\infty}^{+\infty}$ indicates that the integral must be taken in the sense of the Cauchy principal value.

Due to the electric field E(z, t) is real, its Fourier transform has Hermitian symmetry, since only the positive (or negative) frequency part of the spectrum carries information. With these definitions, the Fourier transform of the analytic signal: $E_\omega = [\mathcal{E}_\omega + (\mathcal{E}_{-\omega})^*]/2$.The analytic signal satisfies the following requirements:

$$\mathcal{E}_{\omega>0} = 2E_\omega,$$

$$\mathcal{E}_{\omega=0} = 0,$$

$$\mathcal{E}_{\omega<0} = 0. \tag{2-16}$$

Finically, we can define the complex electric field envelope as:

$$A(z,t) = \mathcal{E}(z,t)e^{-i\beta_0 z + i\omega_0 t} \tag{2-17}$$

2.5 Nonlinear Analytical Envelope Equation (NAEE)

The unidirectional pulse propagation equation (UPPE) can be derive from Maxwell's equations with the SVSAA, which only accounts for the forward propagating part of the electric field but uses the full oscillating electric field:

$$\mathrm{i}\frac{\partial \mathrm{E}_\omega}{\partial \mathrm{z}} + \mathrm{k}(\omega)\mathrm{E}_\omega + \frac{\omega}{2\mathrm{cn}(\omega)}\mathrm{P}_{\mathrm{NL},\omega} = 0 \tag{2-18}$$

where $\mathrm{k}(\omega)$ the full propagation is constant of the medium, c is the speed of light in vacuum, $\mathrm{n}(\omega)$ is the linear refractive index.

We now introduce the complex envelopes A and their Fourier transforms,

$$\mathrm{E}_\omega(\mathrm{z}, \omega - \omega_0) = \left[\mathrm{A}(\mathrm{z},\mathrm{t})\mathrm{e}^{-\mathrm{ik}_0\mathrm{z}} + \mathrm{c.c}\right]/2, \tag{2-19}$$

$$\mathrm{P}_{\mathrm{NL},\omega}(\mathrm{z}, \omega - \omega_0) = \left[\mathrm{A}_\mathrm{P}(\mathrm{z},\mathrm{t})\mathrm{e}^{-\mathrm{ik}_0\mathrm{z}} + \mathrm{c.c}\right]/2, \tag{2-20}$$

Substituting envelopes (2-19), (2-20) into equations (2-18), we can obtain the nonlinear analytical envelope equation (NEE) by using co-moving frame:

$$\frac{\partial \mathrm{A}(\mathrm{z},\tau)}{\partial \xi} + \mathrm{DA}(\mathrm{z},\tau) = -\mathrm{i}\frac{\omega_0}{2\mathrm{c}\varepsilon_0\mathrm{n}(\omega_0)}\left(1 - \frac{\mathrm{i}}{\omega_0}\frac{\partial}{\partial \tau}\right)\mathrm{A}_\mathrm{P}\,(\mathrm{z},\tau) \tag{2-21}$$

where dispersion operator is $\mathrm{D} = \sum_{\mathrm{m}=2}^{\infty}\frac{1}{\mathrm{m!}}\frac{\mathrm{d}^\mathrm{m}\beta(\omega_0)}{\mathrm{d}\omega^\mathrm{m}}\left(-\mathrm{i}\frac{\partial^\mathrm{m}}{\partial \tau^\mathrm{m}}\right)$, $\mathrm{k}_1(\omega_0)$ is reference group velocity at ω_0.The co-moving frame is $\xi = \mathrm{z}, \tau = \mathrm{t} - \mathrm{k}_1(\omega_0)\mathrm{z}$.

In order to obtain the NEE for the analytic signal, we defined the analytic signal of the electric field which only the positive frequency part of the field [6]:

$$\mathcal{E}(\mathrm{z},\mathrm{t}) = \frac{1}{\pi}\int_0^{+\infty}\mathrm{E}(\mathrm{z},\mathrm{t})\exp(-\mathrm{i}\omega\mathrm{t})\mathrm{dt} \tag{2-22}$$

With the above definitions, we now consider an instantaneous second-order $\chi^{(2)}$ nonlinearity and $\chi^{(3)}$ nonlinearity, the nonlinear polarization can be written as:

$$\mathrm{P}_{\mathrm{NL},\omega} = \mathrm{P}_{\mathrm{NL},\omega}^{(2)} + \mathrm{P}_{\mathrm{NL},\omega}^{(3)} \tag{2-23}$$

and in time domain they are given by:

$$\mathrm{P}_{\mathrm{NL}}^{(2)}(\mathrm{z},\mathrm{t}) = \int_{-\infty}^{+\infty}\mathrm{dt}_1\int_{-\infty}^{+\infty}\chi^{(2)}(\mathrm{t},\mathrm{t}_1,\mathrm{t}_2)\mathrm{E}(\mathrm{t}_1)\mathrm{E}(\mathrm{t}_2)\mathrm{dt}_2 \tag{2-24}$$

$$\mathrm{P}_{\mathrm{NL}}^{(3)}(\mathrm{z},\mathrm{t}) = \int_{-\infty}^{+\infty}\mathrm{dt}_1\int_{-\infty}^{+\infty}\mathrm{dt}_2\int_{-\infty}^{+\infty}\chi^{(3)}(\mathrm{t},\mathrm{t}_1,\mathrm{t}_2,\mathrm{t}_3)\mathrm{E}(\mathrm{t}_1)\mathrm{E}(\mathrm{t}_2)\mathrm{E}(\mathrm{t}_3)\mathrm{dt}_3 \tag{2-25}$$

We consider an instantaneous$\chi^{(2)}(t,t_1,t_2)=\chi^{(2)}\delta(t-t_1)\delta(t_1-t_2)$ nonlinearity, so that nonlinear polarization $P_{NL}^{(2)}(z,t)=\chi^{(2)}E(z,t)^2$.

For the cubic case, the standard Born-Oppenheimer approximation implies that for optical fields one can write:

$$P_{NL}^{(3)}(z,t)=\chi_{el}^{(3)}E^3(z,t)+E(t)\int_{-\infty}^{+\infty}ds\chi_R^{(3)}(t-s)E^2(s) \tag{2-26}$$

which is equivalent to taking $\chi^{(3)}(t,t1,t2,t3)=\chi_{el}^{(3)}\delta(t-t_1)\delta(t_1-t_2)\delta(t_2-t_3)+\delta(t-t_1)\chi_R^{(3)}(t-s)\delta(t_2-t_3)$.To be simple, we ignored the Raman nonlinearity.

In frequency domain only have the Kerr nonlinearity this can be written as,

$$P_{NL}^{(3)}(\omega)=\chi_{el}^{(3)}\mathcal{F}[E^3(z,t)]=\chi_{el}^{(3)}\mathcal{F}[E^3(z,t)] \tag{2-27}$$

The total nonlinear polarization is：

$$P_{NL}(z,t)=\chi^2[E(z,t)^2]+\chi_{el}^{(3)}[E(z,t)^3]=\frac{\chi^2}{4}\left[A^2e^{2i\beta_0z-2i\omega_0t}+A^{*2}e^{-2i\beta_0z+2i\omega_0t}+2AA^*\right]+$$

$$\frac{\chi_{el}^{(3)}}{8}\left[A^3e^{3i\beta_0z-3i\omega_0t}+A^{*3}e^{-3i\beta_0z+3i\omega_0t}+3|A|^2Ae^{i\beta_0z-i\omega_0t}+\right.$$

$$\left.3|A|^2A^*e^{-i\beta_0z+i\omega_0t}\right] \tag{2-28}$$

The nonlinear polarization envelope can write:

$$A_P(z,t)=\tilde{\mathcal{P}}\left(P_{NL}(z,t)\right)e^{-i\beta_0z+i\omega_0t}$$

$$=\frac{\chi^2}{2}\left[A^2e^{i\beta_0z-i\omega_0t}+2AA^*e^{-i\beta_0z+i\omega_0t}\right]_+ +\frac{3\chi^3}{4}\left[|A|^2A+|A|^2A^*e^{-2i\beta_0z+2i\omega_0t}+\frac{1}{3}A^3e^{2i\beta_0z-2i\omega_0t}\right]_+ \tag{2-29}$$

where $\tilde{\mathcal{P}}\left(P_{NL}(z,t)\right)$ is the analytic signal for the nonlinear polarization, the '+' subscript indicates that only the positive frequencies must be accounted for. By using operated in the time domain by the Hilbert transform, the A^{*2} and A^{*3} term are no longer present.

We can write Eq. (2-21) for the analytic signal envelope A, which only positive frequencies,

$$i\,\partial_\xi A + \widehat{D}(i\,\partial_\tau)A = -\frac{\chi^2}{2} i \frac{\omega_0}{2c\varepsilon_0 n(\omega_0)} \left[A^2 e^{i\beta_0 z - i\omega_0 t} + 2AA^* e^{-i\beta_0 z + i\omega_0 t}\right]_+ - i \frac{\omega_0}{2c\varepsilon_0 n(\omega_0)} \frac{3\chi_{el}^{(3)}}{4} \left[|A|^2 A + |A|^2 A^* e^{-2i\beta_0 z + 2i\omega_0 t} + \frac{1}{3} A^3 e^{2i\beta_0 z - 2i\omega_0 t}\right]_+ \quad (2\text{-}30)$$

This nonlinear envelope equation (2-30) provides a powerful means of describing light pulse propagation in nonlinear media. The right first term in the first square brackets is responsible for second harmonic generation (SHG) which only positive frequencies. But the second term AA^* so called three wave mixing (TWM) like term has both the positive and negative frequencies usually in cubic media. This term acts as the TWM process. In the second square brackets, the first $|A|^2A$ is typical self-phase modulation term. The interaction between positive and negative frequencies $|A|^2A^*$ term was proved to explain the formation of the negative-frequency resonant radiation emitted by optical solitons by Matteo Conforti [8]. The $\frac{1}{3}A^3$ term is responsible for third harmonic generation (THG).

2.6 Couple Analytic Wave Equations (CAWEs)

NAEE can correctly describe the nonlinear interaction between the positive and the negative frequency parts of the spectrum of optical pulses. However, in the quadratic nonlinear medium the AA^* called TWM like term brings more physical, such as SHG, SFG, DFG etc. Such an interaction is able to generate phase-matched TWM radiation that would not exist in any model based on the conventional envelope equation. For one NAEE is not able to distinguish the detailed physical processes.

Thus, in this section work we introduce the CWEs defined complex envelope that is able to capture the rich interaction between positive and negative frequency components in quadratic nonlinear medium during the propagation of an ultrashort pulse. In order to investigate these TWM process, here we ignore all of the 3-order nonlinearity, such as Kerr and Raman nonlinearity.

Now, we expand the electric field into waves propagating at the fundamental (FF) and second harmonic (SH) frequencies which we assume the FF and SH spectra do not overlap. For the noncritical SHG process, the FW and SH have the same polarization direction.

The FW can be written as:

$$E_1(z,t) = \left[A_1(z,t)e^{-ik(\omega_1)z+i\omega_1 t} + c.c\right]/2, \tag{2-31}$$

and then the SH is:

$$E_2(z,t) = \left[A_2(z,t)e^{-ik(\omega_2)z+i\omega_2 t} + c.c\right]/2, \tag{2-32}$$

where $\omega_2 = 2\omega_1$, c.c. represents the complex conjugate term since the electric field is real-valued. The quadratic nonlinear polarization is：

$$\begin{aligned} P_{NL}(z,t) &= \chi^2[E_1(z,t) + E_2(z,t)]^2 \\ &= \frac{\chi^2}{4}[2A_1^*A_2e^{-i[k(\omega_2)-k(\omega_1)]z+i\omega_1 t} + 2A_2^*A_1e^{-i[k(\omega_1)-k(\omega_2)]z-i\omega_1 t} + \cdots \\ &+ A_1A_1^* + A_1A_1e^{-i2k(\omega_1)z+i\omega_2 t} + A_1^*A_1^*e^{i2k(\omega_1)z-i\omega_2 t} + A_2A_2^*] \end{aligned} \tag{2-32}$$

The nonlinear polarization envelope for the FW is:

$$\begin{aligned} A_{P,1}(z,t) &= \tilde{\mathcal{P}}\left(P_{NL,1}(z,t)\right)e^{ik(\omega_1)z-i\omega_1 t} \\ &= \frac{\chi^2}{4}\left[4A_1^*A_2e^{-i\Delta kz} + A_1A_1^*e^{i\beta_1(\omega_1)z-i\omega_1 t}\right]_+ \end{aligned} \tag{2-33}$$

The nonlinear polarization envelope for the SH is

$$\begin{aligned} A_{P,2}(z,t) &= \tilde{\mathcal{P}}\left(P_{NL,1}(z,t)\right)e^{i\beta_1 z-i\omega_1 t} \\ &= \frac{\chi^2}{4}\left[4A_1A_1e^{i\Delta kz} + A_2A_2^*\, e^{i\beta_2 z-i\omega_2 t}\right]_+ \end{aligned} \tag{2-34}$$

where the phase match between the FW and SH is $\Delta k = k(\omega_2) - 2k(\omega_1)$, $P_{NL,1}(z,t)$ and $P_{NL,2}(z,t)$ respectively represents the nonlinear polarization regarding the FW and the SH. In these expanded equations, terms regarding the FW should has the carrier wave term $e^{i\omega_1 t}$ and the SH has $e^{i\omega_2 t}$.

Substituting envelopes (2-32), (2-33) into Eq. (2-18), the full CWEs regarding the quadratic SHG by the analytic signal are derived, i.e.:

$$\frac{\partial A_1(\xi,\tau)}{\partial \xi} + iD_1A_1(\xi,\tau) = i\frac{\chi^{(2)}\omega}{4cn(\omega_1)}\left(\omega_1 - i\frac{\partial}{\partial\tau}\right)[4A_1^*A_2e^{-i\Delta k\xi} + A_1A_1^*e^{-i\Delta k_{pg}\xi - i\omega_1\tau} \quad (2\text{-}35)$$

$$\frac{\partial A_2(\xi,\tau)}{\partial z} + (-d_{12}\frac{\partial}{\partial\tau} + iD_2)A_2(\xi,\tau) = -i\frac{\chi^{(2)}\omega}{4cn(\omega_2)}(\omega_2 - i\frac{\partial}{\partial\tau})[\,4A_1A_1e^{i\Delta kz} + A_2A_2^*e^{ik(\omega_2)z - i\omega_2\tau}]_+$$

(2-36)

where the group velocity factor $\Delta k_{pg} = k_1(\omega_1)\omega_1 - k(\omega_1)$,the dispersion operators are : $D_{1,2} = \sum_{m=2}^{\infty}\frac{1}{m!}\frac{d^m\beta(\omega_0)}{d\omega^m}(-i\frac{\partial^m}{\partial\tau^m})$, and the group velocity mismatch d_{12} is defined as $d_{12} = k_1(\omega_1) - k_1(\omega_2)$.

2.7 Conclusion

As a conclusion, in this chapter we derived the models for pulse propagations in nonlinear media. NWEFs are derived from the Maxwell equation with the SVSAA which proved the a generalized model for pulse propagations in nonlinear media. By using analytic signal in the optical field, the NAEE is derived which can correctly describe the nonlinear interaction between the positive and the negative frequency parts of the spectrum of optical pulses. To separate the AA^* term, the analytic envelope dynamics of the FW and the SH are both formulated with analytic signal.

Bibliography

[1] Yariv and P. Yeh, Photonics: Optical Electronics in Modern Communications, The Oxford Series in Electrical and Computer Engineering (Oxford University Press, Incorporated, 2007).

[2] R. Boyd, Nonlinear Optics, Nonlinear Optics Series (Elsevier Science, 2008).

[3] G. Agrawal, Nonlinear Fiber Optics, Academic Press (Academic Press, 2013).

[4] M. Kolesik, P. Townsend, and J. Moloney, “Theory and simulation of ultrafast intense pulse

propagation in extended media," IEEE J. Sel. Topics Quantum Electron. 18, 494–506 (2012).

[5] H. Guo, X. Zeng, B. Zhou, and M. Bache, "Nonlinear wave equation in frequency domain: accurate modeling of ultrafast interaction in anisotropic nonlinear media," J. Opt. Soc. Am.B 30, 494-504 (2013).

[6] M. Conforti, F. Baronio, and C. De Angelis, "Nonlinear envelope equation for broadband optical pulses in quadratic media," Phys. Rev. A 81, 053841 (2010).

[7] M. Conforti, F. Baronio, and C. De Angelis, "Modeling of ultrabroadband andsingle-cycle phenomena in anisotropic quadratic crystals," J.Opt.Soc. Am. B 28, 1231–1237 (2011).

[8] M. Conforti, A. Marini, T. X. Tran, D. Faccio, and F. Biancalana, , "Interaction between optical fields and their conjugates in nonlinear media," Opt. Express 21, 31239 (2013)

Chapter 3

Mid-IR femtosecond frequency conversion by soliton-probe collision in phase-mismatched quadratic nonlinear crystals

3.1 Introduction

The optical soliton is remarkably robust as it can both retain its shape despite dispersive or dissipative effects and survive wave collisions. Yet it is quite susceptible to perturbations as it can shed phase-matched resonant radiation to a so-called soliton-induced optical Cherenkov wave (or dispersive wave) when perturbed by higher order dispersion [1]. On the other hand, the soliton can also act as a potential barrier when colliding with a linear (i.e. dispersive) wave, creating the analogy to an optical equivalent of an ”event horizon” [6]. Such a collision can be well understood by generalizing the Cherenkov phase-matching condition – degenerate four wave mixing (FWM) – to non-degenerate FWM where a soliton interacts with two linear dispersive waves [8]. This interaction is mediated by cross-phase modulation (XPM): the collision between the soliton (ω_s) and a linear ”probe” wave (ω_p) can become resonantly phase-matched to a new frequency (the ”resonant” wave ω_r) according to the FWM phase-matching condition. This frequency-converts the probe to the resonant wave, which – when completely depleting the probe – gives rise to the peculiar appearance of the probe reflecting on the soliton: when the probe group velocity is higher than the soliton, the resonant wave group velocity will be lower than the soliton, and therefore travel away from the soliton after formation. This frequency-conversion process therefore in time domain leads to an apparent reflection of the probe on the soliton.

Soliton-probe collisions have been studied in fibers, which have a positive Kerr nonlinearity. However, through cascaded (strongly phase-mismatched) quadratic nonlinear interactions an effective negative Kerr-like nonlinearity may be generated (in bulk this corresponds to a self-defocusing effect) [12]. As a consequence soliton formation requires normal dispersion [13], and Cherenkov phase-matching naturally occurs towards the red side of the soliton spectrum [15]. This allows for efficient near- to mid-IR conversion [16].

In this chapter, we study the collision of near-IR probe waves and self-defocusing solitons to generate long-wavelength resonant waves. The self-defocusing soliton may reflect the probe wave

when the probe XPM term is negative, and this is possible if the sum-frequency generation (SFG) between soliton and probe is detuned sufficiently away from its phase-matching point to induce a negative cascaded XPM term.

3.2 Theoretical background

Let us first stress that the code we use models the o-and e-polarized electrical fields and include all possible $\chi^{(2)}$ and $\chi^{(3)}$ interactions. However, an analytical understanding of the processes behind the interaction is more convenient in the slowly varying envelope approximation. We will now consider the interaction of a strong soliton envelope E_s at the frequency ω_s and a weaker (but not weak) probe envelope Ep at the frequency ω_p. Let us focus on the two equations for the soliton and probe and disregard dispersion for the moment. For the soliton

$$id_z E_{\omega_s} + \frac{\omega_s d_{eff}}{c n_o(\omega_s)}\left[E^*_{\omega_s} E_{2\omega_s} e^{i\Delta k^{SHG}_{\omega_s} z} + E_{\omega_p} E_{\omega_s-\omega_p} e^{-i\Delta k^{DFG}_{\omega_s-\omega_p} z} + E^*_{\omega_p} E_{\omega_s+\omega_p} e^{i\Delta k^{SFG}_{\omega_s+\omega_p} z}\right]$$

$$+\frac{3\omega_s}{8 c n_o(\omega_s)} E_{\omega_s}\left[\chi^{(3)}_{SPM}\left|E_{\omega_s}\right|^2 + 2\chi^{(3)}_{XPM}\left|E_{\omega_p}\right|^2\right] = 0 \qquad (3\text{-}1)$$

where n_o is the o polarized refractive index, modelled by the BBO Sellmeier equations. Here we have only included the type I oo → e SHG, SFG and DFG possibilities, all having the same effective nonlinearity

$$d_{eff}(\theta, \emptyset) = d_{31}\sin\theta - d_{22}\cos\theta \sin 3\emptyset \qquad (3\text{-}2)$$

For the cut we use this is optimized for $\emptyset = -\pi/2$, $d_{22}/d_{31} < 0$, and this implies that $d_{eff} = 0$ for the type II interaction oe → e and the type 0 interaction oo → o. For the cubic terms only included the XPM terms that involve the strong soliton and probe fields, and not the weak e-polarized SHG, SFG and DFG modes. We also note that even if BBO is anisotropic then the XPM term between two o-polarized modes is the same as the SPM term, i.e. $\chi^{(3)}_{SPM} = \chi^{(3)}_{XPM} = c_{11}$. In this identity Miller's scaling is neglected, as it actually is in our code (a single frequency-

independent $\chi_{jk}^{(3)}$ is used for each tensor element). However, for clarity let us keep them separated, as one could imagine cases where the probe is not the same polarization as the soliton. For the probe we equivalently have

$$id_z E_{\omega_p} + \frac{\omega_p d_{eff}}{c n_o(\omega_p)}\left[E^*_{\omega_p} E_{2\omega_p} e^{i\Delta k^{SHG}_{\omega_p} z} + E_{\omega_p} E_{\omega_{s-\omega_p}} e^{-i\Delta k^{DFG}_{\omega_s-\omega_p} z} + E^*_{\omega_p} E_{\omega_{s+\omega_p}} e^{i\Delta k^{SFG}_{\omega_s+\omega_p} z}\right]$$

$$+\frac{3\omega_s}{8 c n_o(\omega_s)} E_{\omega_s}\left[\chi^{(3)}_{SPM}\left|E_{\omega_s}\right|^2 + 2\chi^{(3)}_{XPM}\left|E_{\omega_p}\right|^2\right] = 0 \qquad (3\text{-}3)$$

The phase-mismatch coefficients are:

$$\Delta k^{SHG}_{\omega_j}(\theta) = k_e(2\omega_j, \theta) - 2k_o(2\omega_j)$$

$$\Delta k^{SFG}_{\omega_j}(\theta) = k_e(\omega_s+\omega_p, \theta) - k_o(\omega_s) - k_o(\omega_p)$$

$$\Delta k^{DFG}_{\omega_j}(\theta) = k_o(\omega_s) - k_o(\omega_p) - k_e(\omega_s - \omega_p, \theta) \qquad (3\text{-}4)$$

where $k_e(\omega, \theta) = n_e(\omega, \theta)\omega/c$ and as per usual $n_e(\omega, \theta) = [\cos^2\theta/n_o^2 + \sin^2\theta/n_e^2(\omega)]^{-1/2}$, $n_e(\omega, \theta)$ is the BBO e-polarized refractive index. In what follows we drop the explicit dependence of the $\Delta k'$s and d_{eff} on θ and $\emptyset$.

Let us now write the basic plane-wave equations for the SHG, SFG and DFG e-polarized modes, disregarding irrelevant quadratic contributions (i.e. the ee → e type 0 interaction, which is very weak since it will be heavily phase mismatched and the relevant d_{eff} is not as high as d_{33} in, e.g., $LiNbO_3$), cubic nonlinearities (which we assume to a very good approximation to be irrelevant for the harmonics, as the phase mismatch is larger and thus their intensities too low) and chromatic dispersion (we are only interested in the nonlinear terms at the moment).

$$id_z E_{2\omega_j} + \frac{2\omega_j d_{eff}}{c n_e(\omega_j, \theta)} \frac{1}{2} E^2_{\omega_j} e^{-i\Delta k^{SHG}_{\omega_j} z} = 0 \qquad (3\text{-}5)$$

$$id_z E_{\omega_s-\omega_p} + \frac{(\omega_s-\omega_p) d_{eff}}{c n_e(\omega_s-\omega_p, \theta)} E_s E^*_{\omega_p} e^{i\Delta k^{DFG}_{\omega_s-\omega_p} z} = 0 \qquad (3\text{-}6)$$

$$id_z E_{\omega_s+\omega_p} + \frac{(\omega_s+\omega_p) d_{eff}}{c n_e(\omega_s+\omega_p, \theta)} E_s E_p e^{-i\Delta k^{SFG}_{\omega_s+\omega_p} z} = 0 \qquad (3\text{-}7)$$

With the usual cascading ansatz $\Delta kL \geq 2\pi$ we can find the harmonic fields in the cascading limit.

$$E_{2\omega_j} = -\frac{2\omega_j d_{eff}}{cn_e(\omega_j,\theta)\Delta k_{\omega_j}^{SHG}} E_{\omega_j}^2 e^{-i\Delta k_{\omega_j}^{SHG} z} \tag{3-8}$$

$$E_{\omega_s-\omega_p} = \frac{(\omega_s-\omega_p)d_{eff}}{cn_e(\omega_s-\omega_p,\theta)\Delta k_{\omega_s-\omega_p}^{DFG}} E_s E_{\omega_p}^* e^{i\Delta k_{\omega_s-\omega_p}^{DFG} z} \tag{3-9}$$

$$id_z E_{\omega_s+\omega_p} = \frac{(\omega_s+\omega_p)d_{eff}}{cn_e(\omega_s+\omega_p,\theta)\Delta k_{\omega_s+\omega_p}^{SFG}} E_s E_p e^{-i\Delta k_{\omega_s+\omega_p}^{SFG} z} \tag{3-10}$$

When plugging these into Eqs. (3-1)-(3-3) we get

$$id_z E_{\omega_s} + \frac{3\omega_s}{8cn_o(\omega_s)} E_{\omega_s}\left[\chi_{eff,SPM}^{(3)}(\omega_s)\left|E_{\omega_s}\right|^2 + 2\chi_{eff,XPM}^{(3)}\left|E_{\omega_p}\right|^2\right] = 0 \tag{3-12}$$

$$id_z E_{\omega_p} + \frac{3\omega_p}{8cn_o(\omega_p)} E_{\omega_p}\left[\chi_{eff,SPM}^{(3)}(\omega_p)\left|E_{\omega_p}\right|^2 + 2\chi_{eff,XPM}^{(3)}\left|E_{\omega_s}\right|^2\right] = 0 \tag{3-13}$$

$$\chi_{eff,SPM}^{(3)}(\omega_j) = \chi_{SPM}^{(3)} + \chi_{cas}^{(3),SHG}(\omega_j) \tag{3-14}$$

$$\chi_{eff,XPM}^{(3)} = \chi_{XPM}^{(3)} + \chi_{cas}^{(3),SFG}(\omega_s+\omega_p) + \chi_{cas}^{(3),DFG}(\omega_s-\omega_p) \tag{3-15}$$

$$\chi_{cas}^{(2),SHG}(\omega_j) = -\frac{8\omega_j d_{eff}^2}{3cn_e(2\omega_j,\theta)\Delta k_{\omega_j}^{SHG}} \tag{3-16}$$

$$\chi_{cas}^{(2),SFG}(\omega_s+\omega_p) = -\frac{4(\omega_s+\omega_p)d_{eff}^2}{3cn_e((\omega_s+\omega_p)\theta)\Delta k_{\omega_s+\omega_p}^{SFG}} \tag{3-17}$$

$$\chi_{cas}^{(2),DFG}(\omega_s-\omega_p) = -\frac{4(\omega_s-\omega_p)d_{eff}^2}{3cn_e(\omega_s-\omega_p,\ \theta)\Delta k_{\omega_s-\omega_p}^{DFG}} \tag{3-18}$$

In the field normalized to the intensity case we have $A_{\omega_j} = E_{\omega_j}\sqrt{2/\varepsilon_0 cn_o(\omega_j)}$, $j = s, p$ and

$$id_z A_{\omega_s} + \frac{\omega_s}{c} A_{\omega_s}\left[n_{2,eff}^{SPM}(\omega_s)\left|A_{\omega_s}\right|^2 + 2n_{2,eff}^{XPM}\left|A_{\omega_p}\right|^2\right] = 0 \tag{3-19}$$

$$id_z A_{\omega_p} + \frac{\omega_p}{c} A_{\omega_p}\left[n_{2,eff}^{SPM}(\omega_p)\left|E_{\omega_p}\right|^2 + 2n_{2,eff}^{XPM}\left|A_{\omega_s}\right|^2\right] = 0 \tag{3-20}$$

where $n_{2,eff}^{SPM}(\omega_j) = n_{2,Kerr}^{SPM}(\omega_j) + n_{2,cas}^{SHG}(\omega_j)$ (3-21)

$$n_{2,eff}^{SPM} = n_{2,Kerr}^{XPM} + n_{2,cas}^{SFG}(\omega_s+\omega_p) + n_{2,cas}^{DFG}(\omega_s-\omega_p) \tag{3-22}$$

$$n_{2,Kerr}^{SPM}(\omega_j) = \frac{3\chi_{SPM}^{(3)}}{4\varepsilon_0 cn_o(\omega_j)} \tag{3-23}$$

$$n_{2,Kerr}^{XPM}(\omega_j) = \frac{3\chi_{XPM}^{(3)}}{4\varepsilon_0 cn_o(\omega_s)n_o(\omega_p)} \tag{3-24}$$

while the cascading contributions are

$$n_{cas}^{(2),SHG}(\omega_j) = -\frac{2\omega_j d_{eff}^2}{\varepsilon_0 c^2 n_o^2(\omega_j) n_e(2\omega_j)\Delta k_{\omega_j}^{SHG}} \tag{3-25}$$

$$n_{cas}^{(2),SFG}(\omega_s + \omega_p) = -\frac{(\omega_s+\omega_p) d_{eff}^2}{\varepsilon_0 c^2 n_o(\omega_s) n_o(\omega_p) n_e(\omega_s+\omega_p,\theta)\Delta k_{\omega_s+\omega_p}^{SFG}} \tag{3-26}$$

$$n_{cas}^{(2),DFG}(\omega_s - \omega_p) = -\frac{(\omega_s-\omega_p) d_{eff}^2}{\varepsilon_0 c^2 n_o(\omega_s) n_o(\omega_p) n_e(\omega_s-\omega_p,\theta)\Delta k_{\omega_s-\omega_p}^{DFG}} \tag{3-27}$$

A requirement for the soliton to ”reflect” the probe is that the potential imposed by the soliton on the probe is scattering, i.e. a barrier. As the probe is launched in the anomalous dispersion regime, a scattering potential requires that the XPM effective nonlinear index of the probe ($n_{2,Kerr}^{XPM}$) is negative, i.e. self-defocusing. As we showed above this has three contributions:

$$n_{2,eff}^{XPM} = n_{2,Kerr}^{XPM} + n_{cas}^{(2),SFG}(\omega_s + \omega_p) + n_{cas}^{(2),DFG}(\omega_s - \omega_p) \tag{3-28}$$

viz. the material Kerr XPM as well as cascaded SFG and DFG between the soliton and probe.

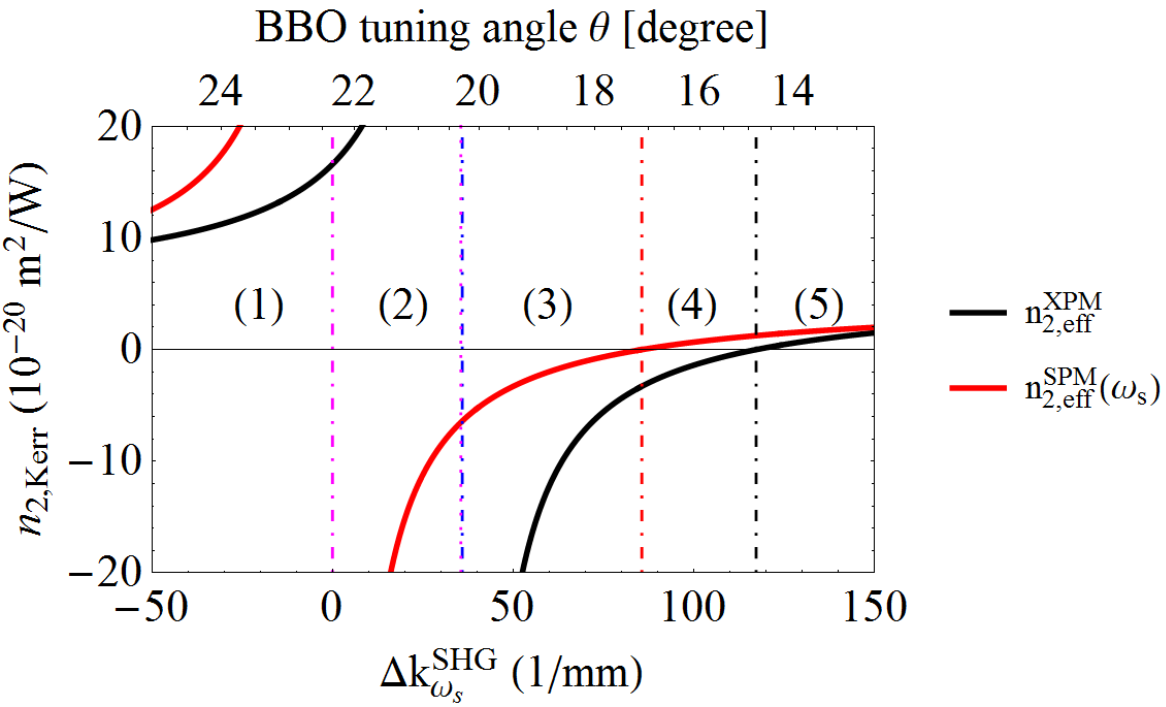

Fig.3-1. The induced cascaded nonlinear refractive indices vs. the SHG phase-mismatch parameter (controlled by the crystal angle θ),calculated for $\lambda_s = 1.1$ μm and $\lambda_p = 1.65$ μm. The domains are divided as follows: (1+4+5) Effective self-focusing SPM regimes ($n_{2,eff}^{SPM}(\omega_s) > 0$), so solitons cannot be excited; (2+3) Effective self-defocusing SPM regimes ($n_{2,eff}^{XPM}(\omega_s) < 0$), i.e. soliton regimes; (1+2+5) positive XPM regimes ($n_{2,eff}^{XPM}(\omega_s) > 0$); (3+4) negative XPM regimes ($n_{2,eff}^{SPM}(\omega_s) < 0$); (1+2) resonant nonlocal cascaded SHG regimes; (3+4+5) non-resonant nonlocal cascaded SHG regimes.

In Fig. 3-1 we show how the crystal tuning angle θ controls the regimes; the self-defocusing soliton can only be excited in regimes (2+3). In turn the effective XPM term is only negative in regimes (3+4); at the boundary to regime (2) it becomes phase matched, and thus in (1+2) it is positive. Coincidentally the boundary between regimes (2) and (3) also marks the transition where the cascaded SHG becomes non-resonant, which it is in regime (3+4+5). In the non-resonant regime the cascading is ultrabroadband and induces minimal self-steepening on the soliton. Thus, for the wavelengths and tuning angles considered here, $n_{cas}^{(2),DFG}(\omega_s - \omega_p)$ is negligible due to a large phase mismatch. Therefore the XPM scattering potential sign and magnitude is by and large a competition between the material Kerr XPM effect and the cascaded SFG effect.

3.3 The general FWM phase-matching condition

The general FWM phase-matching condition is

$$k_{lin}(\omega_r) = k_{sol}(\omega_r) + J[k_{lin}(\omega_r) - k_{sol}(\omega_p)] \tag{3-29}$$

where $k_{lin}(\omega)$ describes the dispersion relation of the linear wave (in bulk media simply determined, e.g., by the Sellmeier equation). $k_{sol}(\omega_r) = k_{lin}(\omega_s) + (\omega - \omega_s)/v_g + q_{sol}$ is the soliton dispersion relation; its non-dispersive nature is reflected in the fact it is simply a wave packet with a constant group velocity v_g. Its accumulated nonlinear phase q_{sol} will cancel out for the J = +1 case that we will focus on here. The parameter J switches between the degenerate case (J = 0, Cherenkov radiation and the non-degenerate case (J = ±1, where the presence of the probe at frequency ω_p invokes the FWM resonant phase-matching condition). In a BBO quadratic nonlinear crystal (β-barium borate, BaB_2O_4) the resonant waves are phase-matched in the mid-IR beyond $\lambda = 2.0$ μm, as seen from the dispersion relations in Fig. 3-2 for the main case considered here, namely a 1.65 μm probe colliding with a 1.1 μm soliton.

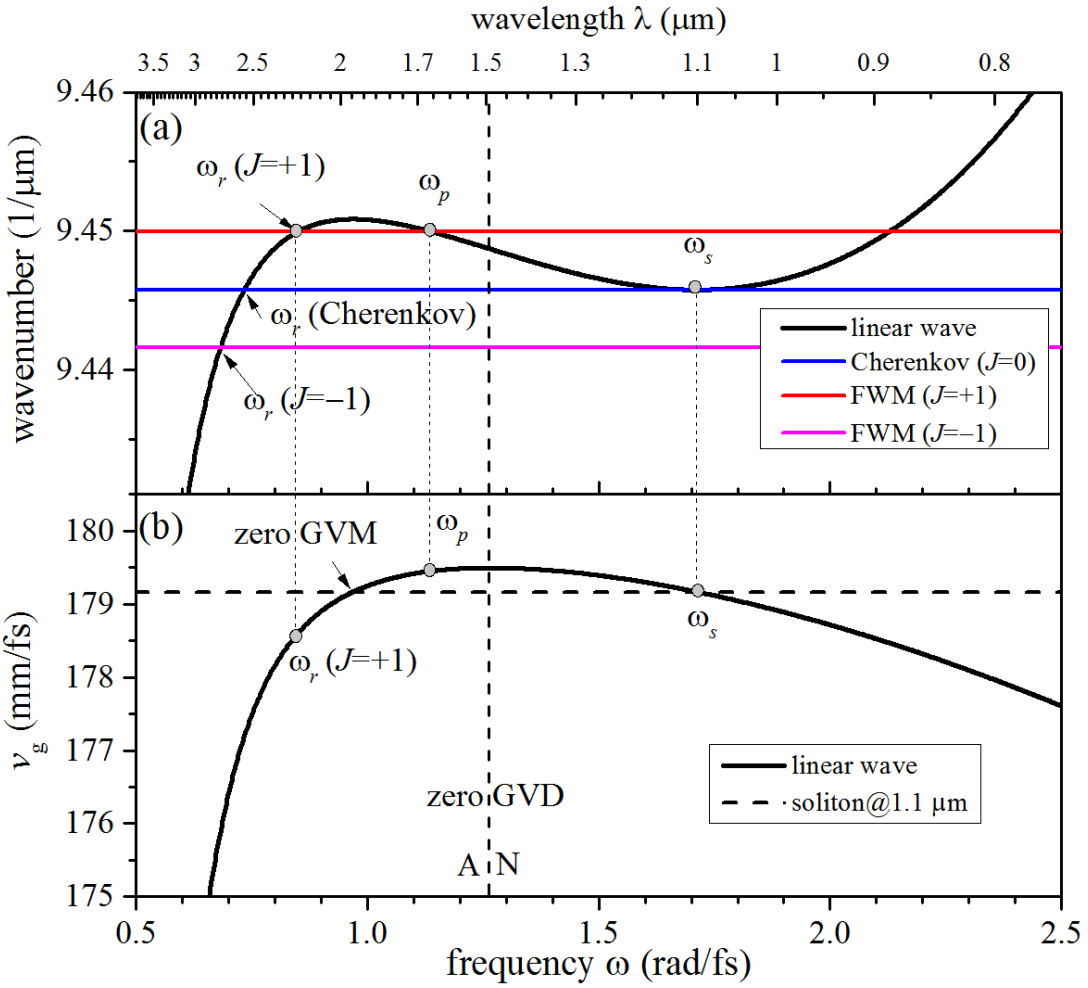

Fig. 3-2 (a) The dispersion relations for BBO in frequency domain, reported in the soliton group-velocity frame. Black line: left-hand side of Eq. (3-29), colored lines: right-hand side of Eq. (3-29), taking a soliton at λ_s = 1.1 μm and a probe at λ_p = 1.65 μm. "A" and "N" denote regimes with anomalous and normal dispersion, respectively. (b) The group velocities of a linear wave (black) and the soliton at λ_s = 1.1 μm (blue).

3.4 Mid-IR femtosecond frequency conversion

The BBO crystal is assumed cut for type-I second harmonic generation (SHG), where two o-polarized photons at the fundamental wave (FW) frequency ω_2 generate a second-harmonic (SH) e-polarized photon at the frequency $\omega_1 = 2\omega_2$. The numerics use the nonlinear wave equations in frequency domain [18] model; the values of the $\chi^{(2)}$ and $\chi^{(3)}$ tensor components were chosen from [19], and the Raman effect is neglected as it is usually considered weak in BBO. Here we pump in the o-wave and through phase-mismatched SHG to the e-wave a nonlinear phase shift accumulates

on the pump pulse, which we exploit to excite a self-defocusing soliton. Importantly, since we also pump with a weak o-polarized probe wave, the numerical model also includes any possible $\chi^{(2)}$ interaction, such as sum- and difference frequency generation (SFG and DFG), and both inter- and intra-polarization (i.e. type 0, I and II) interactions. For simplicity the BBO mid-IR material loss is neglected.

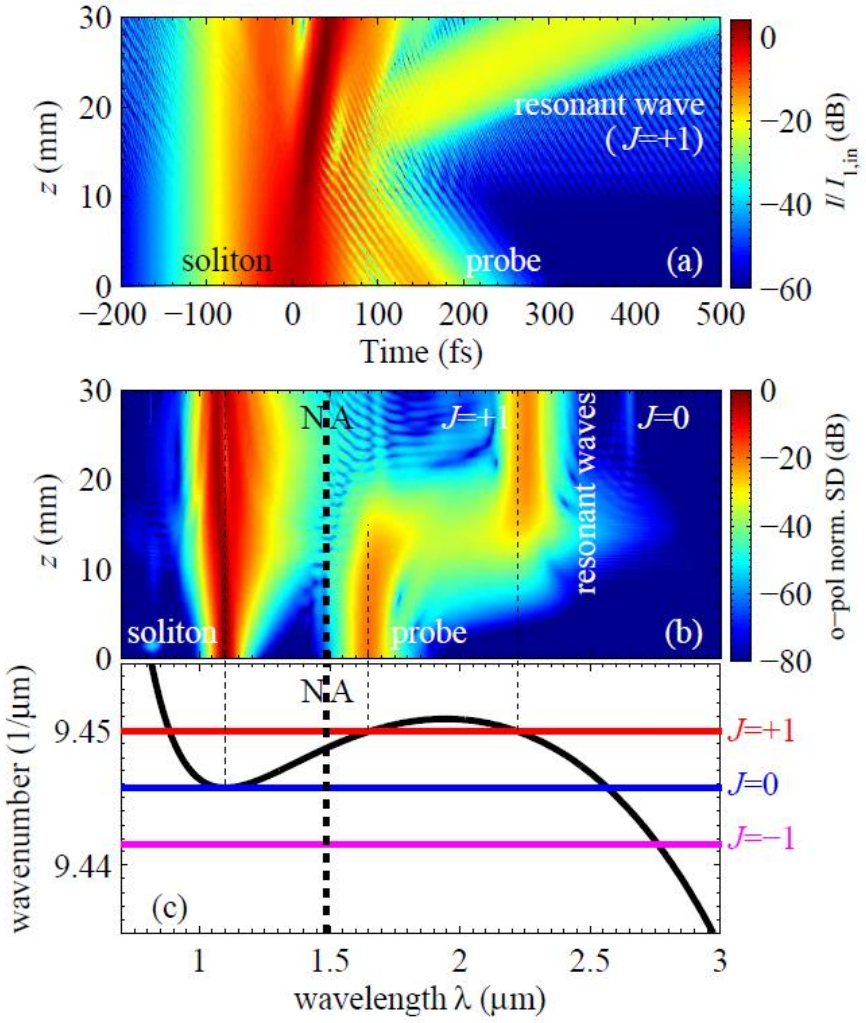

Fig.3-3 Evolution of the o-polarized field in (a) time domain (normalized intensity of the electrical field envelope) and (b) wavelength domain. (c) The dispersion curves of Fig. 3-2(a) in wavelength domain for $\lambda_s = 1.1$ μm (thick) and $\lambda_s = 1.075$ μm(thin). Input pulses: 50 fs FWHM@$\lambda_s = 1.1$ μm, I_1,in = 200 GW/cm^2 (soliton) and 50 fs FWHM@$\lambda_p = 1.65$ μm, Ip,in =5 GW/cm^2, T =150 fs (probe). The BBO crystal had $\Delta k^{SHG}_{\omega_1} = 60\text{mm}^{-1}$($\theta = 18.8^\circ$ and $\varphi = -90^\circ$).the SHG phase mismatch $\Delta k^{SHG}_{\omega_1} = k_e(2\omega_1, \theta) - 2k_o(\omega_1)$ small enough; (b) the group-velocity dispersion (GVD) must be normal [$k_o^{(2)}(\omega_1) > 0$], which in BBO means $\lambda_1 < 1.488$ μm; (c) the effective soliton order [21] $N_{eff} \geq 1$,where $N^2_{eff} = L_D\omega_1 I_{in}|n^{SPM}_{2,eff}(\omega_1)|/c$, $I_{1,in} = \varepsilon_0 n_1(\omega_1)c|E_{1,in}|^2/2$ and $L_D = T_1^2/k_0^{(2)}(\omega_1)$.

The collision is modelled by launching two co-propagating o-polarized fields $E_{1,in}\cos(\omega_1 t)\,\mathrm{sech}(t/T_1) + E_{p,in}\cos(\omega_p t)\,\mathrm{sech}[(t-\tau)/T_p]$, where τ is the delay time between them and we will use identical input pulse durations $T_1 = T_p$.A self-defocusing soliton can form at $\omega_1 = \omega_s$ if the following criteria are fulfilled:(a) The effective Kerr self-phase modulation (SPM) nonlinearity $n_{2,\mathrm{eff}}^{\mathrm{SPM}}(\omega_1) = n_{2,\mathrm{casc}}^{\mathrm{SHG}}(\omega_1) + n_{2,\mathrm{kerr}}$ must be negative, and this is controlled by $n_{2,\mathrm{casc}}^{\mathrm{SHG}}(\omega_1) \propto -d_{\mathrm{eff}}^2/\Delta k_{\omega_1}^{\mathrm{SHG}}$ by making

Fig. 3-3 shows the results from a typical simulation. The BBO crystal angle is suitably chosen to give nonresonant negative SPM and XPM nonlinearities (which occurs between $17.5^\circ < \theta < 20.0^\circ$. The soliton input intensity is chosen so $N_{\mathrm{eff}} = 2.0$, allowing a higher-order self-defocusing soliton to form. A weak probe is launched in the anomalous dispersion regime, which from Fig. 3-2(b) implies that its group velocity is larger than the soliton. It is therefore suitably delayed at the input so the interaction occurs over realistic crystal lengths. The time plot in (a) shows the probe colliding with the trailing edge of the strong soliton at around 10 mm. After the collision a reflected wave emerges; this is the resonant wave phase-matched to the soliton through the negative XPM nonlinearity. According to Fig. 3-2(b) the resonant wave will have a lower group velocity than the soliton and this explains why it is traveling away from the soliton trailing edge. In wavelength domain (b) the normalized spectral density (SD, calculated as $S(\lambda) = |\overline{A}(\omega = 2\pi c/\lambda)|^2\lambda^2/c$) shows that the probe is almost completely converted to the resonant wave, and this occurs between 10 and 20 mm propagation. It is exactly in this propagation range the collision takes place in time domain. There is a good agreement between the predicted phase-matching frequency of the resonant wave, which is evident from the wavelength domain phase-matching curves plotted in (c).We note that the soliton blue-shifts slightly during propagation as a consequence of cascading-induced self steepening. This means that at the final stage $\omega_s > \omega_1$, and this leads to a new set of soliton curves for the phase matching conditions, indicated as thin lines in (c). As these represent solitons they are in frequency domain still straight curves, but they are now tilted instead of flat as the group velocity

is different from that at ω_1; in wavelength domain this means that they are no longer represented as straight curves, but this is simply due to the $\lambda \propto 1/\omega$ relation. These curves explain how the resonant wave is found slightly more red-shifted than the $\omega_s = \omega_1$ case predicted. We also see that the Cherenkov (J = 0) case can be seen in the spectrum, accurately predicted by the blue-shifted soliton phase-matching condition. This is the degenerate case, where the soliton alone becomes phase-matched to a resonant wave.

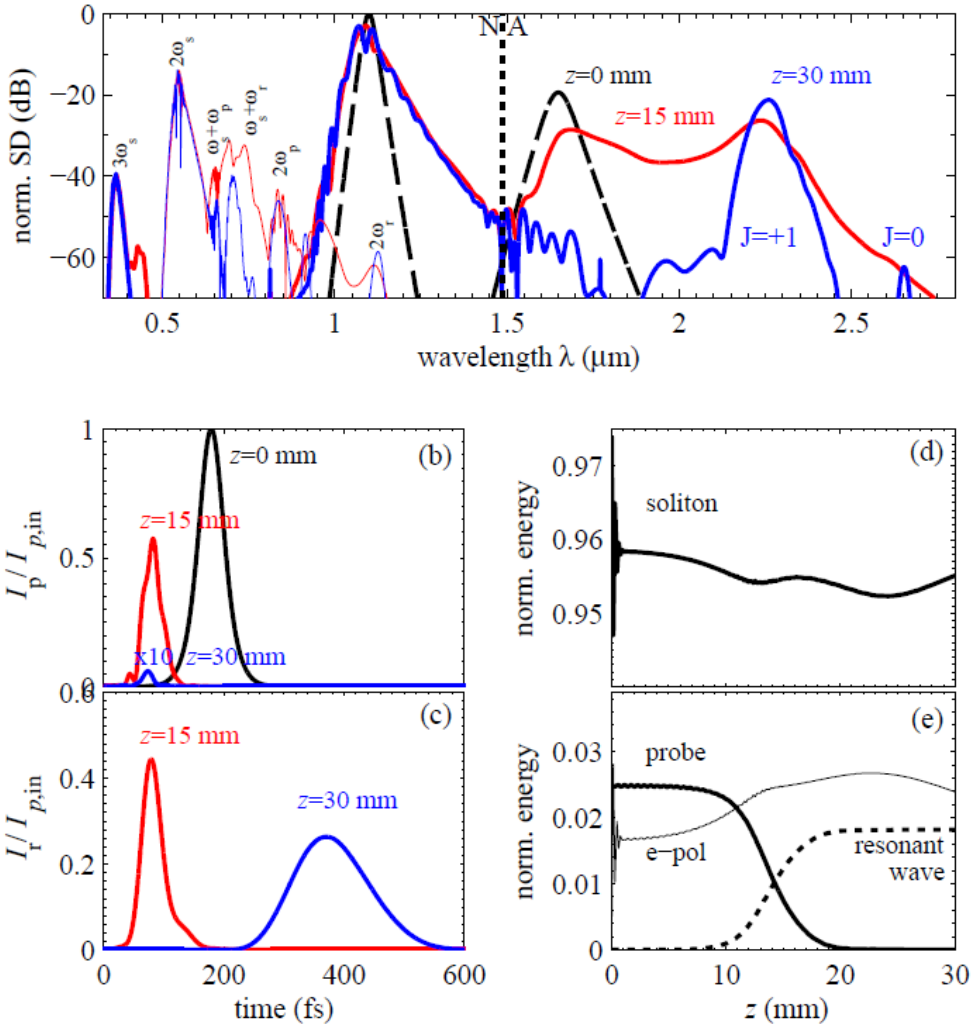

Fig.3-4. Cuts from Fig. 3-3: (a) the normalized o- (thick) and e-polarized (thin) SD; (b) the band-pass filtered probe and (c) the long-pass filtered resonant wave envelopes vs. time.(d+e) Normalized energy vs. z in the collision (full) and no collision (dashed) cases of (d) the soliton and (e) the entire e-polarized spectrum, the filtered probe and resonant waves.

Detailed spectral and temporal cuts are shown in Fig.3-4 (a) shows the SD at input, during (z = 15 mm) and after collision (z = 30 mm). Since the soliton order is above unity, the o-polarized spectra (thick lines) show that the soliton at collision is considerably extended towards the probe spectrum, and the final spectrum shows that the probe is almost completely depleted leaving only the J = +1 and J = 0 resonant waves. The o-polarized third harmonic is also evident, and in the e-polarized spectra (thin lines) the various SHG and SFG components are evident as well. The same cuts are shown in time domain focusing in (b) on the probe (using a band-pass filter) and in (c) on the resonant wave (using a long-pass filter). The probe at 15 mm is around half depleted, giving most of its depleted energy to the resonant wave that is located at the same temporal position. After 30 mm the weak probe does not show on a linear scale (in the plot it is amplified 10 times). The resonant wave is now delayed 400 fs and it is reduced in intensity and increased in time due to dispersion. It has a Gaussian profile since it is a linear and not a soliton wave. Finally (d+e) show the energy, normalized to the total input energy, of the soliton, probe and resonant waves.The soliton initially looses around 2% of its energy through SHG to the e-polarized SH [(e) also shows the total e-polarized energy], causing the initial ripples at z < 1 mm. The soliton-probe interaction occurs between z = 5 − 20 mm, and the resonant wave builds up in energy. After 20 mm the probe is depleted. The energy ratio (conversion efficiency) of the resonant wave to the probe is around 0.72, close to the limit posed by the photon-to-photon ratio $\omega_r/\omega_p = 0.73$ as dictated by the Manley-Rowe relation. The energies from a simulation where the probe never collides with the soliton (dashed lines) show as expected no energy at the resonant wave and the probe remains unaffected.

Fig. 3-4 shows the probe and resonant wave energies vs. N_{eff} (controlled by $I_{1,in}$) for (a) $\lambda_p = 1.65$ μm fixed and four different $I_{p,in}$ values, and (b) $I_{p,in} = 10\ \mathrm{GW/cm^2}$ fixed and three different λ_p values. In (a) the complete depletion of the probe happens for intensities up to $30\ \mathrm{GW/\ cm^2}$, all

ending up at the same plateau, whose level is dictated by the Manley-Rowe relation (as ω_p is fixed). For $I_{p,in} = 40\ GW/cm^2$ the probe conversion is incomplete, which is a result of nonlinear spectral broadening occurring before collision. It is therefore important that the probe does not experience any nonlinear phase shifts before the collision. In (b) a fixed moderate probe intensity was therefore used to ensure complete depletion of the probe. Since different probe frequencies are used the plateau levels vary, in accordance with the Manley-Rowe relation. Clearly probe depletion requires follows a logistic sigmoid function, whose slope scales as $I_{p,in}^{-0.5}$ and the midpoint $N_{eff,0}$ increases linearly with $I_{p,in}$ and decreases linearly with λ_p. This latter scaling comes from the fact that as λ_p increases it approaches the zero group-velocity mismatch (GVM) wavelength, where the probe and soliton have identical group velocities, see Fig.3-2 (b). The detuning from GVM has traditionally

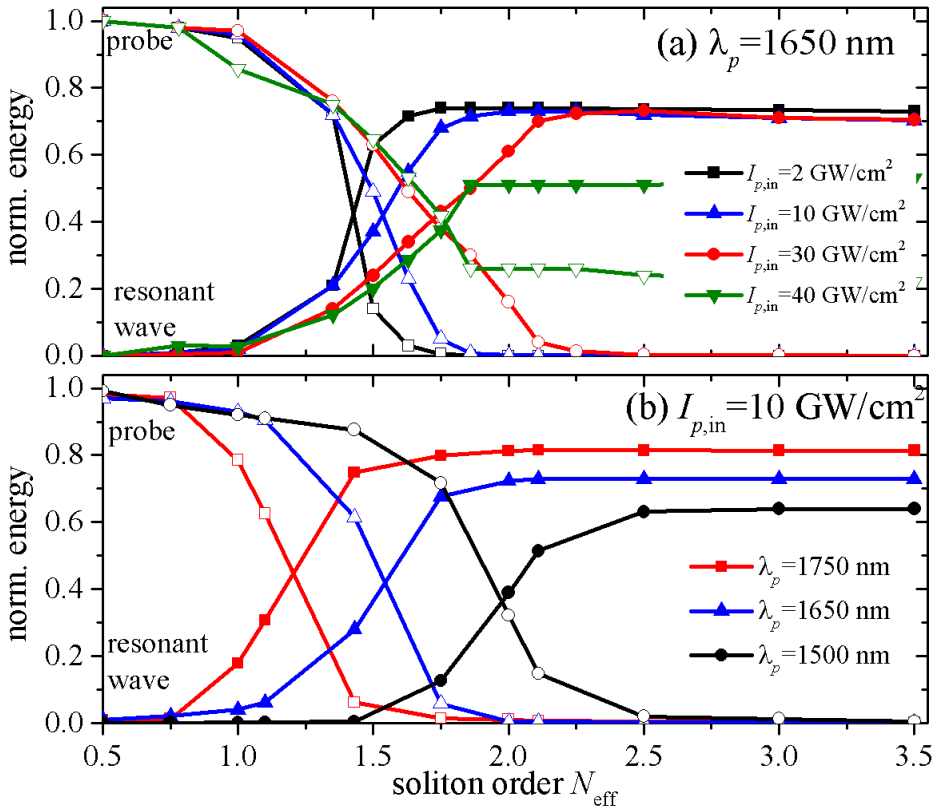

Fig. 3-4. The probe and resonant wave energies (normalized to probe input energy) vs. N_{eff} at z = 40 mm. (a) Fixing $\lambda_p = 1.65\mu m$ and (b) fixing $I_{p,in} = 10\ GW/cm^2$.

been kept small to get a large reflection, with the dilemma that the resonant wavelength is almost identical to the probe [see again Fig. 3-2(b)] and the collision will only take place through very longinteraction distances. Still a decent conversion should be possible even with large detunings from the zero GVM point.

The emission wavelength of the mid-IR resonant wave is tunable from $\lambda = 2.2 - 2.4\mu m$ through changing the probe wavelength, see Fig. 3-5. Note that the mid-IR wave remains quite significant even when probe-depletion is incomplete and when IR losses are taken into account. Besides, this process can be generalized to mid-IR transparent crystals like $LiNbO_3$, where the phase matching point will also lie further into the mid-IR.

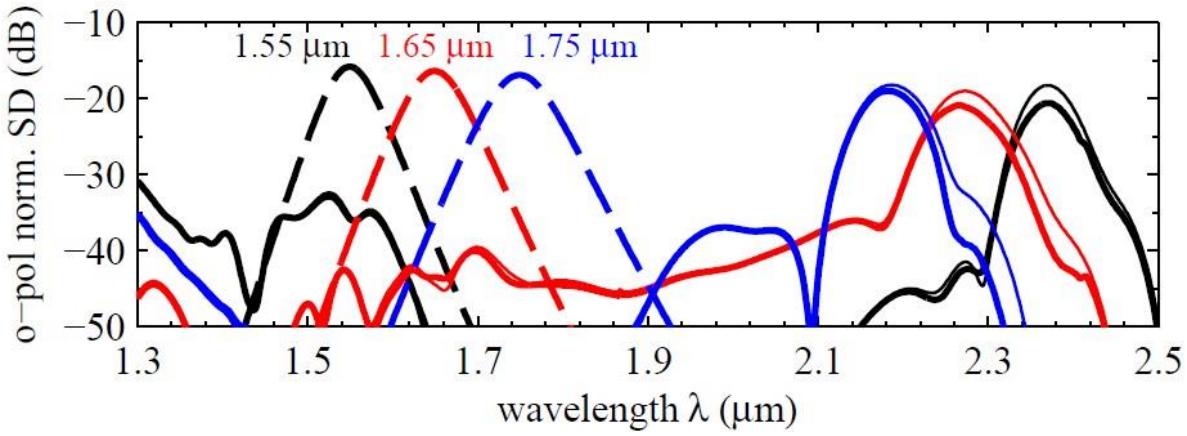

Fig.3-5. Long-wavelength part of the o-polarized SD for various probe wavelengths shown after z = 20 mm (except $\lambda_p = 1.75$ µm where z = 30 mm) with (thick) and without (thin) IR losses of BBO. The dashed lines show the input states. The soliton was the same as in Fig. 3-2 and $I_{p,in} = 10 GW/cm^2$.

3.5 Conclusion

In a quadratic nonlinear crystal multiple cascaded nonlinear effects allow firstly the formation of a self-defocusing near-IR soliton (through cascaded SHG generating a self-defocusing Kerr-like SPM term), which when colliding with a weak near-IR probe induces a cascaded SFG nonlinearity generating a self-defocusing Kerr-like XPM term. This allows a resonant mid-IR wave to become phase matched. A complete probe-resonant wave conversion is possible when colliding with a higher-order soliton, a case which has not been considered before in Kerr systems, and for a given soliton wavelength the resonant wavelength is tunable by varying the probe wavelength. Obtaining

phase matching further into the mid-IR is possible in other crystals, and interestingly the system allows to change the XPM term sign to study the barrier vs. hole potential effect.

Bibliography

[1] P. K. A.Wai, C. R. Menyuk, Y. C. Lee, and H. H. Chen,"Nonlinear pulse propagation in the neighborhood of the zero-dispersion wavelength of monomode optical fibers,"Opt. Lett. 11, 464–466 (1986).

[2] P. Beaud, W. Hodel, B. Zysset, and H. Weber, "Ultrashort pulse propagation, pulse breakup, and fundamental soliton formation in a single-mode optical fiber,"IEEE J. Quantum Electron. 23, 1938 – 1946 (1987).

[3] F. W. Wise, I. A. Walmsley, and C. L. Tang, "Simultaneous formation of solitons and dispersive waves in a femtosecond ring dye laser," Opt. Lett. 13, 129–131(1988).

[4] A. S. Gouveia-Neto, M. E. Faldon, and J. R. Taylor,"Solitons in the region of the minimum group-velocity dispersion of single-mode optical fibers," Opt. Lett. 13,770–772 (1988).

[5] D. V. Skryabin and A. V. Gorbach, "Colloquium: Looking at a soliton through the prism of optical supercontinuum,"Rev. Mod. Phys. 82, 1287–1299 (2010).

[6] T. G. Philbin, C. Kuklewicz, S. Robertson, S. Hill,F. K¨onig, and U. Leonhardt, "Fiber-optical analog of the event horizon," Science 319, 1367–1370 (2008).

[7] A. Demircan, S. Amiranashvili, and G. Steinmeyer,"Controlling light by light with an optical event horizon,"Phys. Rev. Lett. 106, 163901 (2011).

[8] A. V. Yulin, D. V. Skryabin, and P. S. J. Russell,"Four-wave mixing of linear waves and solitons in fibers with higher-order dispersion," Opt. Lett. 29, 2411–2413(2004).

[9] D. V. Skryabin and A. V. Yulin, "Theory of generation of new frequencies by mixing of solitons and dispersive waves in optical fibers," Phys. Rev. E 72, 016619 (2005).

[10] A. Efimov, A. V. Yulin, D. V. Skryabin, J. C. Knight,N. Joly, F. G. Omenetto, A. J. Taylor, and P. Russell,"Interaction of an Optical Soliton with a Dispersive Wave," Phys. Rev. Lett. 95, 213902 (2005).

[11] G. Genty, M. Erkintalo, and J. M. Dudley, “Do optical event horizons really exist? the physics of nonlinear reflection at a soliton boundary,” in “Advanced Photonics Congress,” (Optical Society of America, 2012), p.NW3D.2.

[12] R. DeSalvo, D. Hagan, M. Sheik-Bahae, G. Stegeman,E. W. Van Stryland, and H. Vanherzeele, “Self-focusingand self-defocusing by cascaded second-order effects in KTP,” Opt. Lett. 17, 28–30 (1992).

[13] S. Ashihara, J. Nishina, T. Shimura, and K. Kuroda,“Soliton compression of femtosecond pulses in quadratic media,” J. Opt. Soc. Am. B 19, 2505–2510 (2002).

[14] B. B. Zhou, A. Chong, F. W. Wise, and M. Bache,“Ultrafast and octave-spanning optical nonlinearities from strongly phase-mismatched quadratic interactions,”Phys. Rev. Lett. 109, 043902 (2012).

[15] M. Bache, O. Bang, B. B. Zhou, J. Moses, and F. W.Wise, “Optical Cherenkov radiation in ultrafast cas caded second-harmonic generation,” Phys. Rev. A 82,063806 (2010).

[16] M. Bache, O. Bang, B. B. Zhou, J. Moses, and F. W.Wise, “Optical Cherenkov radiation by cascaded nonlinear interaction: an efficient source of few-cycle energetic near- to mid-IR pulses,” Opt. Express 19, 22557–22562(2011).

[17] B. Zhou, H. Guo, and M. Bache, “Energetic mid-IR femtosecond pulse generation by self-defocusing solitoninduced dispersive waves in a bulk quadratic nonlinear crystal,” Opt. Express 23, 6924–6936 (2015).

[18] H. Guo, X. Zeng, B. Zhou, and M. Bache, “Nonlinear wave equation in frequency domain: accurate modeling of ultrafast interaction in anisotropic nonlinear media,”J. Opt. Soc. Am. B 30, 494–504 (2013).

[19] M. Bache, H. Guo, B. Zhou, and X. Zeng, “The anisotropic Kerr nonlinear refractive index of the betabarium borate (β-BaB2O4) nonlinear crystal,” Opt.Mater. Express 3, 357–382 (2013).

Chapter 4

Three wave mixing resonant radiation in phase-mismatched quadratic nonlinear crystals

4.1 Introduction

In the nonlinear optics, the balance of the second order fiber dispersion and the nonlinearity can lead to formation a soliton, Cherenkov or resonant radiation (RR) emitted by solitons in the presence of higher-order dispersion sheds light through a four wave mixing (FWM) resonant process to a new frequency, which determined by a phase-matching condition between the dispersive resonant radiation and the soliton. The theoretical and experimental studies have demonstrated the crucial role of these processes in the expansion of supercontinuum generated in nonlinear fibers [2] and nonlinear bulk crystals [7].

Theoretical and experimental studies have also shown the mid-IR Cherenkov wave generated by the cascaded quadratic solitons through degenerate FWM resonant interaction[8]. In chapter 3, we showna non-degenerate FWM in the quadratic crystal, where a soliton interacts with linear waves. While in a nonlinear medium without the center of symmetry (quadratic medium), resonant radiation results in parametric three-wave mixing (TWM) when two waves create a third wave is possible to appear.

The aim of this chapter is to develop a physical understanding and analytical methods of the TWM RR in phase-mismatched quadratic nonlinear crystals.

4.2 Three wave mixing radiation phase-matching conditions

We started with study the couple analytic wave equations (CAWEs) in chapter 2, eliminating the Kerr nonlinearity and Raman nonlinearity.

$$\frac{\partial A_1(\xi,\tau)}{\partial \xi} + iD_1 A_1(\xi,\tau) = i\frac{\hat{\chi}^{(2)}_{e;ee}}{4cn(\omega_1)}\left(\omega_1 - i\frac{\partial}{\partial\tau}\right)\left[4A_1^* A_2 e^{-i\Delta k\xi} + A_1 A_1^* e^{-ik_{pg}\xi - i\omega_1\tau}\right]_+ \quad (4\text{-}1)$$

$$\frac{\partial A_2(\xi,\tau)}{\partial z} + [-d_{12}\frac{\partial}{\partial\tau} + iD_2]A_2(\xi,\tau) = -i\frac{\hat{\chi}^{(2)}_{e;ee}}{4cn(\omega_2)}(\omega_2 - i\frac{\partial}{\partial\tau})[\,4A_1 A_1 e^{i\Delta kz} + A_2 A_2^* e^{ik(\omega_2)z - i\omega_2\tau}]_+ \quad (4\text{-}2)$$

In a largely phase mismatched second-harmonic (SH), we assume a SH A_2:

$$A_2(\xi,\tau) = \varphi(\tau)e^{i\Delta k\xi} \tag{4-3}$$

Inserting the Eq. (4-3) into Eq. (4-1) gives the SH:

$$A_2(\xi,\tau) = -i\frac{\hat{\chi}^{(2)}_{e;ee}}{4cn(\omega_2)\Delta k}(\omega_2 - i\frac{\partial}{\partial\tau})e^{i\Delta k\xi}(R(t)\otimes A_1^2)$$

$$= -i\frac{\hat{\chi}^{(2)}_{e;ee}}{4cn(\omega_2)\Delta k}\left(\omega_2 - i\frac{\partial}{\partial\tau}\right)e^{i\Delta k\xi}\int_{-\infty}^{+\infty}d\tau' R(t)A_1^2(t-\tau') \tag{4-4}$$

where $R(\Omega) = \frac{1}{\sqrt{2\pi}}\Delta k/(\frac{1}{2}\beta_2^{(2)}\Omega^2 - d_{12}\Omega + \Delta k)$ is the response function, Ω is set by $\Omega = \omega - \omega_2$, R(t) is the inverse Fourier transform of the response function. Inserting $A_2(\xi,\tau)$ into Eq. (4-1), we get the nonlinear Schrödinger-like (NLS-like) equation only contain positive frequency in the largely phase mismatched SHG process [14]:

$$\frac{\partial A_1(\xi,\tau)}{\partial\xi} + iD_1A_1(\xi,\tau) =$$

$$\frac{\hat{\chi}^{(2)}_{e;ee}}{cn(\omega_1)}\left(\omega_1 - i\frac{\partial}{\partial\tau}\right)\left[\left(-i\frac{\hat{\chi}^{(2)}_{e;ee}}{4cn(\omega_2)\Delta k}\left(\omega_2 - i\frac{\partial}{\partial\tau}\right)(A_1^*A_1^2 - i\tau'_{R,SHG}A_1^*\frac{\partial}{\partial\tau}A_1^2)\right) + \frac{1}{4}A_1A_1^*e^{-i\Delta k_{pg}\xi - i\omega_1\tau}\right]_+ \tag{4-5}$$

where group velocity match(GVM) term $\tau'_{R,SHG} = 2|d_{12}|/\Delta k$,which act as Raman-like redshift of the FW. In our case, we eliminated the GVM term, thus the NLS-like equation only have the positive frequency can be written as :

$$i\frac{\partial A_1(\xi,\tau)}{\partial\xi} - D_1A_1(\xi,\tau) = \left[N_{casc}^2|A_1|^2A_1 + \kappa_2A_1A_1^*e^{-i\Delta k_{pg}\xi - i\omega_1\tau}\right]_+ \tag{4-6}$$

The pre-factor is understood as the dimensionless soliton number $N_{casc}^2 = \frac{\hat{\chi}^{(2)}_{e;oo}{}^2}{4\Delta kc^2n(\omega_1)n(\omega_2)}$ and $\kappa_2 = \frac{\hat{\chi}^{(2)}_{e;oo}}{4cn(\omega_1)}$.

In order to derive three wave mixing radiation phase-matching conditions between a soliton and its resonant radiations, we follow a standard procedure described in [5].We look for solutions of Eq. (4-5) in the form:

$$A_1(\xi,\tau) = F(\tau)e^{iq\xi} + g(\xi,\tau) \tag{4-7}$$

where $F(\tau)$ is the envelope of the optical soliton, q is the shift of the soliton wave number and g is a small amplitude generated dispersive wave .

After substitution into Eq. (4-5), we only consider first order terms for simplicity. Assuming that g is a linear wave we derive：

$$\left[\mathrm{i}\,\partial_\xi + \widehat{\mathrm{D}}_1(\mathrm{i}\,\partial_\tau)\right]\mathrm{g} + \mathrm{N}_{\mathrm{casc}}^2\mathrm{F}^2(\tau)\mathrm{g}^*(\xi,\tau)\mathrm{e}^{2\mathrm{iq}\xi} + 2\mathrm{N}_{\mathrm{casc}}^2\mathrm{F}^2(\tau)\mathrm{g}(\xi,\tau)$$

$$+ \kappa_2\mathrm{F}(\tau)\mathrm{g}^*(\xi,\tau)\mathrm{e}^{-\mathrm{i}\omega_1\tau+\mathrm{i}\Delta\mathrm{k}_{\mathrm{pg}}\xi+\mathrm{iq}\xi}$$

$$= -[\widehat{\mathrm{D}}(\mathrm{i}\,\partial_\tau) + 1/2\beta_2\,\partial_\tau^2]\mathrm{F}(\tau)\mathrm{e}^{\mathrm{iq}\xi} \qquad (4\text{-}8)$$

Eq. (4-8）is the solution of dispersive wave which should have continuum mode on the right-hand side. Thus, the phase-matching conditions are easily found:

$$\mathrm{D}_1(\Omega) = \mathrm{q} \qquad (4\text{-}9)$$

$$\mathrm{D}_1(\Omega) = 2\mathrm{q} \qquad (4\text{-}10)$$

$$\mathrm{D}_1(\Omega) = 0 \qquad (4\text{-}11)$$

$$\mathrm{D}_1(\Omega) = \mathrm{q} + \Delta\mathrm{k}_{\mathrm{pg}} \qquad (4\text{-}12)$$

Equation (4-9) is Cherenkov resonances, (4-10) and (4-11) are degenerated FWM resonances driven between the solitons and generated RR, seeing $\mathrm{F}^2(\tau)\mathrm{g}^*(\xi,\tau)$ and $\mathrm{F}^2(\tau)\mathrm{g}(\xi,\tau)$ terms. The term $\mathrm{F}(\tau)\mathrm{g}^*(\xi,\tau)$ contain both positive frequency and negative frequency, which is the typical three wave mixing interaction. The $\mathrm{g}^*(\xi,\tau)$ operator is the classical analogues of the annihilation operator in quantum optics, which correspond to absorption and emission of a photon. Thus, this $\mathrm{F}(\tau)\mathrm{g}^*(\xi,\tau)$ interaction called like difference frequency generation TWM-RR (TWM-RR (DFG)).The TWM-RR(DFG) only appears in quadratic nonlinear medium when match the phase matching condition (4-12). The TWM-RR(DFG) is strongly detuned to longer wavelength ($-\omega_1$ represents lower shifted frequency relative to the pumping frequency). Thus, TWM-RR (DFG) needs the FW dispersion operator $\mathrm{D}_1(\Omega) < 0$. But in the bulk crystal we have examined the group velocity factor Δkpg > 0, thus TWM-RR (DFG) would not happen. However, there might well be

waveguide structures with a range of frequencies for which Δkpg < 0 or slowdown of group velocity of light by employing electro-optic effect.

For the SH which only have linear wave,

$$[i\partial_{\xi}+ -d_{12}\frac{\partial}{\partial\tau}+iD_2]g = \ -i\frac{\hat{\chi}^{(2)}_{e;ee}}{cn(\omega_2)}(\omega_2 - \ i\frac{\partial}{\partial\tau})F^2(\tau)e^{i2q\xi+i\Delta k\xi} \tag{4-13}$$

The phase matching condition is：

$$D_2(\Omega) - d_{12}\Omega = \Delta k \tag{4-14}$$

Equation (4-14) represents the phase-matching condition of the non-solitonic radiation due to SFG, called TMW-RR (SFG) or nonlocal side which has been experimental and theoretical proved [14].

4.3 Three wave mixing radiation with linear pump

Parametric amplification based on three-wave mixing is a fundamental process in nonlinear optics [17] .They have been widely application for temporal compression, ultrafast all optical switching [18].

Here, the idea of using cascaded quadratic effects in the SHG process to balance dispersion and nonlinearity as to produce solitons. Three-wave resonant interaction is possible in the presence of the quadratic nonlinearity. We study parametric generation of new frequencies resulting from TWM of solitons and linear wave in quadratic crystal. The phase-matching conditions are expected to be different from those generated by the mixing of cw's.

A particular case of the three-wave interaction is known in nonlinear optics as type I birefringent (o+o→e). The quadratic crystal is assumed cut for type-I SHG for generating the self-defocusing soliton field A_1, with the weak linear wave A_2 input. The interaction is modelled by launching two co-propagating o-polarized fields,the generated wave A_3 can be described as:

$$\frac{\partial A_3(\xi,\tau)}{\partial z} + [-d_{13}\frac{\partial}{\partial\tau} + iD_3(\Omega)]A_3(\xi,\tau) = \tilde{\chi}^{(2)}\ A_1A_2e^{i\,\Delta k_{SFG}\xi} \tag{4-15}$$

The dispersion operator in Eq. (4-15) is given by:

$$D_3(\Omega) = \sum_{m=2}^{\infty} \frac{\Omega^m k_e^{(m)}(\omega_3)}{m!} \tag{4-16}$$

where the phase match of sum frequency $\Delta k_{SFG} = k_e(\omega_3) - k_o(\omega_1) - k_o(\omega_2)$, $k_o^{(1)}(\omega_1)$ is the group velocity of the soliton and d_{13} is the GVM between the soliton and the SFG ω_3, $d_{13} = k_o^{(1)}(\omega_1) - k_e^{(1)}(\omega_3)$.

We launched soliton with optical field $A_1(\xi,\tau) = F(\tau)e^{iq\xi}$, and the weak probe is the linear wave which can be written as $A_2 = g(\xi,\tau)$.For the A_3, there only have solution for the linear wave, thus we derive,

$$[i\partial_\xi - d_{13}\frac{\partial}{\partial\tau} + iD_3]g = \tilde{\chi}^{(2)}(\tau)F(\tau)g(\xi,\tau)e^{iq\xi+i\Delta k_{SFG}\xi} \tag{4-17}$$

The SFG between soliton and probe phase matching condition can be described as:

$$D_3(\Omega) - d_{13}\Omega = \Delta k_{SFG} + q \tag{4-18}$$

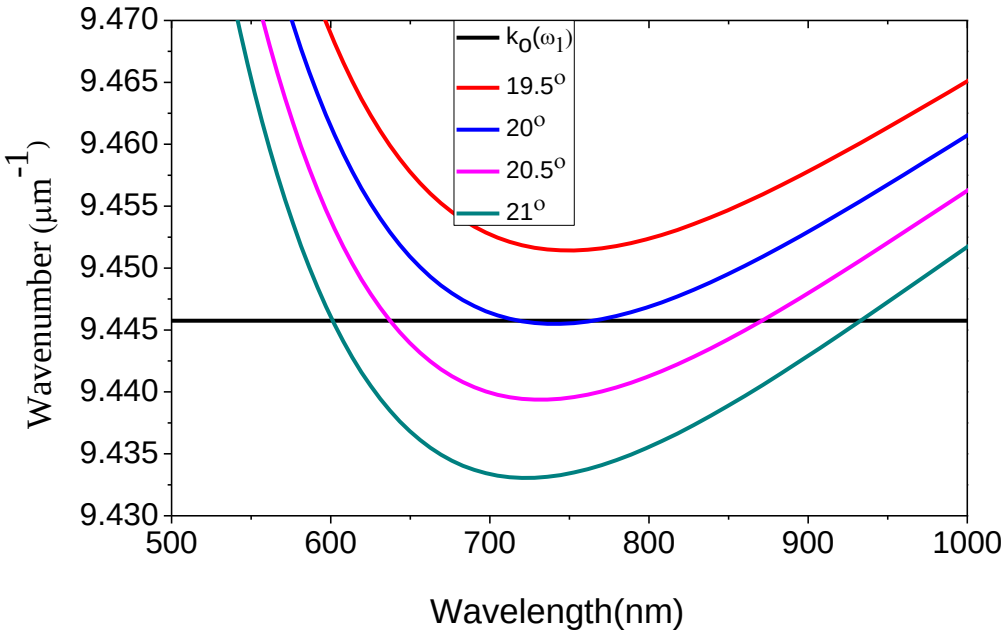

Figure 4-1. The TWM-linear resonances wavelengths calculated for type I birefringent (o+o→e) in BBO.

The TWM resonances curve $k(\Omega) = D_3(\Omega) - d_{13}\Omega + k_o(\omega_2) - k_e(\omega_3)$ is tunable through θ this is indicated with color curves for taken 0.5^o larger and smaller. This resonance is driven by the

TWM between the solitons and linear wave pump (see terms $F(\tau)g(\xi,\tau)$ on Eq. (4-17). Therefore, we call them TWM-linear resonances. In a BBO quadratic nonlinear crystal TWM resonant waves are phase-matched at $\theta = 21^{\circ}$, as seen from the phase matching curve in Fig. 4-2. (a 1.65 μm probe colliding with a 1.1 μm soliton).

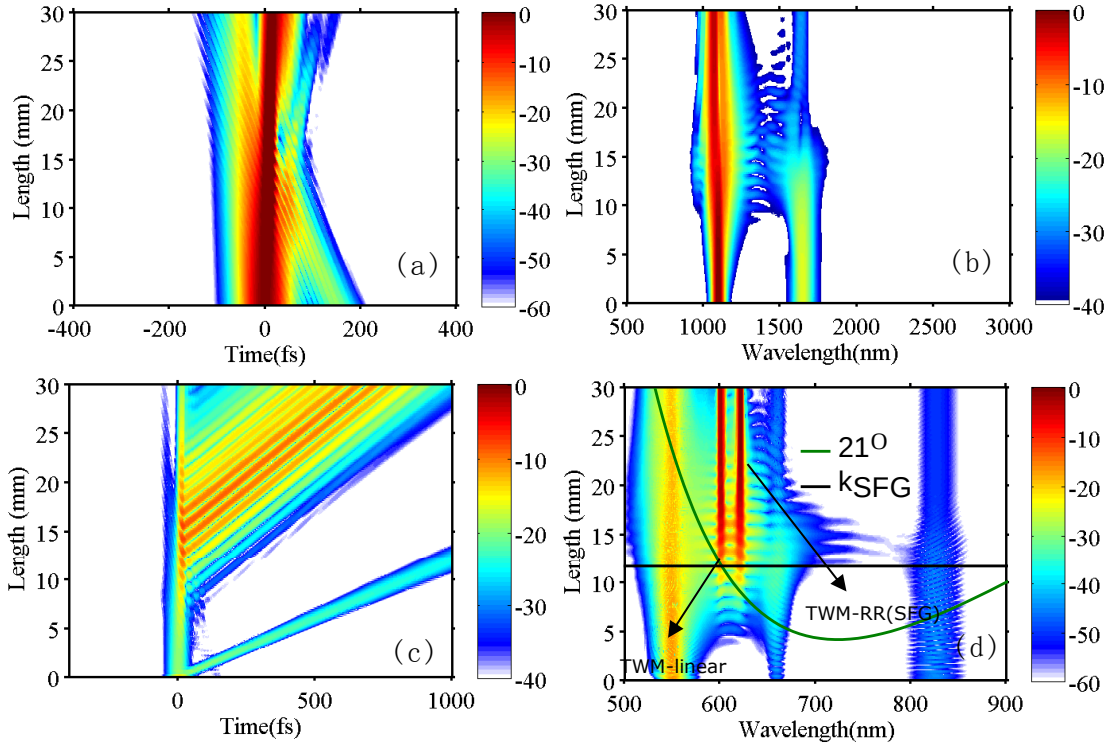

Figure 4-2. Numerical simulations use the NWEF. (a) Evolution of the o-polarized field in time domain and (b) wavelength domain. (c) Evolution of the e-polarized field in time domain and (d) wavelength domain. Input pulses: 50 fs FWHM @$\lambda_s = 1.1$ μm, Iin = 25 GW/cm^2 (soliton) and 50 fs FWHM@$\lambda_p = 1.65$ μm, $I_{pr,in}$ = 1.25 GW/cm^2,(probe). The BBO crystal had ($\theta = 21^{\circ}$ and $\varphi = -90^{\circ}$).

Fig. 4-2 shows the results from a typical simulation using NWFWs model, the BBO phase-mismatch ($\theta = 21°$) where the cascaded SHG becomes non-resonance. The soliton with 50 fs duration, pumping wavelength at λ_0 =1.1 μm, the peak intensity I=25 Gw/cm^2 to give an effective self-defocusing soliton order N_{eff}=2.0. A weak probe with 50fs duration, pumping wavelength at λ_p =1.65 μm and input intensity I_p=1.25 Gw/cm^2 is launched in the normal dispersion regime. As we expected, the TWM (o+o→e) between soliton and linear wave becomes non-resonant, see the

TWM-linear resonances curve Fig 4-1. The Fig 4-2 (a) and (c) show the propagation FW and SH dynamics time domain, (b) and (d) show the propagation FW and SH dynamics wavelength domain. Because of GVD, the linear wave approaches the soliton, until it reaches the soliton. When the pulses begin to interact, positive cross phase modulation (chapter 3, Fig 3-1) induces a TWM-linear resonant wave formed at wavelength 607 nm at length z=15mm. There is a perfect agreement between the predicted phase-matching frequencies of the TWM resonant wave, which is evident from the wavelength domain phase-matching curves plotted insert Fig 4-2 (d).

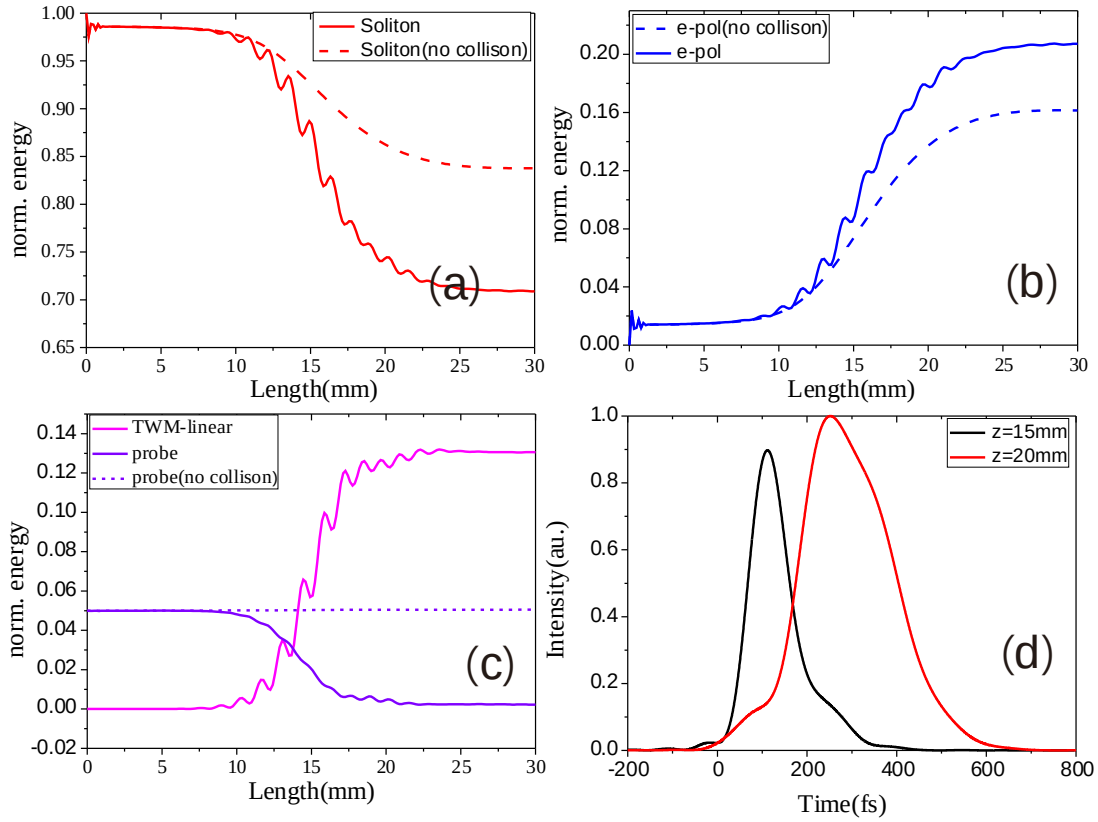

Figure 4-3 (a) The energy of soliton, (b) the energy of e-pol except the TWM resonant wave (c) the energy of the probe and TWM resonant wave (d) the filtered resonant wave envelopes vs. time.

Fig 4-3(a, b, c) show the energy, normalized to the total input energy, of the soliton, probe and resonant waves. The energies from a simulation where the probe never collides with the soliton (dashed lines) show as expected no energy at the resonant wave and the probe remains unaffected.

The soliton-probe interaction occurs between z = 10 − 20 mm, and the TWM resonant wave builds up in energy. After 20 mm the probe is depleted. The energy ratio (conversion efficiency) of the resonant wave to the probe is around 2.4, which means this is an optical parametric amplification process. The photon of the soliton and the probe convert the energy to the TWM resonant wave by TWM process. As the Fig 4-3 (d) show, the duration of the TWM resonant wave is in the fs scale.

4.4 Conclusion

In conclusion, we have introduced the concept of TWM radiation in the BBO Crystal and demonstrated a possibility of the TWM resonant wave created by soliton in quadratic media. The parametric amplification process was also demonstrated by the collision of the soliton and a weak probe. We believe our results open a new direction in quadratic soliton, and may bring new ideas into other fields of nonlinear optics where parametric wave interactions are important.

Bibliography

[1] D.V. Skryabin and A.V. Gorbach, “Looking at a soliton through the prism of optical supercontinuum”, Rev. Mod.Phys. 82, 1287-1299 (2010).

[2] J.M. Dudley, G. Genty, and S. Coen, “Supercontinuum generation in photonic crystal fiber”, Rev. Mod. Phys 78,1135-1184 (2006).

[3] N. Akhmediev and M. Karlsson, “Cherenkov radiation emitted by solitons in optical fibers”, Phys. Rev. A 51,2602-2607 (1995).

[4] D.V. Skryabin, F. Luan, J.C. Knight, and P.S. Russell, “Soliton self-frequency shift cancellation in photonic crystal fibers”, Science 301, 1705-1708 (2003).

[5] D.V. Skryabin and A.V. Yulin, “Theory of generation of new frequencies by mixing of solitons and dispersive waves in optical fibers”, Phys. Rev. E 72, 016619 (2005).

[6] Efimov, A. and Yulin, A. V. and Skryabin, D. V. and Knight, J. C. and Joly, N. and Omenetto,

F. G. and Taylor, A. J. and Russell, P. “Interaction of an Optical Soliton with a Dispersive Wave”, Phys. Rev. Lett. 95 213902 (2005).

[7] F. Silva, D. Austin, A. Thai, M. Baudisch, M. Hemmer, D. Faccio, A. Couairon, and J. Biegert, “Multi-octave supercontinuum generation from mid-infrared filamentation in a bulk crystal,” Nature Comms. 3, 807 (2012).

[8] B. Zhou, H. Guo, and M. Bache, “Energetic mid-IR femtosecond pulse generation by self-defocusing soliton induced dispersive waves in a bulk quadratic nonlinear crystal,” Opt. Express 23, 6924–6936 (2015).

[9] R. DeSalvo, D. Hagan, M. Sheik-Bahae, G. Stegeman,E. W. Van Stryland, and H. Vanherzeele, “Self-focusingand self-defocusing by cascaded second-order effects in KTP,” Opt. Lett. 17, 28–30 (1992).

[10] S. Ashihara, J. Nishina, T. Shimura, and K. Kuroda,“Soliton compression of femtosecond pulses in quadratic media,” J. Opt. Soc. Am. B 19, 2505–2510 (2002).

[11] B. B. Zhou, A. Chong, F. W. Wise, and M. Bache,“Ultrafast and octave-spanning optical nonlinearities from strongly phase-mismatched quadratic interactions,”Phys. Rev. Lett. 109, 043902 (2012).

[12] M. Bache, O. Bang, B. B. Zhou, J. Moses, and F. W.Wise, “Optical Cherenkov radiation in ultrafast cas caded second-harmonic generation,” Phys. Rev. A 82,063806 (2010).

[13] M. Bache, O. Bang, B. B. Zhou, J. Moses, and F. W.Wise, “Optical Cherenkov radiation by cascaded nonlinear interaction: an efficient source of few-cycle energetic near- to mid-IR pulses,” Opt. Express 19, 22557–22562(2011).

[14] M. Bache, J. Moses, and F. W. Wise, “Scaling laws for soliton pulse compression by cascaded quadratic nonlinearities,”J. Opt. Soc. Am. B 24, 2752–2762 (2007).[erratum: ibid., 27, 2505 (2010)].

[15] M. Bache, O. Bang, J. Moses, and F. W. Wise, “Nonlocal explanation of stationary and nonstationary regimes in cascaded soliton pulse compression,” Opt. Lett. 32,2490–2492 (2007).

[16] B. B. Zhou, H. R. Guo, and M. Bache, “Soliton-induced nonlocal resonances observed through high-intensity tunable spectrally compressed second-harmonic peaks,” Phys. Rev. A 90, 013823 (2014).

[17] For a comprehensive overview of cascading, see G. Stegeman,D.J. Hagan, and L. Torner, Opt. Quantum Electron. 28, 1691~1996

[18] For an overview of quadratic spatial solitons, see L. Torner, in Beam Shaping and Control with Nonlinear Optics, edited by F. Kajzer and R. Reinisch ~Plenum, New York, 1998, p. 229;Yu.S. Kivshar, in Advanced Photonics with Second-Order Optically Nonlinear Processes, edited by A.D. Boardman, L. Pavlov,and S. Tanev ~Kluwer, Dordrecht, 1998), p. 451

[19] Y. Wang and R. Dragila, “Efficient conversion of picosecond laser pulses into second-harmonic frequency using group-velocity dispersion,” Phys. Rev. A 41, 5645–5649 (1990)

[20] A. Stabinis, G. Valiulis and E.A. Ibragimov, “Effective sum frequency pulse compression in nonlinear crystals,” Optics Comm. 86, 301–306 (1991)

.

Chapter 5

The soliton optical parametric generator: single-pumped tunable generation of mid-IR femtosecond pulses

5.1 Introduction

Periodically poled lithium niobate (PPLN) is a quasi-phase matched material that offers a high nonlinear coefficient, high resistance to photorefractive damage and broad spectral transmission range (0.35-5.5 μm), allowing efficient wavelength conversion into the mid-IR from low pulse energy. Several approaches have been explored for generating the mid-IR pulse based on the PPLN crystal, such as optical parametric oscillators (OPOs)[1], difference frequency generation (DFG)[2], and optical parametric pulse amplification (OPA)[4], despite the great complexity implementing critical phase-matching conditions and synchronous pumping scheme.

In this chapter, a defocusing soliton-driven tunable mid-IR optical parametric amplifier is proposed in a standard PPLN bulk crystal. It relies only on a single input pulse entering a quadratic nonlinear crystal, which is appropriately phase-mismatched so a self-defocusing temporal soliton forms. This temporal soliton drives resonant radiation in the mid-IR through a three-wave mixing (TWM) process with a large degree of tunability in the wavelength by shifting the grating pitch value.

5.2 Quasi-phase-matching

Quasi phase-matching (QPM) is a very well-known technique in nonlinear optics which relying on the periodic modulation of the nonlinear susceptibility in the nonlinear medium. Momentum is conserved, that can compensate for the phase-mismatch between the FF and SH wave-number, through an additional momentum contribution corresponding to the wavevector of the periodic structure. Moreover, QPM structures can be engineered by varying the period, duty cycle of the grating, crystal widths and lengths, enabling several applications for efficient frequency conversion, high harmonic generation[8], all-optical processing[9], pulse shaping[10], supercontinuum generation[11] and other nonlinear processes.

The phases mismatch between FW and SH is for the QPM interaction is given by：

$$\Delta k_{eff} = \Delta k - \frac{2\pi m}{\Lambda}$$

where Λ is the poling period,m the QPM order, Δk is the natural phase mismatch between FW and SH.

In a QPM device, the second-order nonlinear optical coefficient distributed along the z-axis coinciding with the direction of wave-vectors：

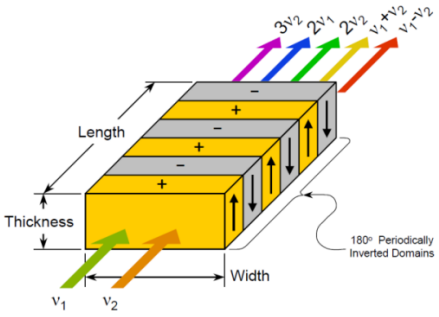

Fig 5-1 The device PPLN [13]

$$d(z) = d_{ij}g(z) \tag{5-1}$$

where second-order nonlinear coefficient $d_{ij} = \chi^{(2)}_{ikl}/2, \chi^{(2)}_{ikl}$ is the second-order susceptibility tensor and g(z) can take values of ±1 inside the nonlinear medium.

By approximating this periodic modulation of g(z) with discrete Fourier series:

$$g(z) = \sum_{m=-\infty}^{+-\infty} G_m \, e^{-im\frac{2\pi}{\Lambda}z} \tag{5-2}$$

where $G_m = \frac{2}{m\pi}\sin(\frac{m\pi}{2})$ is Fourier coefficients.

5.3 Soliton generation in QPM crystal

The cascading quadratic nonlinearity in a material with first-order QPM structure can be writing as:

$$n_{2,casc} = -\frac{2\omega_1(\frac{2}{\pi}d_{eff})^2}{\epsilon_0 c^2 n(\omega_2) n^2(\omega_1)\Delta k_{eff}} \tag{5-3}$$

which a positive-valued Δk_{eff} provide self-defocusing in the normal dispersion region.

The cubic nonlinearity stemming from the electronic Kerr effect is always characterized through the Z-Scan measurement:

$$n_{2,\mathrm{cubic}} = \frac{3\chi^3(\omega)}{4\epsilon_0 c n^2(\omega)} \tag{5-4}$$

LN is reported to have quite strong Raman response [14], f_R > 50%, so the competing Kerr nonlinear-rity is $n_{2,\mathrm{kerr}} = (1 - f_R)n_{2,\mathrm{cubic}}$.

The total nonlinearity is given by a combination of competing cascaded second-order nonlinearity and cubic nonlinearity：

$$n_2 = n_{2,\mathrm{casc}} + n_{2,\mathrm{kerr}} \tag{5-5}$$

The effective soliton order is $N_{\mathrm{eff}}^2 = L_D\omega_1 I_0(|n_{2,\mathrm{casc}}^2| - |n_{2,\mathrm{Kerr}}^2|)/c$, where I_0 is input intensity, $L_D = T_0/k_1^{(2)}(\omega)$ is the effective dispersion length, $k_1^{(2)}(\omega)$ is the GVD coefficient of FW and T_0 is input pulse duration. Fig 5.2 shows the nonlinearities n_2 as a function of the wavelength in the LN crystal and PPLN crystal.

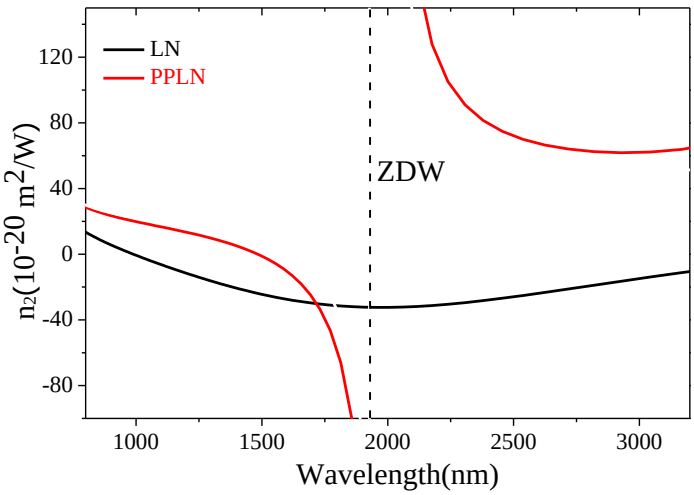

Fig. 5-2 The nonlinearities as a function of the wavelength in LN and PPLN cut for the interaction (e; ee); quadratic and cubic susceptibilities used are [15] d_{33} = 15.6 (pm/V), c_{33} = 75 (pm^2/V^2), f_R =0.35 @ 1060nm.The pith $\Lambda = 29$ μm.

5.3 Phase-matching conditions

Since the largest quadratic susceptibility in LN is d_{33}, we consider type 0 QPM geometry in this quadratic cascading interaction. The analytic signal coupled wave equations governing the propagation of the FF and SH waves in the PPLN can be described as:

$$\frac{\partial A_1(\xi,\tau)}{\partial \xi} + iD_1A_1(\xi,\tau) =$$

$$-\mathrm{i}\frac{\hat{\chi}^{(2)}_{e;ee}\omega}{4cn_e(\omega_1)}(\omega_1-\mathrm{i}\frac{\partial}{\partial\tau})[4A_1^*A_2e^{-\mathrm{i}\Delta k_{eff}\xi}+A_1A_1^*e^{-\mathrm{i}(\Delta k_{pg}-\frac{2\pi}{\Lambda})\xi-\mathrm{i}\omega_1\tau}]_+ \tag{5-6}$$

$$\frac{\partial A_2(\xi,\tau)}{\partial z}+[-d_{12}\frac{\partial}{\partial\tau}+\mathrm{i}D_2]A_2(\xi,\tau)=-\mathrm{i}\frac{\hat{\chi}^{(2)}_{e;ee}\omega}{4cn_e(\omega_2)}(\omega_2-\ \mathrm{i}\frac{\partial}{\partial\tau})[\,4A_1A_1e^{\mathrm{i}\Delta k_{eff}\xi}]_+ \tag{5-7}$$

where$k_1(\omega_1)$ is the group velocity, the group velocity phase-mismatch factor is $\Delta k_{pg}=k_1(\omega_1)\omega_1-k(\omega_1)$,$D_{1,2}=\sum_{m=2}^{\infty}\frac{1}{m!}\frac{d^m\beta(\omega_0)}{d\omega^m}(-\mathrm{i}\frac{\partial^m}{\partial\tau^m})$ are group velocity dispersion, the group velocity mismatch is defined as $d_{12}=\ k_1(\omega_1)-\ k_1(\omega_2),\ \hat{\chi}^{(2)}_{e;ee}=2d33$ denotes the effective nonlinear coefficient.

The nonlinear Schrödinger-like (NLS-like) equation in the largely phase-mismatched SHG process in the PPLN can be derived as the standard procedures[16]：

$$\mathrm{i}\frac{\partial A_1(\xi,\tau)}{\partial\xi}-D_1A_1(\xi,\tau)$$
$$=\left[N^2_{casc}|A_1|^2A_1+\kappa_2A_1A_1^*e^{-\mathrm{i}(\Delta k_{pg}-\frac{2\pi}{\Lambda})\xi-\mathrm{i}\omega_1\tau}\right]_+ \tag{5-8}$$

The pre-factor is understood as the dimensionless soliton number $N^2_{casc}=\frac{\hat{\chi}^{(2)\ 2}_{e;ee}}{4\Delta k_{eff}c^2n_e(\omega_1)n_e(\omega_2)}$ and $\kappa_2=\frac{\hat{\chi}^{(2)}_{e;ee}}{4cn_e(\omega_1)}$.

We look for solutions of Eq. (5-8) in the form

$$A_1(\xi,\tau)=F(\tau)e^{\mathrm{i}q\xi}+g(\xi,\tau), \tag{5-9}$$

where $F(\tau)$ is the envelope of the optical soliton, q is the shift of the soliton wave number and g is a small amplitude dispersive wave.After substitution into Eq. (5-8), assuming that g is a linear wave we derive：

$$\left[\mathrm{i}\,\partial_\xi+D_1(\mathrm{i}\,\partial_\tau)\right]g+\gamma_2F^2(\tau)g^*(\xi,\tau)e^{2\mathrm{i}q\xi}+2\gamma_2F^2(\tau)g(\xi,\tau)+\gamma_{22}F(\tau)g^*(\xi,\tau)e^{\mathrm{i}q\xi+\mathrm{i}(\Delta k_{pg}-\frac{2\pi}{\Lambda})\xi-\mathrm{i}\omega_1\tau}$$
$$=-[D_1(\mathrm{i}\,\partial_\tau)+1/2\beta_2\,\partial_\tau^2]F(\tau)e^{\mathrm{i}q\xi} \tag{5-10}$$

Eq. (5-10) is the solution of dispersive wave which should have continuum mode on the right-hand side. Thus, the phase-matching conditions are easily found:

$$D_1\,(\Omega)=q, \tag{5-11}$$

$$D_1(\Omega)=2q-D_1(dw), \tag{5-12}$$

$$D_1(\Omega) = D_1(dw), \tag{5-13}$$

$$D_1(\Omega) = q + \Delta k_{pg} - \frac{2\pi}{\Lambda}. \tag{5-14}$$

where $D_1(dw) = q$, Equation (5-11) is a well-known condition giving the frequencies of the resonance waves emitted by the soliton so-called Cherenkov resonances. Equations (5-12) and (5-13) are degenerate FWM resonances, which are driven between the solitons and dispersive wave see $F^2(\tau)g^*(\xi,\tau)e^{2iq\xi}$ and $F^2(\tau)g(\xi,\tau)$ terms on the left-hand side of Eq. (5-10). Equations (5-14) give negative frequencies regarding TWM (DFG) resonances which depend on the $F(\tau)g^*(\xi,\tau)$ term.

For the SH only linear wave:

$$[i\partial_\xi + -d_{12}\frac{\partial}{\partial\tau} + iD_2]g = \frac{\hat{\chi}^{(2)}_{e;ee}\omega}{cn_e(\omega_2)}F^2(\tau)e^{i2q\xi+i\Delta k_{eff}\xi} \tag{5-15}$$

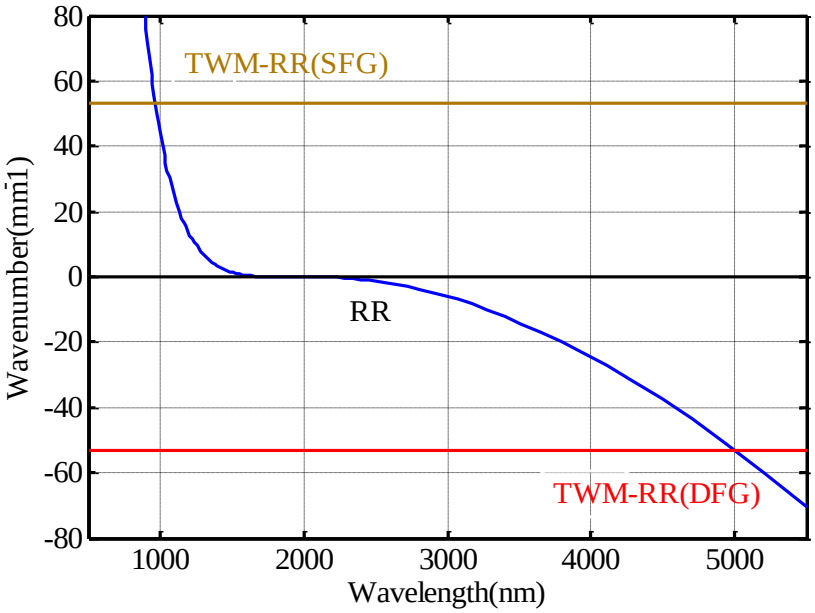

Fig 5-3.The phase matching conditions in PPLN, The soliton wavelength at 1730nm, and the pith $\Lambda = 29$ μm.

The three wave mixing radiation phase matching is：

$$D_2(\Omega) = \Delta k_{eff} + 2q$$

$$= d_{12}\Omega - \sum_{m=2}^{+\infty}\frac{\beta^{(m)}(\omega_2)\Omega^m}{m!}$$

Thus, the phase matching condition depends on the $F^2(\tau)e^{i2q\xi+i\Delta k_{eff}\xi}$ term can be written as:

$$D_1(\Omega) = -\Delta k_{pg} + \frac{2\pi}{\Lambda} + 2q. \tag{5-16}$$

The TWM (DFG) resonances is strongly redshifted with respect to the pump, if $\Delta k_{pg} - \frac{2\pi}{\Lambda} < 0$. Figure 5-3 shows the phase matching curve $D_1(\Omega)$ versus pump wavelength together with its intersections with q, $-\Delta k_{pg} + \frac{2\pi}{\Lambda}$ and $\Delta k_{pg} - \frac{2\pi}{\Lambda}$, which give respectively the RR, TWM (SFG) and TWM (DFG) frequencies.

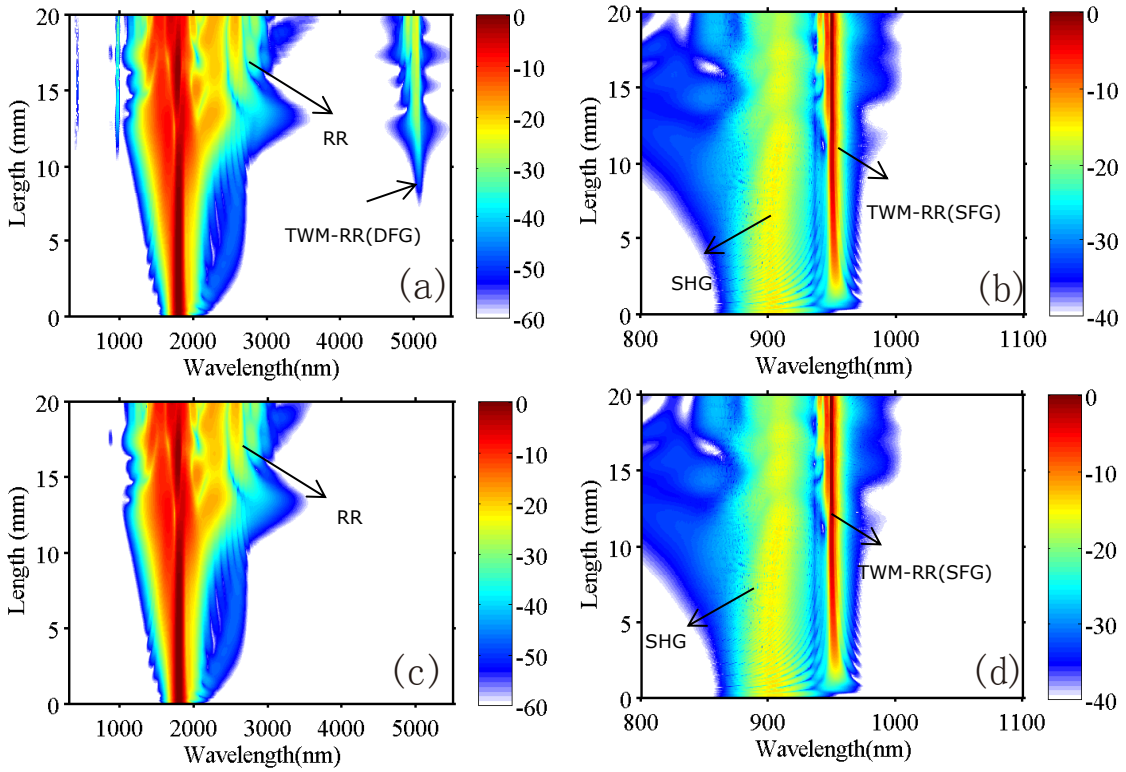

Fig.5-4 (a) Contour plot of the spectral evolution of a short pulse in PPLN, obtained by direct simulation of Eq. (5-5) and Eq. (5-6) The pulse is pumped at λ_0 =1.730 nm, with a peak intensity of 50 GW/cm^2 and a duration 60 fs. All plots are in logarithmic scale.

Here we support the above theory with numerical simulations performed by analytic signal coupled equations Eq. (5-5) and (5.6). Fig. 5-4 we show the spectral evolution in the PPLN crystal, with a pump wavelength $\lambda = 1.73$ μm,, a 60 fs pulse, and peak intensity I=50 GW/cm^2. Figure 3(a, d) show FW and SH spectral evolution obtained by solving Eq. (5-5) and (5.6). Both TWM-RR (SFG) and TWM-RR (DFG) emissions are visible; see Fig. 5-4 (a) and (b). Figure 3(c, d) show the same

simulation as in Fig. 3(a, b) but when switching off the $A_1 A_1^*$ term. No TWM-RR (DFG) is generated in this case, showing that such radiation is indeed coming from the interaction between the positive and the negative frequency spectral components $A_1 A_1^*$. This resonant radiation is the standard three wave mixing process; unlike the well know soliton-induced optical Cherenkov radiation which due to degenerate four wave mixing. It is here worth to emphasize that ordinary coupled-wave envelope equations do not contain the results shown here, in particular the tunable mid-IR RR is absent.

5.4 Experiments and discuses

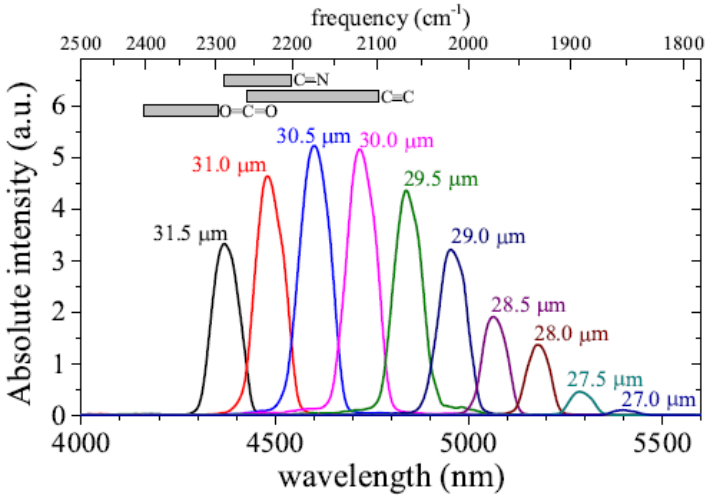

Figure 5-5 Parametrically tunable mid-IR dispersive wave for various PPLN grating pitch values.

The pump laser is a 1 kHz OPA system and we tune the OPA output wavelength from 1.55 to 1.85 μm during the experiment, which in normal dispersion region in LN. The pulse duration of the pump is around 60 fs. A few pieces of bulk PPLN crystals with multi-grating structures were investigated. All spectra (Fig 5-5) were recorded one after another in the same bulk PPLN crystal with the pump laser fixed (λ = 1.73 μm, 60 fs FWHM, peak intensity 55 GW/cm^2), and the pitch was varied by displacing the multiple-grating PPLN crystal. The intensity magnitude of each recording is therefore absolute and can be related to the other measurements. The inset bars indicate the IR absorption bands present in this range when exciting the main IR stretching modes in the

ground tone, which, apart from the well-known band for CO_2 in the gas phase, include the important alkyne and nitrile stretching modes.

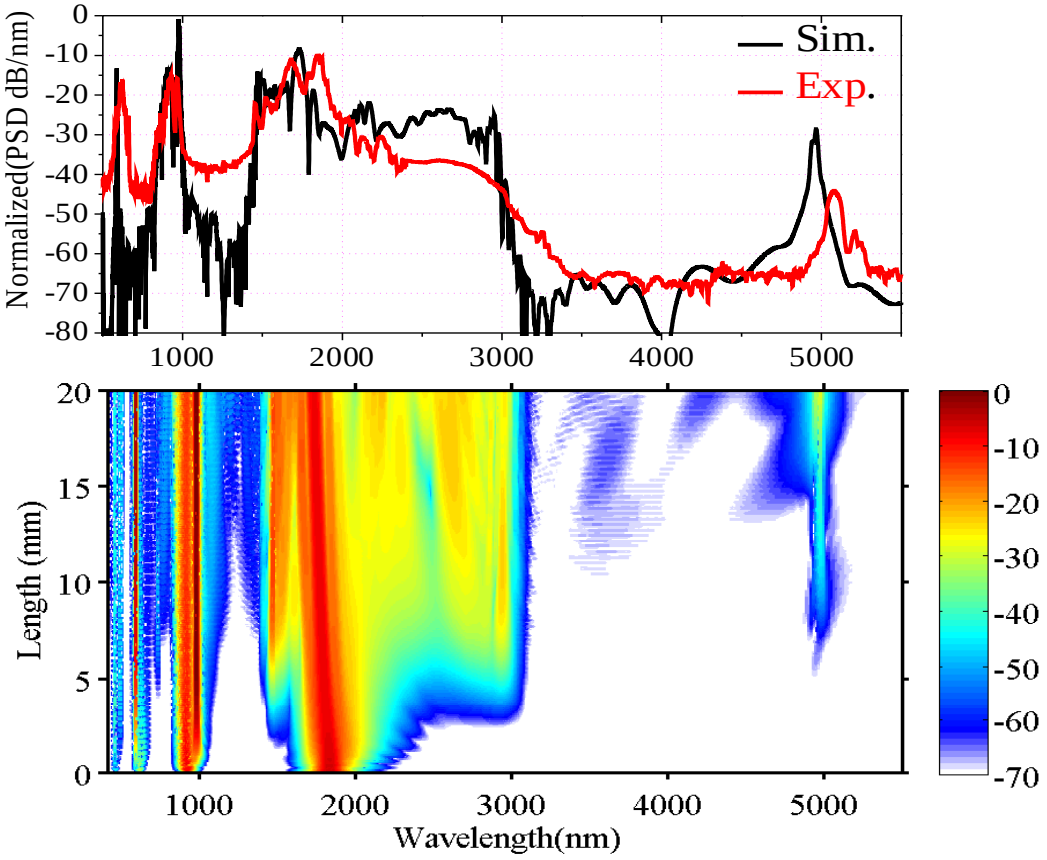

Fig. 5-6 Top: Typical decade-spanning supercontinuum, here recorded for λ = 1.73 μm, peak intensity 55 GW/cm^2 and Λ= 29 μm. Bottom: NFWEs simulation of PPLN propagation. The pump laser was λ = 1.73 μm, 60 fs FWHM, peak intensity 55 GW/cm^2, and the pitch is Λ= 29 μm

We have simulated the propagation of a pulse of duration 60 fs launched in a 20-mm PPLN with a grating pitch value Λ= 29 μm. Numerical simulation used nonlinear wave equations in frequency domain model. The supercontinuum spans over a decade (0.4−5.5 μm), practically the entire LN transmission range. At z= 5mm coincides with maximum spectral broadening, there is a RR emission in the anomalous dispersion regime at 3000 nm. This phenomenon previously observed numerically and experimentally in the LN, can be explained as phase-matched resonant transfer of energy between soliton and RR [17].The spectrum around 1.0 μm stems from an up-converted RR in the SH sideband [18].The most striking observation in Fig. 5-6 is the strong emission of a band of

mid-IR light at ~5μm, which wavelength longer than the RR, exactly like in the experiment (see Fig 5-5). We verified that it was caused by the TWM phase-matching to the soliton. The recorded MIR tuning data shows excellent agreement with the theoretically calculated curve, as shown in Fig.5-7.

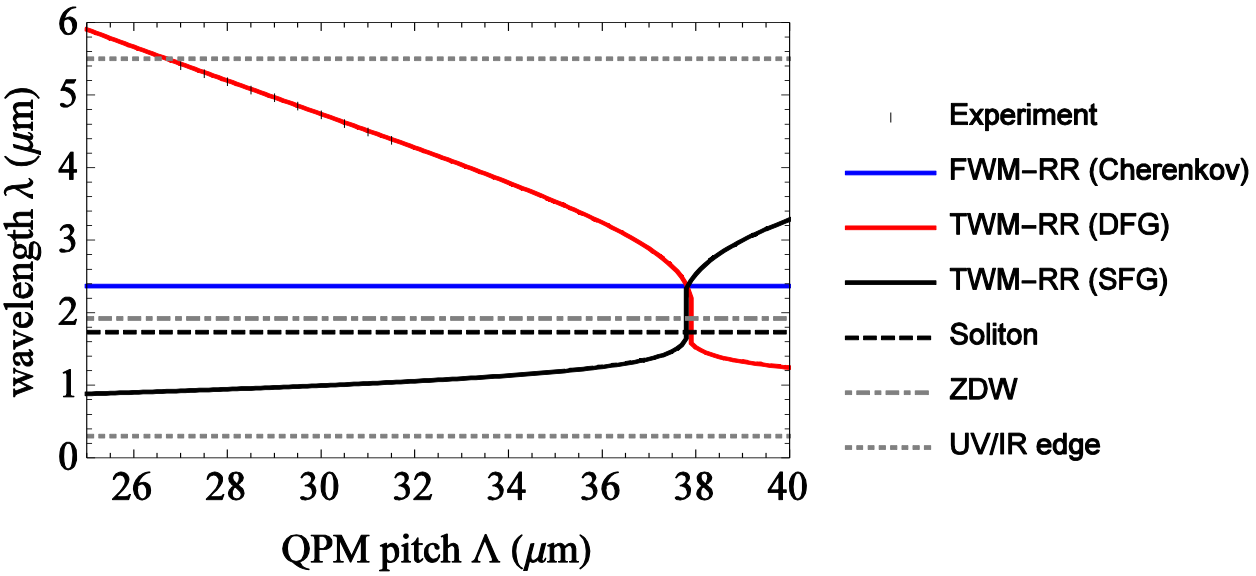

Fig. 5.7. The tuning curves predicted by theory, showing excellent agreement with the experimental data.

5.5 Conclusion

In conclusion, we demonstrate the concept by pumping a standard PPLN bulk crystal with an energetic near-IR femtosecond pump laser, and show efficient generation of mid-IR broadband pulses, tunable in the 4.0-5.5 μm regimes simply by changing the pitch length of the poling. Since the whole process requires only a single near-IR pump, it constitutes an entirely different approach to ultrafast mid-IR parametric amplification.

Bibliography

[1] L. E. Myers and W. R. Bosenberg, "Periodically poled lithium niobate and quasi-phase-matched optical parametric oscillators," IEEE J. Quantum Electron. 33(10), 1663–1672 (1997).

[2] C. Erny, K. Moutzouris, J. Biegert, D. Kühlke, F. Adler, A. Leitenstorfer, and U. Keller, "Mid-infrared difference-frequency generation of ultrashort pulses tunable between 3.2 and

4.8 μm from a compact fiber source," Opt. Lett. 32(9), 1138–1140 (2007).

[3] K. Krzempek, G. Sobon, J. Sotor, G. Dudzik, and K. M. Abramski, "Widely tunable, all-polarization maintaining, monolithic mid-infrared radiation source based on differential frequency generation in PPLN crystal," Laser Phys. Lett. 11(10), 105103 (2014).

[4] A. Galvanauskas, A. Hariharan, D. Harter, M. A. Arbore, and M. M. Fejer, "High-energy femtosecond pulse amlification in a quasi-phase-matched parametric amplifier," Opt. Lett. 23(3), 210–212 (1998).

[5] C. Heese, C. R. Phillips, B. W. Mayer, L. Gallmann, M. M. Fejer, and U. Keller, "75 MW few-cycle mid-infrared pulses from a collinear apodized APPLN-based OPCPA," Opt. Express 20(24), 26888–26894 (2012).

[6] J. Moses, S.-W. Huang, K.-H. Hong, O. D. Mücke, E. L. Falcão-Filho, A. Benedick, F. Ö. Ilday, A. Dergachev, J. A. Bolger, B. J. Eggleton, and F. X. Kärtner, "Highly stable ultrabroadband mid-IR optical parametric chirped-pulse amplifier optimized for superfluorescence suppression," Opt. Lett. 34(11), 1639–1641 (2009).

[7] M. Baudisch, M. Hemmer, H. Pires, and J. Biegert, "Performance of MgO:PPLN, KTA, and $KNbO_3$ for mid-wave infrared broadband parametric amplification at high average power," Opt. Lett. 39(20), 5802–5805 (2014).

[8] X. Zhang, A. L. Lytle, T. Popmintchev, X. Zhou, H. C. Kapteyn, M. M. Murnane, and O. Cohen, "Quasi-phase-matching and quantum-path control of high-harmonic generation using counterpropagating light," Nat. Phys. 3(4), 270–275 (2007).

[9] C. Langrock, S. Kumar, J. E. McGeehan, A. E. Willner, and M. M. Fejer, "All-optical signal processing using $\chi(2)$ nonlinearities in guided-wave devices," J. Lightwave Technol. 24(7), 2579–2592 (2006).

[10] G. Imeshev, A. Galvanauskas, D. Harter, M. A. Arbore, M. Proctor, and M. M. Fejer,

"Engineerable femtosecond pulse shaping by second-harmonic generation with Fourier synthetic quasi-phase-matching gratings," Opt. Lett.23, 864-866 (1998)

[11] C. R. Phillips, Carsten Langrock, J. S. Pelc, M. M. Fejer, I. Hartl, and Martin E. Fermann, "Supercontinuum generation in quasi-phasematched waveguides," Opt. Express 19, 18754-18773 (2011)

[12] C. R. Phillips, Carsten Langrock, J. S. Pelc, M. M. Fejer, J. Jiang, Martin E. Fermann, and I. Hartl, "Supercontinuum generation in quasi-phase-matched LiNbO3 waveguide pumped by a Tm-doped fiber laser system," Opt. Lett. 36, 3912-3914 (2011)

[13] http://deltroniccrystalindustries.com/deltronic_crystal_products/pp_materials/ppln

[14] M. Bache and R. Schiek, "Review of measurements of kerr nonlinearities in lithium niobate: the role of the delayed raman response," arXiv e-print p. 1211.1721 (2012).

[15] D. Nikogosyan, Nonlinear Optical Crystals: A Complete Survey (Springer- Science, 2006).

[16] M. Bache, "Scaling laws for soliton pulse compression by cascaded quadratic nonlinearities," J. Opt. Soc. Am. B 24, 2752–2762 (2007).

[17] Binbin Zhou, Hairun Guo, and Morten Bache, "Energetic mid-IR femtosecond pulse generation by self-defocusing soliton-induced dispersive waves in a bulk quadratic nonlinear crystal," Opt. Express 23, 6924-6936 (2015)

[18] B. B. Zhou, H. R. Guo, and M. Bache, "Soliton-induced nonlocal resonances observed through high-intensity tunable spectrally compressed second-harmonic peaks," Phys. Rev. A 90, 013823 (2014).

Chapter 6

Octave-spanning Supercontinuum Generation in a Silicon-rich Nitride Waveguide

6.1 Introduction

Recently, there is a growing interest in supercontinuum generation (SCG) in photonic integrated waveguides. This promises highly efficient SCG in different regions of the electromagnetic spectrum with extremely low pump pulse energies delivered by near-IR ultrafast femtosecond fiber lasers. Some of the recent waveguide platforms that have demonstrated near-IR pumped octave-spanning broadened spectra include lithium niobate (LN) [1], chalcogenides [4], InGaP membranes [5] and silicon [6].

Silicon nitride is a material platform highly suitable for nonlinear optics applications. The nonlinear coefficient in bulk is ten times larger than silica glass and its transparency window covers from the UV to >6 mm. This material does not display two-photon absorption in the telecommunications wavelength band and waveguides can be engineered with very low propagation losses. Nonlinear applications demonstrated so far include microresonator comb generation [7] , supercontinuum [8], and other high-speed optical signal processing.

However, a well-known challenge with silicon nitride is that in order to achieve anomalous dispersion in the telecom band, the waveguide core requires a thickness beyond 500 nm where silicon nitride films tend to crack [11].Advanced fabrication methods to overcome film cracking have been recently developed [11]. An alternative procedure to circumvent the fabrication challenges of thick silicon nitride films is increasing slightly the silicon content during deposition (silicon-rich nitride [12]). The resulting material structure shows a higher refractive index and nonlinear Kerr coefficient than stoichiometric silicon nitride [13].

In this chapter, we report an octave-spanning supercontinuum in a silicon-rich nitride waveguide pumped with a mode-locked femtosecond erbium fiber laser. The simulations indicate that the spectra are highly coherent.

6.2 Supercontinuum generation and results

Our silicon nitride film is fabricated in a low-pressure chemical vapor deposition process [14]. The waveguide patterns are transferred by standard deep UV contact lithography followed by dry etching. The silica top cladding is done in a plasma enhanced chemical vapor deposition process. The waveguides feature losses of 1.5 dB/cm and a Kerr parameter of 6 $(Wm)^{-1}$ around 1550 nm. The waveguide dimensions are displayed in Fig.6-1. The slight tilt in the walls is a consequence of the etching process. The effect is included in the numerical finite-element simulations (COMSOL) of the group-velocity dispersion (GVD) parameter shown in Fig. 6-1. It has two zero-dispersion wavelengths (ZDWs) giving a broad region (spanning 700 nm) with flat and moderate anomalous dispersion, centered around 1550 nm. The long-wavelength ZDW is controllable by varying the waveguide height. Such a dispersion profile is desired for efficient supercontinuum generation.

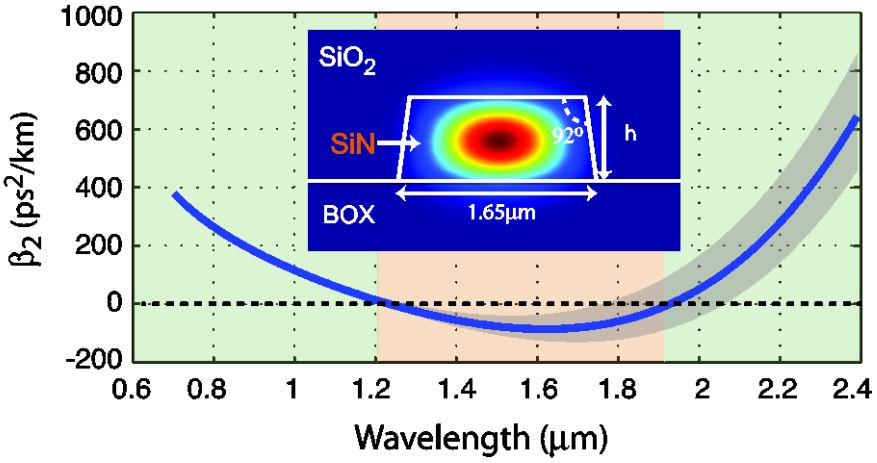

Fig. 6-1 Numerically calculated GVD for the waveguide. As described by the shadowed area, by varying the height of the waveguide h from 650 nm to 740 nm the second ZDW can be tuned from 1.7 to 2.1 μm. The blue solid line corresponds to h= 695 nm. (Inset) Cross-section geometry and modal confinement of power for fundamental quasi TE mode.

The experimental setup is displayed in Fig. 6-2.The femtosecond fiber laser (Toptica) produces laser pulses at 90 MHz repetition rate, centered at 1550 nm. The bandwidth (33 nm FWHM) supports a transform-limited 105 fs (FWHM) Gaussian shaped pulse. The pulses were free-space coupled by an objective lens into a DCF that compensated for the accumulated chirp before the

waveguide. NDFs were used to control the pulse energy, and the polarization was controlled with an FPC. This was followed by a piece of single-mode fiber spliced to a tapered lensed fiber (based on SMF-28, from OZ Optics), which focuses to a 2.0 μm FWHM spot size. We used an intensity autocorrelator to estimate the pulse duration to 130 fs FWHM (assuming a Gaussian shape) at the waveguide entrance, revealing some remaining chirp in the pulse. The maximum total power before the waveguide was measured to 42 mW. The output from the waveguide is collected with a tapered lensed fiber and sent to an optical spectrum analyzer (OSA). To record the supercontinuum, we used two OSAs with spectral ranges 600–1700 nm and 1200–2400 nm, whose spectra were overlapped to get the final spectrum. The coupling loss is estimated at 6.5 dB/facet (TE) and 5.3 dB/facet (TM), providing a maximum input pulse energy of 105 pJ (TE) and 140 pJ (TM) inside the waveguide.

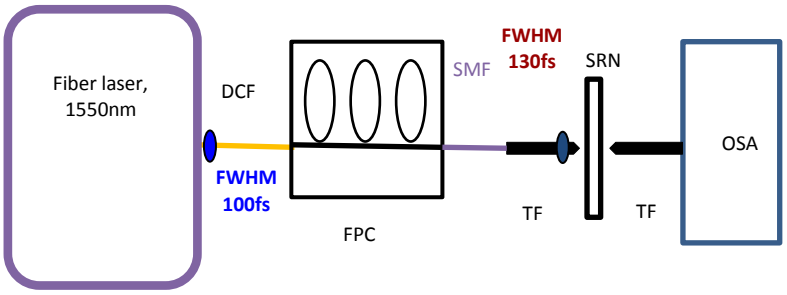

Figure. 6-2 Sketch of experimental setup for supercontinuum generation. DCF: dispersion compensating fiber; SMF: single-mode fiber; FPC: fiber polarization controller; OSA: optical spectrum analyzer.

The spectral evolution of the generated supercontinuum With a TE-polarized pump as a function of input pulse energy is shown in Fig. 6-3. The spectra for low pulse energies are clearly dominated by self-phase modulation (SPM), i.e. early stage broadening before soliton formation occurs. At 78 pJ the soliton has formed, accompanied by two soliton-induced dispersive waves, one on each side of the two ZDWs. The strongest dispersive wave is found at low wavelengths, peaked around 820 nm, while the mid-IR dispersive wave, peaked around 2250 nm, is less powerful and changes

significantly when increasing the pulse energy further to the maximum value of 105 pJ (9 mW average power).

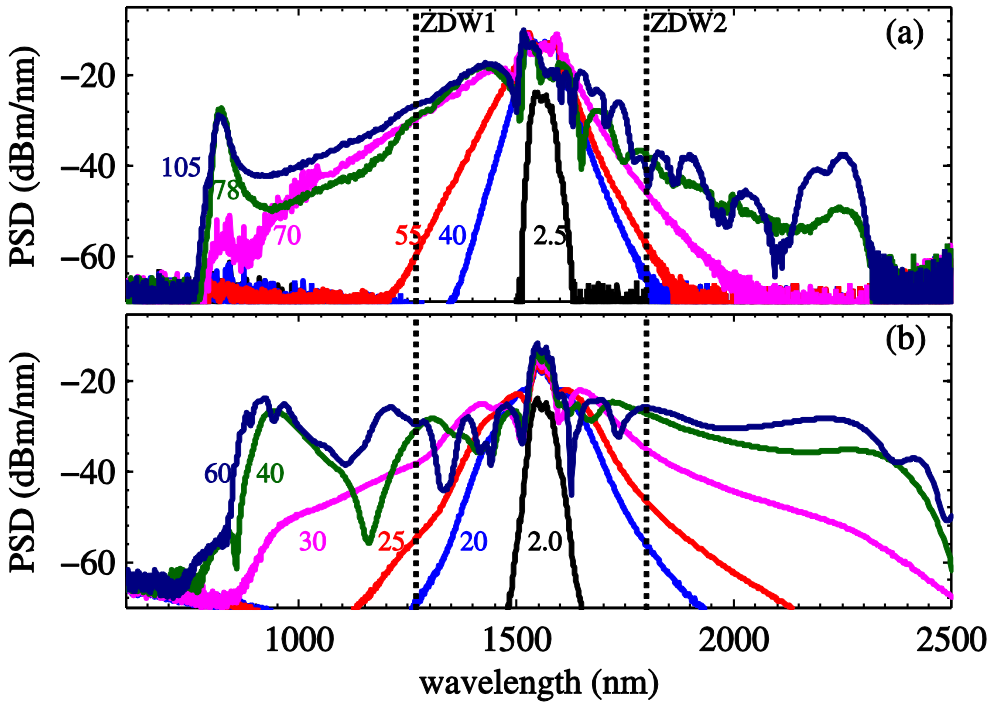

Fig.6-3. (a) Experimentally recorded PSD at the end of the waveguide (corrected for end-facet coupling loss). The numbers show the estimated input pulse energies in pJ. (b) Results of numerical simulations of the TE FM. The spectra show the total PSD at the waveguide end averaged over 50 noise realizations. The pulse was prechirped using GDD = +3500 fs^2, andthe waveguide height was h = 660 nm. The ZDWs are those calculated for a TE-polarization mode using h = 660 nm.

The results are verified with numerical simulations using the so-called nonlinear analytic envelope equation (NAEE) [15], which resolves sub-cycle carrier-wave dynamics and includes a full expansion of the cubic nonlinearity. We only model the waveguide fundamental mode (FM). Its mode effective index and effective area vs. wavelength from the COMSOL calculations were included in the model without truncation. The frequency dependence of the effective mode area was modeled as shown in [16]. The cubic nonlinear coefficient was 5.7 $(Wm)^{-1}$, which is a slightly modified value to that reported in s due to an improved estimate of the linear propagation loss. This propagation loss (1.5 dB/cm was taken constant across the modeled wavelength range. The NAEE model was extended to include delayed Raman nonlinearities[15].A simple model was implemented

based on the Si-N phonon mode centered at 410 cm^{-1}, and having a broadband 70 cm^{-1} linewidth (reflecting the amorphous nature of the silicon nitride thin film). The relative Raman strength was set to $f_R = 0.2$, which is a typical value for amorphous materials. Generally, the Raman effect gave only minor contributions, in line with previous studies of silicon nitride waveguides. An explanation might be that the dispersion engineering leaves only a moderate anomalous dispersion range where the Raman effect can influence the soliton by red-shifting it. Finally, noisy initial conditions were used based on the one-photon-per-mode model [17].

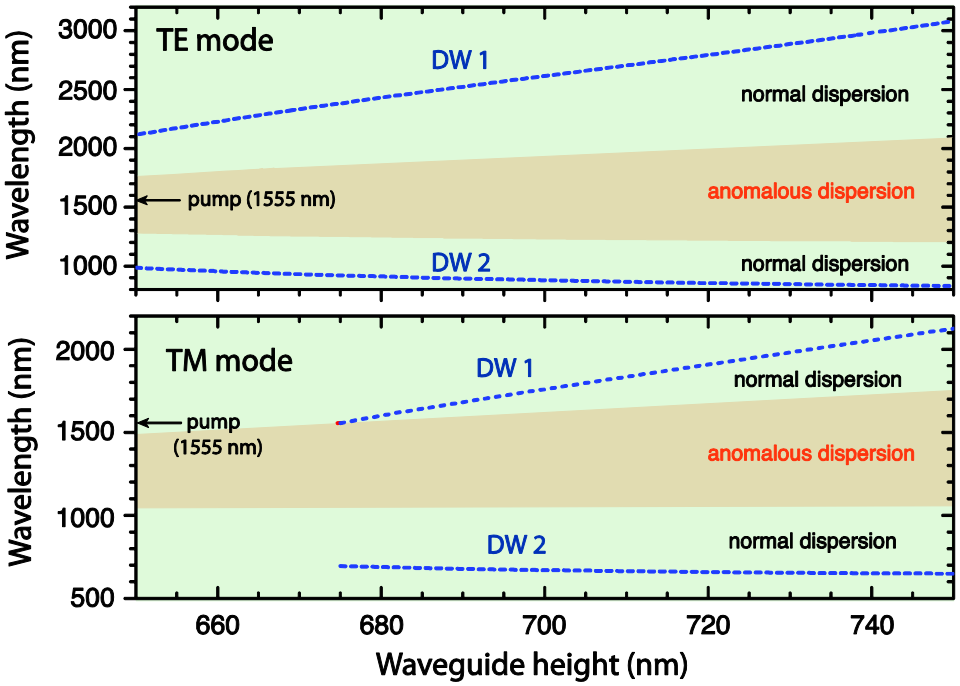

Fig. 6-4. Calculated ZDWs vs. waveguide height h for TE and TM modes. The phase-matching wavelengths for dispersive waves coupling to a soliton at 1555 nm are also shown. Note that for the TM case h > 675 nm to support a soliton at 1555 nm, so no DWs can be found for h < 675 nm.

In Fig. 6-3(b) we show a direct comparison of the numerical simulations to the experimental spectra. The simulations are able to reproduce the major features of the experimental spectra, but noticeably the dispersive waves seem to be narrower in the experimental case, and the near-IR dispersive wave is also located at a somewhat lower wavelength. The waveguide height is important because as Fig. 6-1(a) indicates, it affects the long-wavelength ZDW. Using a smaller waveguide

height will blue-shift this ZDW, the mid-IR dispersive wave, as well as the anomalous dispersion regime. The calculations in Fig. 6-4(a) summarize this by showing the change in the dispersion landscape when varying the waveguide height from 650 to 750 nm. Along the entire range the TE mode has anomalous dispersion at 1555 nm, but only for values below 675 nm was the mid-IR dispersive wave (denoted DW 1) found below 2500 nm and the near-IR dispersive wave (denoted DW 2) below 900 nm. The best match to the experimental results was found with a 660 nm height; similar results were observed in the range 650-675 nm, but for 700 nm and higher the dispersive wave positions did not match the experiments very well, especially for the TM results below

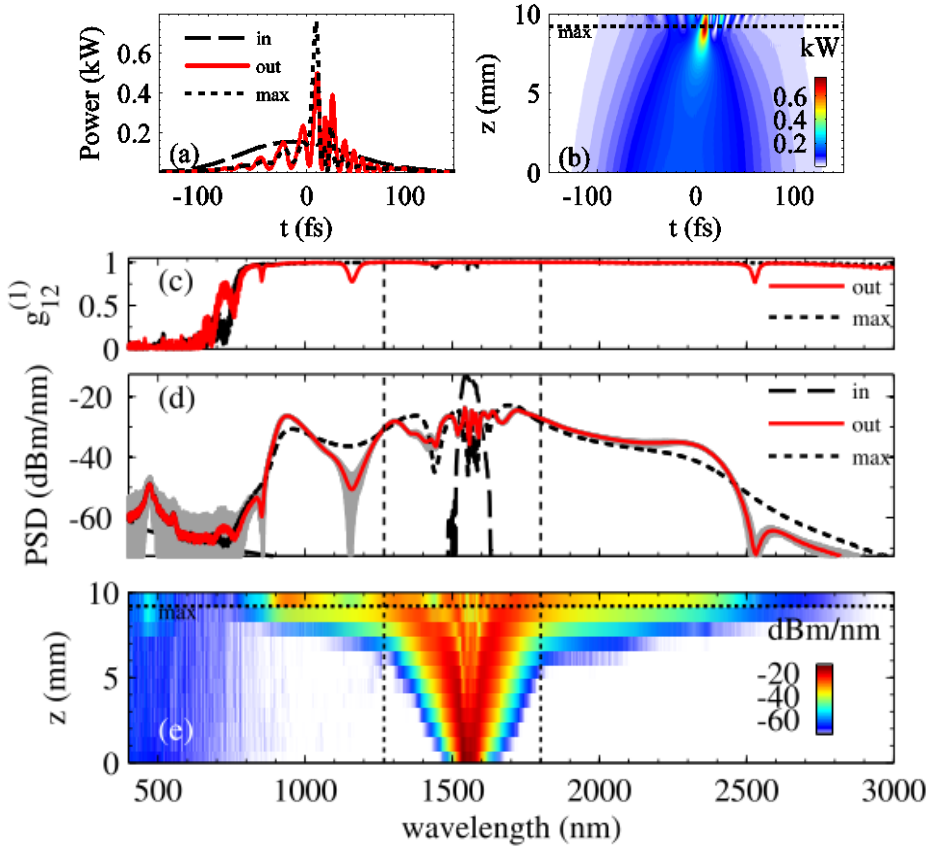

Fig. 6-5. Evolution from a single noise realization of the TE polarization FM (40 pJ total input energy) in (a+ b) time and (e) wavelength. The coherence function (c) and FM spectra (d) were averaged over 50 noise realizations (each shown in gray for the output pulse).

As mentioned, the simulations only model the FM, but from the higher-order modes (HOMs) given by the COMSOL simulations we estimate that around 55% of the input energy will be

coupled to the FM, and the rest goes into the HOMs. The HOMs will typically not show any spectral broadening due to their lower peak powers, higher GVD and mode areas. Experiments therefore often have a portion of the pump input spectrum that remains "undepleted" in the supercontinuum. In the numerical spectra shown in Fig. 6-3(b) we have therefore added the equivalent energy of the HOMs at the end of the simulation as 45% of the total input spectrum. Additionally, combining the 33 nm bandwidth of the input pulse with the measured value of 130 fs FWHM corresponds to a group-delay dispersion of GDD = $\pm$3500 fs^2. The simulations used positive chirp but similar results were found with negative chirp. We note that the simulations used lower energies than the experiments, which can be attributed to uncertainties in coupling efficiencies, waveguide nonlinearity and dispersion, input pulse pre-chirp etc.

In Fig. 6-5 the power was chosen so the soliton forms almost at the waveguide exit. In (a) the soliton forms as a single-cycle spike (5 fs FWHM), and after this self-compression point (’max’ position) the temporal trace quickly develops interference oscillations. This is because the two dispersive waves are now formed by the soliton at the same temporal position but at different wavelengths. In the spectral evolution (e) the dispersive waves are seen to be present at the soliton formation point (’max’), and after this they grow significantly, see also (d). In (d) the shot to shot coherence is shown, as calculated from the first order coherence function. This excellent coherence pertains for lower powers, but it degrades for higher powers; this is quite typical as soliton fission and other nonlinear processes following the soliton formation stage are quite noise sensitive.

The TM case shown in Fig. 6-6(a) does not show strong broadening. Noticeably, though, the spectrum broadens enough to enter the important 1600-1850 nm wavelength range for 3-photon absorption microscopy and coherent anti-Stokes Raman spectroscopy. The spectral shapes indicate normal GVD at the pump wavelength, which leads to optical wave breaking: the pulse in time domain becomes highly chirped and develops steep shock fronts. In frequency domain this is

accompanied by SPM-induced spectral broadening, which has some very characteristic spectral ripples. The spectral broadening is typically much weaker than in the soliton case because no dispersive waves are formed and the pulse does not self-compress. To understand when TM has normal GVD at 1555 nm, Fig. 3 shows this may happen when the height is taken well below 700 nm, as this changes the higher ZDW (ZDW2) from >1900 nm (700 nm height) to <1500 nm (650 nm height). The experimental results therefore again indicate a lower height than the nominal 700 nm, as this would leave the 1555 nm pump pulse in the non-solitonic normal dispersion regime. In fact, the numerical simulations shown in (c) agree well with the experimental results using the exact same parameters as in the TE case.

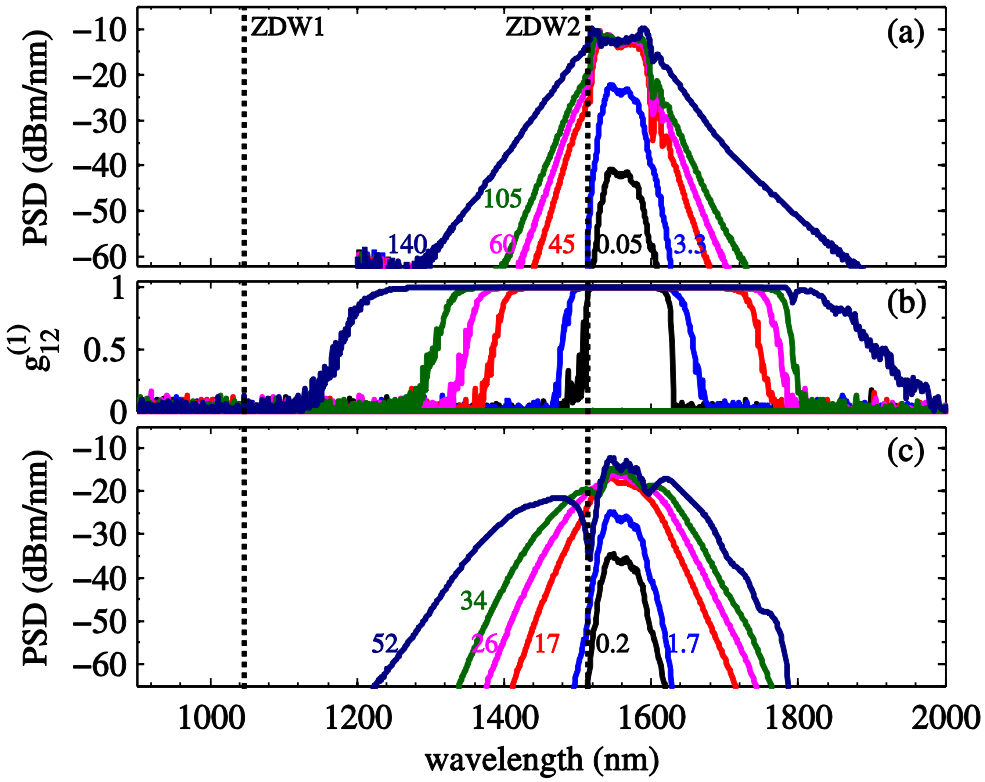

Fig. 6-6 (a) Experimental spectra for various TM pump pulse energies; The ZDWs are those calculated for a TM-polarization mode using a 660 nm waveguide height. (b) and (c) numerical simulations showing the coherence function and average spectra. The simulations used the same waveguide specs (width, height) and input pulse pre-chirp as Fig. 6-3(b).

6.3 Conclusion

In conclusion, we have used a dispersion engineered silicon rich nitride waveguide to study supercontinuum generation by pumping with low-energy pulses (80-140 pJ) from an erbium fiber oscillator. In the TE polarization case a soliton and two dispersive waves were excited to give a 1.5 octave supercontinuum (from 800-2250 nm at -30 dB). With TM polarized pulses, the continuum was generated by optical wave breaking because the waveguide had normal dispersion at the pump wavelength. Numerical results indicate that the supercontinua had an excellent coherence. The dispersion was controlled by varying the stoichiometry of the core material and the cross-section geometry of the waveguide to give anomalous dispersion at the pump wavelength (TE case).

Bibliography

[1] Carsten Langrock, M. M. Fejer, I. Hartl, and Martin E. Fermann, "Generation of octave-spanning spectra inside reverse-proton-exchanged periodically poled lithium niobate waveguides," Opt. Lett. 32, 2478-2480 (2007)

[2] C. R. Phillips, Carsten Langrock, J. S. Pelc, M. M. Fejer, J. Jiang, Martin E. Fermann, and I. Hartl, "Supercontinuum generation in quasi-phase-matched LiNbO3 waveguide pumped by a Tm-doped fiber laser system," Opt. Lett. 36, 3912-3914 (2011).

[3] Hairun Guo, Binbin Zhou, Michael Steinert, Frank Setzpfandt, Thomas Pertsch, Hung-ping Chung, Yen-Hung Chen, and Morten Bache, "Supercontinuum generation in quadratic nonlinear waveguides without quasi-phase matching," Opt. Lett. 40, 629-632 (2015)

[4] Yi Yu, Xin Gai, Ting Wang, Pan Ma, Rongping Wang, Zhiyong Yang, Duk-Yong Choi, Steve Madden, and Barry Luther-Davies, "Mid-infrared supercontinuum generation in chalcogenides," Opt. Mater. Express 3, 1075-1086 (2013)

[5] Utsav D. Dave, Charles Ciret, Simon-Pierre Gorza, Sylvain Combrie, Alfredo De Rossi, Fabrice Raineri, Gunther Roelkens, and Bart Kuyken, "Dispersive-wave-based octave-

spanning supercontinuum generation in InGaP membrane waveguides on a silicon substrate," Opt. Lett. 40, 3584-3587 (2015)

[6] I-Wei Hsieh, Xiaogang Chen, Xiaoping Liu, Jerry I. Dadap, Nicolae C. Panoiu, Cheng-Yun Chou, Fengnian Xia, William M. Green, Yurii A. Vlasov, and Richard M. Osgood, "Supercontinuum generation in silicon photonic wires," Opt. Express 15, 15242-15249 (2007)

[7] Jacob S. Levy, Alexander Gondarenko， Mark A. Foster, Amy C. Turner-Foster, Alexander L. Gaeta and Michal Lipson , “CMOS-compatible multiple-wavelength oscillator for on-chip optical interconnects,” Nature Photon. 4, 37-40 (2010).

[8] Haolan Zhao, Bart Kuyken, Stéphane Clemmen, François Leo, Ananth Subramanian, Ashim Dhakal, Philippe Helin, Simone Severi, Edouard Brainis, Gunther Roelkens, and Roel Baets, "Visible-to-near-infrared octave spanning supercontinuum generation in a silicon nitride waveguide," Opt. Lett. 40, 2177-2180 (2015)

[9] Jörn P. Epping, Tim Hellwig, Marcel Hoekman, Richard Mateman, Arne Leinse, René G. Heideman, Albert van Rees, Peter J.M. van der Slot, Chris J. Lee, Carsten Fallnich, and Klaus-J. Boller, "On-chip visible-to-infrared supercontinuum generation with more than 495 THz spectral bandwidth," Opt. Express 23, 19596-19604 (2015)

[10] Kevin Luke, Avik Dutt, Carl B. Poitras, and Michal Lipson, "Overcoming Si3N4 film stress limitations for high quality factor ring resonators," Opt. Express 21, 22829-22833 (2013)

[11] Jörn P. Epping, Tim Hellwig, Marcel Hoekman, Richard Mateman, Arne Leinse, René G. Heideman, Albert van Rees, Peter J.M. van der Slot, Chris J. Lee, Carsten Fallnich, and Klaus-J. Boller, "On-chip visible-to-infrared supercontinuum generation with more than 495 THz spectral bandwidth," Opt. Express 23, 19596-19604 (2015)

[12] H. T. Philipp, K. N. Andersen, W. Svendsen and H. Ou, "Amorphous silicon rich silicon

nitride optical waveguides for high density integrated optics," in Electronics Letters, vol. 40, no. 7, pp. 419-421(2004).

[13] T. Wang, D. K. T. Ng, S.-K. Ng, Y.-T. Toh, A. K. L. Chee, G. F. R. Chen, Q. Wang, and D. T. H. Tan, "Supercontinuum generation in bandgap engineered, back-end CMOS compatible silicon rich nitride waveguides"Laser & Photonics Reviews 9, 498 (2015).

[14] Clemens J. Krückel, Attila Fülöp, Thomas Klintberg, Jörgen Bengtsson, Peter A. Andrekson, and Víctor Torres-Company, "Linear and nonlinear characterization of low-stress high-confinement silicon-rich nitride waveguides," Opt. Express 23, 25827-25837 (2015)

[15] M. Bache, "The nonlinear analytical envelope equation in quadratic nonlinear crystals," (2016). arXiv:1603.00188

[16] J. Lægsgaard, "Mode profile dispersion in the generalized nonlinear Schrödinger equation," Opt. Express 15, 16110-16123 (2007)

[17] John M. Dudley and Stéphane Coen, "Coherence properties of supercontinuum spectra generated in photonic crystal and tapered optical fibers," Opt. Lett. 27, 1180-1182 (2002)

Chapter 7

Conclusions and Outlooks

7.1 Conclusions

In this thesis, we investigated the Ph.D. project: **Femtosecond few-cycle mid-infrared laser pulses.** The works were forced on optical solitons in near-IR for generating the mid-IR pulses.

Firstly, we demonstrated theoretically and numerically a new method for generating mid-IR pulses which based on the collision of the self-defocusing soliton and a weak probe in quadratic crystal.

A near-perfect conversion efficiency is possible for a high effective soliton order. A near-IR soliton induced by a cascaded quadratic $\chi^{(2)}$ nonlinearity forms in normal GVD regime, and the soliton emitted DW in the anomalous GVD regime in the mid-IR by degenerate four wave mixing. The higher order of the soliton colliding with a weak near-IR probe induces a cascaded sum-frequency generation nonlinearity generating a self-defocusing Kerr-like effective negative cross phase modulation term. The tunable femtosecond mid-IR converted wave is formed between $\lambda = 2.2 - 2.4$ μm as a resonant dispersive wave by non-degenerate four-wave mixing process.

Secondly, we theoretically studied three-wave mixing resonant radiation in the quadratic crystal.

By controlling the angle of incidence light, the higher order of the soliton colliding with a weak near-IR probe induces a cascaded sum-frequency generation nonlinearity generating a self-defocusing Kerr-like effective positive cross phase modulation term. The femtosecond visible converted wave is formed as a resonant dispersive wave by three-wave mixing parametric amplification process.

A defocusing soliton-driven tunable mid-IR optical parametric amplifier is demonstrated for the first time in a standard periodically poled lithium niobate (PPLN) bulk crystal with one fixed near-IR pump wavelength. This unique tunable resonant radiation from $\lambda = 4.2 - 5.5$ μm is generated by three-wave mixing process from the self-defocusing soliton simply by changing the pitch length of the poling.

Finally, a soliton and two dispersive waves were excited in a dispersion engineered silicon rich nitride to give waveguide 1.5 octave supercontinuum in the TE polarization case by pumping with low-energy pulses (80-140 pJ) from an erbium fiber oscillator.

7.2 Outlooks

During the project, we noticed that ultrafast optical solitons in the nonlinear optical not only accompanied with the frequency conversion, but also rich in physical meaning. *But what are the project's unsolved problems and future challenges?*

I .The collision of soliton and a weak probe

We are looking forward to verify experimentally the collision of the soliton and a weak probe in the BBO crystal and other mid-IR transparent crystals [1]. This simple and effective method provide a good solution for mid-IR ultrashort pulse generation. Moreover, this kind of collision contains a lot of physical and applications, such as analog an artificial event horizon [2], all-optical transistor [4] and black hole laser [5].

II .Optical parametric amplifier based on the microresonator

The Kerr comb generation based on continuous-wave-pumped optical microresonators utilizes the high quality factor of microresonators which enhances the cubic nonlinearity of the material by four wave mixing[6].The DWs can be simultaneously excited when pumping in either the anomalous or normal dispersion regimes by four wave mixing. And analogous frequency comb based on cascaded quadratic nonlinearities also have been demonstrated [10]. Thus, using continuous-wave-pumped quasi phase-matching microresonators generate the three-wave mixing resonant radiation will be a promising direction.

III .The silicon-rich nitride waveguide

The silicon-rich nitride approach allows increasing the waveguide height to give mid-IR dispersive waves beyond 3000 nm, making it feasible to generate >2 octaves of bandwidth

with almost perfect coherence. Thus, these show promises for short-range near-IR and mid-IR coherent supercontinua generation in a CMOS-compatible waveguide by exploiting the mature erbium-fiber laser technology.

We are looking forward to more and more researchers interested in the mid-IR pulse, which will bring new insights into nonlinear optics, physics and even to our life.

Bibliography

[1] M. Bache, H. R. Guo, and B. B. Zhou, “Generating mid-IR octave-spanning supercontinua and few-cycle pulses with solitons in phase-mismatched quadratic nonlinear crystals,” Opt. Mater. Express 3, 1647–1657 (2013)

[2] T. G. Philbin, C. Kuklewicz, S. Robertson, S. Hill,F. K¨onig, and U. Leonhardt, “Fiber-optical analog of the event horizon,” Science 319, 1367–1370 (2008).

[3] K. E. Webb, M. Erkintalo, Y. Xu, N. G. R. Broderick, J. M. Dudley, G. Genty, and S. G. Murdoch, “Nonlinear optics of fibre event horizons,” Nat. Commun. 5, 4969 (2014).

[4] A. Demircan, S. Amiranashvili, and G. Steinmeyer,“Controlling light by light with an optical event horizon,”Phys. Rev. Lett. 106, 163901 (2011).

[5] Faccio, D., Arane, T., Lamperti, M. & Leonhardt, U. “Optical black hole lasers”. Class. Quantum Grav. 29, 224009 (2012)

[6] T. J. Kippenberg, S. M. Spillane, and K. J. Vahala, "Kerr-nonlinearity optical parametric oscillation in an ultrahigh-Q toroid microcavity," Phys. Rev. Lett. 93, 083904 (2004).

[7] I. H. Agha, Y. Okawachi, M. A. Foster, J. E. Sharping, and A. L. Gaeta, "Four-wave mixing parametric oscillations in dispersion-compensated high-Q silica microspheres,"Phys. Rev. A 76, 043837 (2007).

[8] P. Del'Haye, T. Herr, E. Gavartin, M. L. Gorodetsky, R. Holzwarth, and T. J. Kippenberg,"Octave Spanning Tunable Frequency Comb from a Microresonator," Phys. Rev.

Lett.107, 063901 (2011).

[9] Y. Okawachi, K. Saha, J. S. Levy, Y. H. Wen, M. Lipson, and A. L. Gaeta, "Octavespanning frequency comb generation in a silicon nitride chip," Opt. Lett. 36, 3398 (2011).

[10] Ville Ulvila, C. R. Phillips, Lauri Halonen, and Markku Vainio, "Spectral characterization of a frequency comb based on cascaded quadratic nonlinearities inside an optical parametric oscillator," Phys. Rev. A 92, 033816 (2015).

Appendix A:

MATLAB Code:CAWEs Equation

```
clear;
clc;
close all;
format long
global   chi2 chi3 dt qpm_k  li  omega_e w n_e c t dk_e dz wfh kfhe delta_k wsh ish isw
li=i;
qpm_k =2*pi/30;%pith
c = 0.299792458; % um/fs
fftw('planner', 'hybrid');
%-------------------------------------------------------------
% --- chi2 & chi3 --- crystal  PPLN
deg=90;
theta = deg*pi/180;
fai   = pi/6;
d22 =  1.92e-6; % um/V                    ( 2.60e-6 um/V at 1064nm, HCP Co.)
d31 = -4.40e-6; % um/V from the handbook! (-4.60e-6 um/V at 1064nm, HCP Co.)
d33 = 20.5e-6; % um/V from the handbook! (25.00e-6 um/V at 1064nm, HCP Co.)
deff = zeros(3,6);
deff(1,1) = -3*d31*cos(theta)^2*sin(theta) ...
          -d33*sin(theta)^2 ...
          -d22*cos(theta)^2*sin(3*fai);   % e,ee
deff(1,2) = -d31*sin(theta) ...
          +d22*cos(theta)*sin(3*fai);     % e,oo
deff(1,6) = -2*d22*cos(theta)^2*cos(3*fai); % e,oe or e,eo

deff(2,1) = -d22*cos(theta)^2*cos(3*fai);   % o,ee
deff(2,2) =  d22*cos(3*fai);                % o,oo
deff(2,6) = -2*d31*sin(theta) ...
          +2*d22*cos(theta)*sin(3*fai);   % o,oe or o,eo
chi2 = deff*2;
c0   = 299792458; % Vacuum speed of light in m/s
mu0  = 4e-7*pi;   % [N/A^2]
eps0 = 1/(c0^2*mu0); % [F/m]
c11 = 0;      % [um^2/V^2]
c33 =52e-10; % [um^2/V^2]
c18 = 0;      % unkown!!!
c110= 0;      % unkown!!!
chi3 = zeros(3,10);
chi3(1,1) =      c11*cos(theta)^4 ...
          -  4*c110*sin(theta)*cos(theta)^3*sin(3*fai) ...
          +3/2*c18*sin(2*theta)^2 ...
          +    c33*sin(theta)^4;                    % e,eee
chi3(1,2) =      c110*sin(theta)*cos(3*fai);          % e,ooo
chi3(1,4) =   -9*c110*sin(theta)*cos(theta)^2*cos(3*fai); % e,eeo or e,eoe or e,oee
chi3(1,6) =      c11*cos(theta)^2 ...
            +3*c18*sin(theta)^2 ...
            +3*c110*sin(2*theta)*sin(3*fai);        % e,ooe or e,oeo or e,eoo

chi3(2,1) =   -3*c110*sin(theta)*cos(theta)^2*cos(3*fai); % o,eee
chi3(2,2) =      c11;                               % o,ooo
chi3(2,4) =      c11*cos(theta)^2 ...
```

```
            +3*c18*sin(theta)^2 ...
            +3*c110*sin(2*theta)*sin(3*fai);          % o,eeo or o,eoe or o,oee
chi3(2,6) =    3*c110*sin(theta)*cos(3*fai);            % o,ooe or o,oeo or o,eoo

% --- reference: FH: lambda_o & SH: lambda_e% ----------------------------------
lambda_e = 1.75;
omega_e  = 2*pi*c/lambda_e;
lambda_sh = 1.75/2;
omega_sh  = 2*pi*c/lambda_sh;
deg = 90;
% --- reference wave vector ---
[k, dk] = MgLN_Wave_Vec_deg(omega_e,1,deg);
n_e  = k.fhe*c/omega_e;
dk_e = dk.fhe;
delta_k = k.she - 2*k.fhe;
%--------------------------- SH
[k, dk] = MgLN_Wave_Vec_deg(omega_sh,1,deg);
n_sh  = k.fhe*c/omega_sh;
KKK=n_sh*omega_sh/c;

dk_sh = dk.fhe;
d12=dk_sh -dk_e;
%-----------------------------------------------
% --- time ---
time_span =8000; % fs
% time_num =10*time_span*c/lambda_e;
nt = 2^14;
dt = time_span/nt;
t  = -time_span/2:dt:time_span/2-dt;
% --- frequency ---
omega_span = 2*pi/dt; % fs^-1
dw = omega_span/nt;
w  = -omega_span/2:dw:omega_span/2-dw;
%------------------------------------------------------- FW
wfh=w+omega_e;
lambda_left  = 0.3;
lambda_right =5.5;
omega_left  = 2*pi*c/lambda_right;
omega_right = 2*pi*c/lambda_left;
w1 = find(wfh > omega_left, 1,'first');
w2 = find(wfh< omega_right,1, 'last');

w3 = find(wfh >-omega_right,1,'first');
w4 = find(wfh <-omega_left, 1, 'last');
isw = (wfh>=omega_left & wfh<=omega_right);
%------------------------------------------------------- SH
wsh=w+omega_sh;
w5 = find(wsh > omega_left, 1,'first');
w6 = find(wsh< omega_right,1, 'last');

w7 = find(wsh >-omega_right,1,'first');
w8 = find(wsh <-omega_left, 1, 'last');
ish = (wsh>=omega_left & wsh<=omega_right);
% --- wave vector ----------------------------------------  wave vector FW
k_e_arr = zeros(1,nt);
```

```
k_right = MgLN_Wave_Vec_deg(wfh(w1:w2),0,deg);
k_left  = MgLN_Wave_Vec_deg(wfh(w3:w4),0,deg);
k_e_arr(w1:w2) = k_right.fhe;
 k_e_arr(w3:w4) =k_left.fhe;
%   plot(2*pi*c./wfh, [k_e_arr*c./wfh; (k.fhe+dk_es.*(w-omega_e))]);
   k_e_arr=(k_e_arr-k.fhe-dk_e.*wfh).*isw;      % phase of FW
   plot(2*pi*c./wfh, k_e_arr)
%   k_e_arr=(k_e_arr-(dk_e).*wfh+(dk_e).*wfh)*c./wfh;      % phase of FW
%   plot(2*pi*c./wfh(w1:w2), k_e_arr(w1:w2))
% --- wave vector ----------------------------------------  wave vector % SH
 k_e_arrsh = zeros(1,nt);
k_right = MgLN_Wave_Vec_deg(wsh(w5:w6),0,deg);
k_left  = MgLN_Wave_Vec_deg(wsh(w7:w8),0,deg);
k_e_arrsh(w5:w6) = k_right.fhe;
 k_e_arrsh(w7:w8) =k_left.fhe;

k_e_arrsh=(k_e_arrsh-KKK-dk_sh.*wfh-(d12).*wfh).*ish;   % phase of SH
plot(2*pi*c./wfh,k_e_arrsh)
% --- z ----------------------------------------
intp =50;
zlength =5000;
    dz =1;
    nz = ceil(ceil(zlength/dz+1)/intp+1)*intp;
    z  = 0:dz:(nz-1)*dz;
fprintf('total steps: %8d\n', nz);
eps0 = eps0*1e-6; % F/um
% --- e light
% ----------------------------------------------------------input pluse
I_in_e =80e-14; % 1GW/cm^2 = 1e-14 V^2*F/(fs*um^2)
E_c_e  = sqrt(eps0*n_e*c/2);
E_in_e = sqrt(I_in_e/E_c_e^2); % V/um
FWHM_in_e = 50; % fs
T_in_e = FWHM_in_e/(2*log(1+2^0.5)); % Guassan: exp(-t^2/T0^2).*(cos(t*omega_e )+0*li*sin(t*omega_e ));
E_in_e_arr = 1*E_in_e*sech((t)/T_in_e);
height = E_in_e*sum(sech(t.^2/T_in_e^2))*dt;
%----------------------------------------
  E_in_e_arrsh = zeros(1,nt);
EFE = zeros(nz/intp,w2-w1+1);
EFSH = zeros(nz/intp,w6-w5+1);
%%-----------------------------------------------------
phs_e_arr = exp(-1i*k_e_arr*dz);
phs_e_arr1 = exp(-1i*k_e_arr*dz/2);
phs_e_arr2 = exp(1i*k_e_arr*dz/2).*isw;%%%%%%%%%%%%%%%%% FW

phs_e_arrsh = exp(-1i*k_e_arrsh*dz);
phs_e_arrsh1 = exp(-1i*k_e_arrsh*dz/2);
phs_e_arrsh2 = exp(1i*k_e_arrsh*dz/2).*ish;%%%%%%%%%%%%%%%%% FW
%-0-----------------------------------------------------------
Ef_e_arr = fftshift((fft(E_in_e_arr)*dt)).*phs_e_arr1 ;
Ef_e_arrsh = fftshift((fft(E_in_e_arrsh)*dt)).*phs_e_arrsh1 ;
kfhe=k.fhe;
tic;
for i = 1:nz
     [ Ef_e_arr2] = rk4(@nlin_func_fR,[Ef_e_arr;Ef_e_arrsh],z(i),dz);
     un_fh=Ef_e_arr2(1,:);
```

```
    un_sh=Ef_e_arr2(2,:);

  Ef_e_arr= un_fh.*phs_e_arr;
 Ef_e_arrsh= un_sh.*phs_e_arrsh;
   %     % --- interloop plot ---
  plot(2*pi*c./wfh,20*log10(abs(Ef_e_arr)/height),2*pi*c./wsh,20*log10(abs(Ef_e_arrsh)/height));
%  plot(2*pi*c./wsh,20*log10(abs(Ef_e_arrsh)/height));
%  plot(2*pi*c./w(w1:w2),2*(abs(Ef_e_arr(w1:w2))/height));
 axis([0.4 5 -100 2]);
  pause(0.001)
     if mod(i,intp)==1;
    disp(i);
     EFE(floor(i/intp)+1,:) = Ef_e_arr(w1:w2);
    EFSH(floor(i/intp)+1,:) = Ef_e_arrsh(w5:w6);
   end

end
toc;



function [dEf_e_arr] = nlin_func_fR( Ef_e_arr, z)
format long
global   chi2  dt   omega_e wfh li n_e c t  dk_e  qpm_k  kfhe mm delta_k wsh isw ish
% % .*exp(delta_k*z)
 dkk=dk_e*omega_e-kfhe;
% %
% % dkk2=dk_e*omega_e*2-2*kfhe;
%

 tt=t-dk_e*z;
mm=1*(square(qpm_k*z+pi/2)  );

Ef_e_arr1=Ef_e_arr(1,:);
Ef_e_arr2=Ef_e_arr(2,:);


E_e_arr1 = ifft(fftshift(Ef_e_arr1))/dt;
E_e_arr2 = ifft(fftshift(Ef_e_arr2))/dt;

% dEf_e_arr1 =-(1./(4*c*n_e))*li.*(1+(wfh-omega_e)/omega_e).*
fftshift(fft( 1*mm*chi2(1,1)*E_e_arr1.*(E_e_arr1).*exp(1*li*omega_e*tt+li*dkk*z)+2*mm*chi2(1,1)*E_e_arr1.
*conj(E_e_arr1).*exp(-1*li*omega_e*tt-li*dkk*z) )*dt);
 dEf_e_arr1 =-(1./(4*c*n_e))*li.*(1+(wfh-omega_e)/omega_e).*
fftshift(fft(  4*mm*chi2(1,1)*(E_e_arr2).*conj(E_e_arr1).*exp(-
li*delta_k*z)+2*mm*chi2(1,1)*E_e_arr1.*conj(E_e_arr1).*exp(-1*li*omega_e*tt-li*dkk*z)   )*dt);

 dEf_e_arr2 =-(1./(4*c*n_e))*li.*(1+(wsh-2*omega_e)/(2*omega_e)).*
fftshift(fft( 4*mm*chi2(1,1)*E_e_arr1.*E_e_arr1.*exp(li*delta_k*z)+2*mm*chi2(1,1)*E_e_arr2.*conj(E_e_arr2)
.*exp(-1*li*omega_e*tt-li*dkk*z))*dt);


  dEf_e_arr=[dEf_e_arr1;dEf_e_arr2];
```

```
function [u_out] = rka(func, u_in, z, dz)
global dt
format long

% full step
u_full = rk4(func, u_in, z, dz);

% half step, twice
u_half = rk4(func, u_in, z, dz/2);
u_half = rk4(func, u_half, z+dz/2, dz/2);

I_full = norm(u_full, 2)^2*dt;
I_half = norm(u_half, 2)^2*dt;

err = (I_full-I_half)/(I_full+I_half);

if (err <= 1e-9)
   u_out = u_full;
else
   u_out_half = rka(func, u_in, z, dz/2);
   u_out = rka(func, u_out_half, z+dz/2, dz/2);
end
```

Appendix B:

Publications during Ph.D.Study

[1]. **Xing Liu**, Binbin Zhou, Hairun Guo, and Morten Bache, "Mid-IR femtosecond frequency conversion by soliton-probe collision in phase-mismatched quadratic nonlinear crystals," Opt. Lett. 40, 3798-3801 (2015)

[2]. **Xing Liu**, Minhao Pu, Binbin Zhou, Clemens J. Krückel, Attila Fülöp, and Victor Torres-Company and Morten Bache, , "Octave-spanning supercontinuum generation in a silicon-rich nitride waveguide," **Submitted** to Opt. Lett (2016)

[3]. **Xing Liu**, Binbin Zhou, Clemens J. Krückel, Attila Fülöp, and Victor Torres-Company and Morten Bache , "Octave-spanning supercontinuum generation in a silicon-rich nitride waveguide," **accepted to** CLEO(2016)

[4]. **Xing Liu**,, B. Zhou, H. Guo, and M. Bache, "Collision Between Soliton and Dispersive Wave in Phase-Mismatched Quadratic Nonlinear Crystals," in 2015 European Conference on Lasers and Electro-Optics - European Quantum Electronics Conference, (Optical Society of America, 2015), paper EF_3_6.

[5]. **Xing Liu**, H. Niu, W. Liu, D. Chen, B. Zhou and M. Bache, "Cross-correlation frequency-resolved optical gating by molecular vibration for ultrashort pulse," Lasers and Electro-Optics Europe (CLEO EUROPE/IQEC), 2013 Conference on and International Quantum Electronics Conference, Munich, 2013, pp.1-1.doi: 10.1109/CLEOE-IQEC.2013.6801114

[6]. **Xing Liu,** H. Niu, W. Liu, D. Chen, B. Zhou and M. Bache, "Completely background free broadband coherent anti-Stokes Raman scattering spectroscopy," Lasers and Electro-Optics Europe (CLEO EUROPE/IQEC), 2013 Conference on and International Quantum Electronics Conference, Munich, 2013, pp.1-1.doi: 10.1109/CLEOE-IQEC.2013.6801508

[7]. H. Guo, **Xing Liu**, X. Zeng, B. Zhou, and M. Bache, "Tunable Mid-infrared Radiations in Quadratic Media through Near-infrared Soliton Interactions with Second-harmonic Resonances," in 2015 European Conference on Lasers and Electro-Optics - European Quantum Electronics Conference, (Optical Society of America, 2015), paper EE_P_11

[8]. B. Zhou, H. Guo, **Xing Liu,** and M. Bache, "Octave-Spanning Mid-IR Supercontinuum Generation with Ultrafast Cascaded Nonlinearities," in CLEO: 2014, OSA Technical Digest (online) (Optical Society of America, 2014), paper JTu4A.24.

[9]. M. Bache, **Xing Liu,** and B. Zhou, "Observation of an Octave-Spanning Supercontinuum in the Mid-Infrared using Ultrafast Cascaded Nonlinearities," in Research in Optical Sciences , OSA Technical Digest (online) (Optical Society of America, 2014), paper HTu1C.4.